Strathclyde Institute of Pharmacy and Biomedical Sciences

Development of novel tumour-targeted gold nanocages for cancer therapy

By

Jamal Almowalad

A thesis presented in fulfilment of the requirements for the degree of

Doctor of Philosophy

2021

This thesis is the result of the author's original research. It has been composed by the author and has not been previously submitted for examination which has led to the award of a degree.

Signed:

Date:

Acknowledgements

First, I would like to thank my God for providing me with the strength, patience and ability to complete this work.

It gives me great pleasure to express my sincere gratitude to my supervisor, Dr Christine Dufès, for her unlimited support, enthusiasm and invaluable guidance on the research project and the writing of this thesis.

I also would like to express my appreciation to the Government of Saudi Arabia, as represented by Umm Al-Qura University and the Saudi Arabian Cultural Bureau in the UK, for funding this project.

This thesis would not have been completed without the help of numerous people. I would like to thank Dr Paul Edwards for assisting with SEM. Many thanks to Mrs Margaret Mullin from the University of Glasgow for her help with TEM. A special thanks to Dr Rothwelle Tate for kindly assisting with the gel retardation assay. Thanks also to Mr Alexander Clunie and Ms Patricia Keating from Pure and Applied Chemistry for their help with ICP-MS and MALDI-TOF. Special thanks to my colleagues Dr Sukrut Somani and Dr Partha Laskar for their kind advice and great support during my studies, not to mention all of my colleagues in Lab 224: Joan, Najla, Intouch and Jitkasem. My gratitude also extends to all my friends in SIPBS, especially Ahmed and Hadi, for their help, encouragement and friendship.

Finally, I expressly appreciate my parents, brothers, and nieces. I cannot thank you enough for your unwavering love, support and unending prayers throughout my years of studying abroad.

Contents

List of Figures

List of Tables

List of abbreviations

AgNCs	Silver nanocubes
ANOVA	One-way analysis of variance
AuNCs	Gold nanocages
AuNCs-DAB-Lf	Lactoferrin-bearing dendrimer-conjugated gold nanocages
AuNCs-Lf	Lactoferrin-bearing gold nanocages
AuNCs-Lf-2xPEG	2xPEG-conjugated, lactoferrin-bearing gold nanocages
AuNCs-Lf-DAB	Dendrimer-conjugated, lactoferrin-bearing gold nanocages
AuNCs-Lf-PEG	PEG-conjugated, lactoferrin-bearing gold nanocages
AuNCs-Lf-PEI	Polyethyleneimine-conjugated, lactoferrin-bearing gold nanocages
AuNCs-Lf-PLL	Polylysine-conjugated, lactoferrin-bearing gold nanocages
AuNCs-PEG	PEGylated gold nanocages
AuNCs-PEG-Lf	Lactoferrin-bearing PEGylated gold nanocages
AuNCs-PLL-Lf	Lactoferrin-bearing polylysine-conjugated gold nanocages
AuNPs	Gold nanoparticles
CD	Circular dichroism
DAB	Diaminobutyric polypropylenimine dendrimer

DAB-Lf	Lactoferrin-bearing generation 3-diaminobutyric polypropylenimine dendrimer
DAPI	4′, 6-diamidino-2-phenylindole
DEG	Diethylene glycol
DI water	Deionized water
DMSO	Dimethyl sulfoxide
DNA	Deoxyribonucleic acid
DOTAP	N-[1-(2,3-Dioleoyloxy) propyl]-N, N, N-trimethylammonium methylsulfate
EPR	Enhanced permeability and retention
FACS	Fluorescence-activated cell sorting
FBS	Foetal bovine serum
FDA	Food and Drug Administration
FTIR	Fourier-transform infrared
IC_{50}	Growth inhibitory concentration
ICP-MS	Inductively coupled plasma mass spectrometry
IV	Intravenous injection
Lf	Lactoferrin
LNCaP	Prostate adenocarcinoma cell line

LSPR	Localised surface plasmon resonance
MALDI-TOF	Matrix-assisted laser desorption/ionization-time of flight
MDR	Multidrug resistance
MEM	Minimum essential medium
MPS	Mononuclear phagocyte system
MTT	3-(4,5-dimethylthiazol-2-yl)-2,5-diphenyltetrazolium bromide
MWCO	Molecular weight cut-off
ONPG	O-nitrophenyl- β-D-galactosidase
PBS	Phosphate buffer saline
pCMV β-Gal	Plasmid DNA encoding β-galactosidase
PEG	Polyethylene glycol
PEI	Polyethyleneimine
PLB	Passive lysis buffer
PLL	Poly-L-lysine
PPI	Polypropylenimine
PVP	Polyvinyl pyrrolidone
RNA	Ribonucleic acid
SEM	Standard error of the mean

SEM	Scanning electron microscope
TBE	Tris-Borate-Ethylenediamine tetra acetate
TEM	Transmission electron microscopy
TNF-α	Tumour necrosis factor alpha
TRAIL	Tumour necrosis factor-related apoptosis-inducing ligand
IL	Interleukin

Abstract

Gold nanocages are a novel class of multimodal nanomaterials with hollow interiors that have received considerable attention in recent years. Because of their unique morphologies and remarkable optical and physicochemical properties, they have been widely explored in various biomedical applications, including imaging, drug delivery and cancer treatments. However, their promise as a gene delivery system for cancer therapy has only been revealed so far in conjunction with chemotherapeutics and photothermal therapy. The purpose of this work is to determine whether conjugating the targeting ligand lactoferrin and various cationic polymers on gold nanocages complexed with plasmid DNA can enhance gene expression, cellular uptake, and anti-proliferation activity in prostate cancer cells without the use of external stimulation. Lactoferrin-bearing gold nanocages (AuNCs-Lf) conjugated with polyethylenimine (PEI), polyethylene glycol (PEG), poly-L-lysine (PLL), and diaminobutyric polypropylenimine (DAB) were synthesised and characterised. Their cellular uptake, transfection efficacy, and anti-proliferative effects were evaluated in PC-3 prostate cancer cells following complexation with plasmid DNA. Our results demonstrated that lactoferrin-bearing gold nanocages alone or conjugated with cationic polymers could condense plasmid DNA at conjugate:DNA weight ratios higher than 1:1. Among all gold conjugates, the highest gene expression was obtained following treatment with AuNCs-DAB-Lf and AuNCs-Lf-PLL on PC-3 cells due to a significant increase in DNA uptake mediated by these conjugates. The anti-proliferative activity of AuNCs-DAB-Lf and AuNCs-Lf-PLL complexed to DNA-encoding TNFα was significantly improved (by up to 9.0-fold and 2.1-fold)

compared with DAB dendriplex and PLL polyplex-encoding TNFα, respectively. In conclusion, lactoferrin-bearing gold nanocage conjugates are, therefore, promising gene delivery systems that might be further used in prostate cancer therapy.

Chapter 1: Introduction

1.1. Application of nanotechnology in cancer therapy

Cancer is considered one of the major causes of mortality in the world. According to estimates from the Global Cancer Incidence, Mortality and Prevalence (GLOBOCAN), 19.3 million people were diagnosed with cancer in 2020, with over 10 million cancer-related deaths. Furthermore, the GLOBOCAN report demonstrated that the incidence of new cancer cases will increase from 19.3 million in 2020 to 28.4 million in 2040 (Sung *et al.*, 2021).

Adding to surgical intervention, current conventional cancer treatments include chemotherapy and radiation therapy. Although chemotherapy is considered the most commonly used cancer treatment, anti-cancer drugs have significant drawbacks because they non-selectively kill normal cells alongside cancer cells. The lack of selective delivery of chemotherapy into the tumour site adversely affects healthy tissues, thereby making patients suffer from unwanted side effects in addition to cancer symptoms. Therefore, selective targeting delivery could be a potential approach for overcoming anticancer drugs' drawbacks.

Current advances in the nanotechnology sciences enable the use of such a tool for enhancing targeting delivery and reducing the side effects of cancer therapeutics (Misra *et al.*, 2010; Wicki *et al.*, 2015). Nanotechnology involves designing, developing and manufacturing materials at the nanometre scale. The term *'nano'* is derived from the Greek word *'nanos'*, which means 'dwarf'. Accordingly, the American Society for Testing and Materials (ASTM International 2006) defines nanoparticles as particles in which two or more dimensions are of the order of 1–100 nm. In the context of medicine, nanotechnology utilisation has induced nanomedicine, thereby making it possible for nano-sized drug-delivery vehicles to be

created. Nanomedicine refers to the therapeutic and diagnostic agents produced at a nanoscale size for treatment, delivery and diagnostic applications. Generally, nanocarriers smaller than 1000 nm can transport therapeutic agents to disease areas.

The transport of cancer drugs plays a vital role in nanocarriers. Compared to conventional chemotherapeutics, anticancer drug delivery using a nanoparticle-based platform presents some advantages. First, nanoparticles can be used to deliver less stable, low-soluble therapeutics to the desired cells, where the poorly water-soluble therapeutics alone show low bioavailability and cellular uptake (Williams *et al.*, 2013). Also, various body enzymes, such as pepsin, trypsin and ribonucleases (RNAses), can biodegrade anticancer therapeutics, which may affect their therapeutic efficacy. These therapeutics can be encapsulated in nanoparticles to prevent their degradation, ultimately resulting in enhanced solubility and chemical stability (Wicki *et al.*, 2015). Nanoparticles also help to improve the biodistribution and selectivity of anticancer agents towards cancer cells. The distribution of cancer medications depends on their physicochemical properties, which determine their ability to penetrate cancer cells. Nanoparticles can be designed to improve anticancer drug penetration into the target tissue, as they can target tumours selectively owing to their enhanced permeability and retention (EPR) effect. This effect ensures that anticancer therapeutics are delivered in higher concentrations to tumour sites and in minimal concentrations to healthy tissues. Finally, nanoparticles can be functionalised with targeting ligands to specifically deliver the drugs into the target site (Minchinton and Tannock, 2006; Lammers *et al.*, 2012; Zhang *et al.*, 2012). Such benefits have made the development of nanoparticle-based cancer medication a high priority.

Due to recent advancements in nanotechnology and the potential of using nanoparticles in drug delivery, new cancer treatment approaches based on nanotechnology and gene therapy can be explored.

1.2. Gene therapy

Gene therapy is a novel therapeutic approach that holds great promise to treat genetic diseases and disorders, such as cancer, cystic fibrosis and Parkinson's disease, alongside many others (Zhou *et al.*, 2017; Salameh *et al.*, 2020). It refers to the process of transferring genetic materials (DNA or RNA) to the host cell for therapeutic benefits, including treating disease or abnormal medical condition. Depending on the therapeutic purpose, gene therapy can be applied by different mechanisms, such as correcting defective genes, replacing faulty or missing genes, and introducing new or modified genes. Consequently, the transferred gene expression could either restore or initiate a new cellular response, thereby achieving the therapy's purpose (Wang *et al.*, 2013a). Gene therapy can be performed using two main methods: *ex vivo* and *in vivo* strategies. For *ex vivo*, the required cells are isolated from the patients, transfected by genetic materials, and then re-implanted into the patients. However, for *in vivo*, the genetic materials are directly administered into the required organ or tissue cells via systemic or local injection (Zhou *et al.*, 2017).

1.2.1. Gene delivery

To achieve successful gene therapy, the therapeutic gene must specifically be delivered to and expressed in the desired cells without affecting non-target cells.

Also, efficient gene therapy depends on the successful transfer of therapeutic genes across biological barriers, such as cell membranes, before integrating with the nucleus of the targeted cells. Consequently, the naked nucleic acids cannot achieve the desired results due to their rapid degradation in blood circulation. To overcome this challenge, gene delivery systems have been developed and studied to deliver foreign genetic materials into target cells. These delivery systems can be classified into viral and non-viral vectors (Wang *et al.*, 2013a).

1.2.1.1. Viral vectors

Viral vectors have been extensively used in gene delivery applications and have been involved in two-thirds of gene therapy clinical trials (Waehler *et al.*, 2007; Zhou *et al.*, 2017). They refer to the use of modified viruses to transfer genetic materials to the target cells owing to the ability of viruses to induce infection. Thus, the main advantages of viral vectors are their high transfection efficacy and long-term gene expression compared to non-viral vectors (Wang *et al.*, 2013a). Adenovirus and retrovirus are the most common viral vectors used in gene therapy-related clinical trials due to their high transfection efficacy *in vivo*. However, viral vectors also have some potential disadvantages that hinder their clinical use, such as their immunogenicity, toxicity, poor targeting ability to specific cells, limited ability to deliver large size nucleic acids and high cost (Wang *et al.*, 2013a).

1.2.1.2. Non-viral vectors

Non-viral vectors have been extensively employed as gene delivery systems due to their favourable advantages compared to viral vectors. First, they provide enhanced

biosafety, biocompatibility and a capacity to condense and transfer large-sized nucleic acids. Second, they are relatively easy to prepare in large quantities at low cost. Finally, they can be modified with targeting ligands for cell- or tissue-specific targeting purposes (Zhou *et al.*, 2017). Various nanomaterials, mainly cationic, such as liposomes, polymers and dendrimers, have been investigated for gene delivery applications (Zhou *et al.*, 2017; Salameh *et al.*, 2020). Nucleic acid complexation occurs through electrostatic interactions between nucleic acids and the non-viral vectors. The complexation induced several advantages, such as protecting the complexed nucleic acids from the surrounding medium and avoiding their degradation by the nuclease enzymes present in the blood circulation (Wang *et al.*, 2013a; Zhou *et al.*, 2017). Furthermore, the DNA complexation minimises the charge repulsion generated from the charge similarity between the DNA and the cell membrane, which subsequently facilitates DNA penetration inside the cell (Zhou *et al.*, 2017).

1.2.1.2.1. Liposomes

Liposomes are closed, spherical-shaped vesicles comprising single or multiple concentric lipid bilayers enclosing an aqueous core (Wang *et al.*, 2012). Initially described in 1965, they were among the earliest nanocarriers used in the medical field (Bangham, 1993). The size of liposomes ranges from tens of nanometres to micrometres according to their design. Their biocompatible and biodegradable composition, alongside their ability to entrap hydrophilic compounds in their aqueous core and hydrophobic molecules inside their lamellae, make them efficient nanocarriers (Wang *et al.*, 2012).

Cationic liposomes have been extensively studied and widely utilised for gene delivery since the first application of cationic lipids in gene delivery was reported in 1987 by Felgner and his colleagues (Felgner *et al.*, 1987). They used N-[1- (2,3-dioleyloxy) propyl]-N,N,N-trimethylammonium chloride (DOTMA), a double chain monovalent quaternary ammonium lipid, to condense and transfer genetic materials, thereby inducing a high level of gene expression. The structure of cationic lipids generally includes three parts: a cationic hydrophilic head group, a hydrophobic anchor and a linker. The cationic hydrophilic head normally contains one or more amino groups necessary to bind the nucleic acid through electrostatic interactions and form a complex called lipoplex (Zhou *et al.*, 2017). Physical factors such as the shape, size and surface charge of the lipoplex can influence its transfection efficacy. As the surface–charge ratio is the most critical parameter, cationic liposomes should have a higher net charge than DNA, thereby forming a DNA lipoplex with a total surface–charge ratio of about one. This feature prevents the enzymatic degradation of the DNA and supports its entry into the cells, owing to the charge attraction between the lipoplex and the cell membrane (Wang *et al.*, 2013a; Zhou *et al.*, 2017). Cationic lipids can be used alone or jointly with another lipid (named co-lipid or helper lipid) to promote transfection efficacy. Dioleoylphosphatidylethanolamine (DOPE) is one of the most widely utilised co-lipids that has demonstrated an enhancement in transfection efficacy when combined with cationic lipids, such as DOTAP (dioleoyl-3-trimethylammonium propane) (Hui *et al.*, 1996). DOPE facilitates endosomal escape and promotes DNA release from the lipoplex, resulting in improved transfection efficacy (Hui *et al.*, 1996; Wang *et al.*, 2013a).

1.2.1.2.2. Polymers

Polymers are macromolecules comprising numerous smaller repeating units, termed monomers, that are chemically attached together. Polymeric-based nanoparticles are extensively used as nanocarriers in drug delivery applications due to their biodegradability and biocompatibility (Sun *et al.*, 2014).

Cationic polymers are macromolecules that have positive zeta potentials owing to the presence of a high density of amine groups in their structures. In recent decades, they have been developed and used as non-viral gene delivery vectors due to their well-defined chemistry and low cost. Also, the tuneable chemical structure of polymers allows surface modification to further improve their transfection or reduce their cytotoxicity (Salameh *et al.*, 2020). Among the cationic and commercialised polymers, polyethyleneimine (PEI), poly-L-lysine (PLL), cationic dendrimers and chitosan are the most used polymers for gene delivery applications. The delivery of nucleic acid using cationic polymers can be achieved via electrostatic interactions between DNA and the polymers. The positively charged amino groups of these polymers would generate electrostatic interactions with the negatively charged phosphate groups of nucleic acid, thereby forming a polyionic complex or polyplex (Wang *et al.*, 2013a; Salameh *et al.*, 2020). These complexes protect the complexed nucleic acid from enzymatic degradation in the circulation and body tissues, improve its cellular uptake via endocytosis through electrostatic interactions between the polyplex and the cell surface, and prolong its half-life in the cytoplasm (Wang *et al.*, 2013a).

1.2.1.2.3. Poly-L-Lysine

Poly-L-Lysine (PLL) is a cationic polymer that is considered one of the earliest polycations used for gene delivery. It has become attractive for *in vivo* applications because of its biodegradable nature (Zhou *et al.*, 2017). Its structure is also rich with primary amine groups that are ionised in a physiological environment and have high affinity to negative ions (Figure 1-1). These positively charged amine groups allow PLL to electrostatically interact with negatively charged DNA and form condensed particles (polyplexes) with a small particle size around 100 nm (Wagner and Kloeckner, 2006). However, the poor transfection efficacy of PLL polyplexes is the main drawback of this vector. This might be because of the low ability of the PLL polyplex to escape from the endosome following its cellular endocytosis and due to the strong binding between DNA and PLL that hinders the release of the DNA into the cytoplasm (Wang *et al.*, 2013a). Thus, the modification of PLL with endosomolytic agents, such as chloroquine, improves transfection efficacy by facilitating the endosomal escape of the polyplex (Pouton *et al.*, 1998).

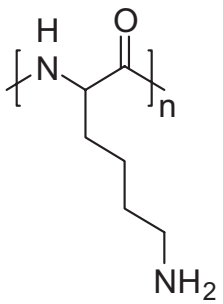

Figure 1-1: Chemical structure of poly-L-lysine (Adapted from Wong *et al.*, 2007).

1.2.1.2.4. Polyethyleneimine

Polyethyleneimine (PEI) is the most common non-viral vector and is considered the gold standard in gene delivery because of its high transfection efficacy *in vitro* and *in vivo* (Patnaik and Gupta, 2013; Zhou *et al.*, 2017). This efficient non-viral vector can be classified based on its chemical structure into branched and linear PEI, which contain different amine groups (primary, secondary and tertiary amines) (Figure 1-2). These features enable PEI to effectively condense the DNA and generate a stable polyplex alongside complex large molecules. The positive charges of PEI polyplexes promote cellular penetration through adhesion to the negatively charged cell membrane. In addition, PEI can facilitate the endosomal escape of the polyplex due to its proton sponge effect, which promotes DNA release into the cytoplasm (Zhou *et al.*, 2017). Upon endocytosis of polyplexes, PEI becomes highly cationic due to its protonation at the low pH of the endosomal microenvironment. This will trigger the influx of chloride counter ions and increase osmotic pressure, inducing endosomal rupture and resulting in the release of the DNA into the cytoplasm. The molecular weight and the architecture of the branched (b-PEI) or linear PEI (L-PEI) can crucially influence the transfection efficacy and the toxicity profile. It has been found that branched PEI induced better transfection efficacy, resulting from its strong ability to condense DNA compared to its linear counterpart (Thapa and Narain, 2016). The molecular weight of PEI also impacts the transfection efficacy. Higher molecular weight PEI displays increased DNA condensation efficacy with enhanced transfection efficacy (Godbey *et al.*, 1999; Monnery *et al.*, 2017). However, the enhanced transfection efficacy obtained from PEI with a high molecular weight was also associated with increased cytotoxicity.

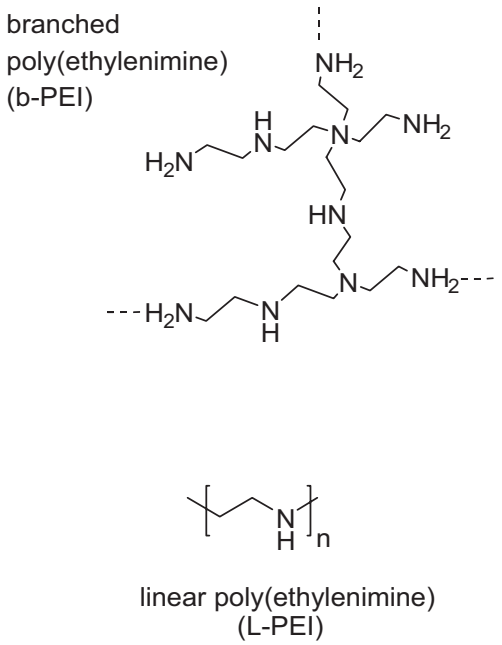

Figure 1-2: Chemical structure of branched and linear PEI (Adapted from Wong *et al.*, 2007).

1.2.1.2.5. Dendrimers

Dendrimers are polymerised macromolecules with highly organised branches, creating a three-dimensional (3D) architecture with a tree-like shape (Baker, 2009). They can be developed from synthetic or natural compounds (e.g. amino acids, sugars and nucleotides). They are composed of a central core, interior layers and external layers (Nanjwade *et al.*, 2009). The central core can be a single or multiple atom with a minimum of two identical functional groups, where the interior layers are attached to the core via branched units. Finally, the external layers contain different terminal functional groups that play a role in conjugating molecules to the dendrimers. Dendrimers can also support drug loading via hydrophobic, hydrophilic bonds or other chemical linkers due to the presence of the central core and layers. In

gene delivery applications, cationic dendrimers, such as polyamidoamine (PAMAM) and diaminobutyric polypropylenimine (DAB), are the most studied dendrimers as non-viral vectors due to their high transfection efficacy and commercial availability (Dufès *et al.*, 2005). The cationic charge, precise structure and tree-like shape of cationic dendrimers enable the effective complexation of genetic materials (Figure 1-3). Cationic dendrimers bind the genetic material through electrostatic interactions between the phosphate groups on the DNA and the amino groups on the dendrimer, thereby forming nanoparticles called dendriplex (Dufès *et al.*, 2005). Also, the generation of these cationic dendrimers was found to influence their transfection efficacy. Higher generations were found to have higher transfection efficacy but were accompanied by high toxicity, probably resulting from the highly positive surface charge (Duncan and Izzo, 2005). However, recently, low generation dendrimers such as generations-1, 2 and 3 DAB (DAB-Am 4, 8 and 16) showed high transfection efficacy with low cytotoxicity, making them potentially attractive as non-viral gene carriers (Zinselmeyer *et al.*, 2002; Altwaijry *et al.*, 2018a).

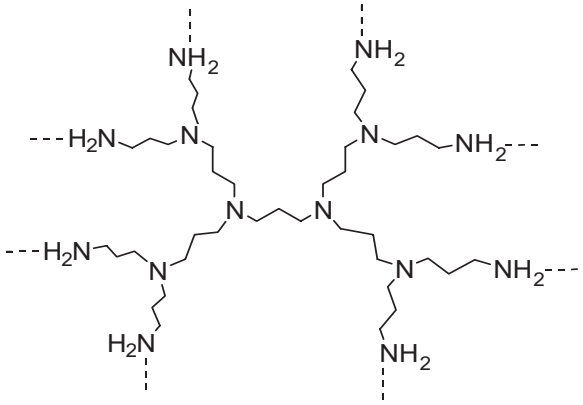

Figure 1-3: Chemical structure of polypropylenimine dendrimer (Adapted from Wong *et al.*, 2007).

1.3. Delivery barriers

To achieve the desired therapeutic effects, efficient cancer gene therapy requires the successful delivery of genetic material specifically to its target cancer site. However, several barriers, classified as extracellular and intracellular barriers, can limit the delivery of the genetic material by non-viral vectors.

1.3.1. Extracellular barriers

Upon systemic administration, free plasmid DNA can undergo rapid degradation by the nuclease enzymes. The half-life of free DNA is about a few minutes in the bloodstream (Zhou *et al.*, 2017). The recognition and uptake of DNA molecules by the reticuloendothelial system (RES) can induce the rapid elimination of DNA from the circulation. This can usually be overcome by DNA complexation with cationic non-viral vectors, thereby protecting the DNA from enzymatic degradation (Wang *et al.*, 2013a). However, following systemic administration, these DNA complexes could interact with blood components, such as plasma proteins, salts and lipids, which may restrict their delivery to target tissue. The interactions between plasma proteins and DNA complexes depend on the physicochemical properties of the nanocarriers, which, in turn, determine the blood circulation and biodistribution of the DNA complexes. For example, the positive charge of cationic vectors attracts plasma proteins, which results in protein deposition on the vector surface. This might affect vector stability and impact its electrostatic interactions with DNA, resulting in premature release of the complexed nucleic acids (Zhou *et al.*, 2017). The adsorption of proteins on cationic vectors may also alter their surface charges resulted in aggregating the vector into larger particles. This would induce the rapid clearance of

DNA complexes by the reticuloendothelial system (RES) or phagocytes, thereby decreasing their transfection efficacy (Moghimi *et al.*, 2012). This could be overcome by surface modification of the vector with hydrophilic molecules, such as polyethylene glycol (PEG), which has been widely used due to its ability to prevent cationic vector aggregation by shielding their total positive charges (McCrudden and McCarthy, 2013). In addition, the PEGylation of polycations prolongs the blood circulation time of cationic DNA complexes owing to the PEG ability to alter the non-specific interactions that may occur between plasma proteins and cationic DNA complexes (Park *et al.*, 2006).

1.3.2. Intercellular barriers

DNA penetration across the cell membrane is one of the most crucial processes for effective gene transfer. Because both DNA and the cell membrane carry negative charges, the formed charge repulsion restricts DNA penetration through the cell (Wang *et al.*, 2013a). DNA complexation with cationic vectors is one of the main techniques that facilitates DNA entry into the cell. Due to the positive charge of the cationic vector, the DNA complex can electrostatically interact with the anionic cell membrane, inducing cellular uptake of the complex via non-specific endocytosis. However, the cellular uptake by non-specific cells is another barrier that challenges cationic complexes due to the lack of cell specificity of the cationic carriers. Therefore, cationic carriers are frequently conjugated to cell-specific targeting ligands to increase the cellular uptake selectivity towards the target cells. These ligands specifically recognise and bind receptors in the cell membranes of the target cells. This enables complex penetration via receptor-mediated endocytosis – a

cellular biological process in which a specific molecule enters or leaves the cell assisted by a specific receptor in the cell membrane (Zhou *et al.*, 2017). Furthermore, nanocarriers can passively target and penetrate cancer cells via the enhanced permeation and retention (EPR) effect due to the leaky vasculature of highly proliferating solid tumours. The entrapment of DNA complexes inside the endosome after their cellular uptake is also considered a barrier for gene delivery. In the endosome, the DNA complex encounters a decrease in pH from neutral to 4.5 and may be degraded by various enzymes (Wang *et al.*, 2013a). To overcome endosomal barriers, cationic polymers with high buffer capacity, such as PEI or dendrimers, can be used for endosomal escape owing to their proton sponge effect (Salameh *et al.*, 2020). The low pH of the endosome triggers the cationic polymers to become ionised. The ionised polymer then draws protons to the endosome, inducing increased osmotic pressure alongside endosomal swelling and disruption, which results in DNA release into the cytoplasm. Following endosomal release, the DNA must be transported to the nucleus through the cytoplasm, where it may be subjected to cytoplasmic degradation. Because only free DNA may enter the nucleus, the DNA must first be separated from its vector. Following nuclear uptake, the transgene is expressed as messenger RNA, which is exported to the cytoplasm and translated into the required protein (Thapa and Narain, 2016).

1.4. Cancer targeting

One of the main aims of the use of nanomedicine for cancer therapy is to reach the tumour following administration into the circulatory system. Two approaches have been used for cancer targeting: passive and active targeting (Ghosh *et al.*, 2008a).

1.4.1. Passive targeting

The passive targeting approach is achieved based on the pathophysiology of the tumour site. Tumour vasculature is generally associated with abnormalities, such as leaky walls of blood vessels (Jain and Stylianopoulos, 2010). The wall leakage occurs due to the rapid proliferation of the endothelial cells. Due to such irregularities, the tumour vasculature displays pores significantly exceeding normal vessel junctions (5–10 nm), with diameters ranging from 100 nm to 800 nm (Sun *et al.*, 2014). Hence, the tumour vasculature is highly permeable, allowing the penetration of macromolecules, such as nanoparticles, into the tumour (Figure 1-4). For healthy tissues, the lymphatic system is responsible for eliminating macromolecules, but this system is dysfunctional in solid tumours (Maeda *et al.*, 2000). The highly permeable nature of tumour vasculature and the impaired lymphatic system therefore generate a phenomenon known as the enhanced permeability and retention (EPR) effect. This effect enables macromolecules and nanoparticles to accumulate in tumours for longer periods and at higher concentrations than in healthy tissue (Wang *et al.*, 2012).

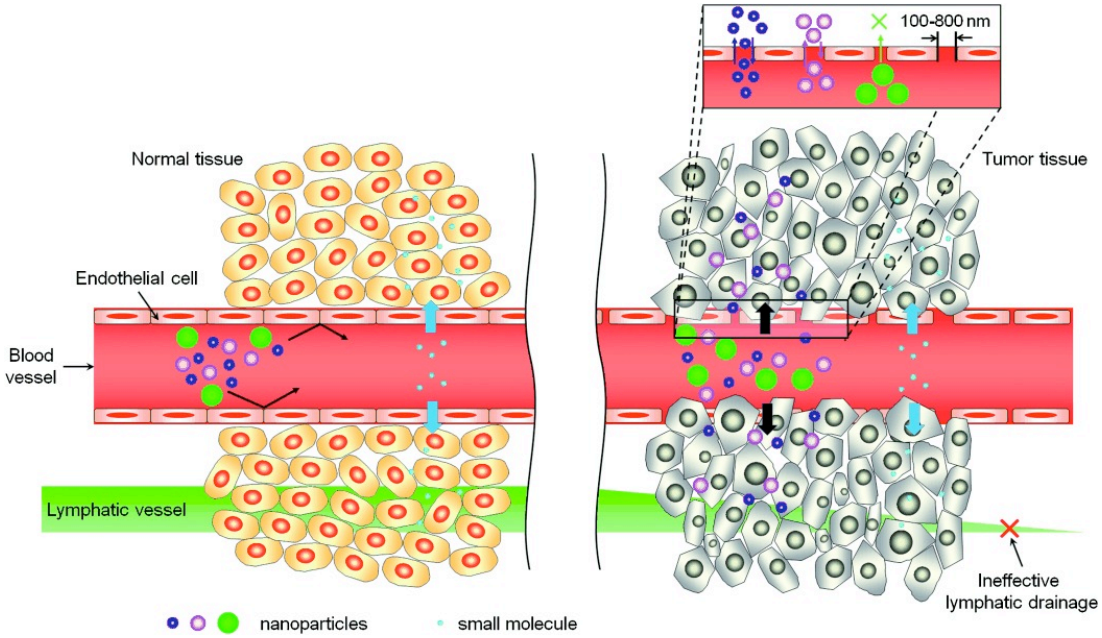

Figure 1-4: Transport of nanoparticles of various sizes through healthy tissue (left) and tumour (right). The EPR effect allows the nanoparticles to accumulate in the tumour more than in normal tissues (Adapted from Sun *et al.*, 2014).

1.4.2. Active targeting

Active targeting is another strategy that is widely used currently for directing nanoparticles to specific areas, such as tumours, without affecting healthy tissues. The active targeting approach involves modifying the nanoparticle surfaces with targeting ligands that can identify and selectively bind to specific receptors on the target cells. The targeting ligands could be antibodies, proteins, peptides, sugars, lipoproteins and nucleic acids (Bertrand *et al.*, 2014). Active targeting mainly aims to promote nanoparticle accumulation in the target tumour tissue and to enhance their cellular penetration via receptor-mediated endocytosis. Therefore, several factors determine its effectiveness, including the overexpression of specific receptors on the surface of target cells over non-target cells, the binding affinity of the targeting

ligands to their receptors and the cellular uptake of nanoparticles (Bertrand *et al.*, 2014). Although the active targeting method can increase payload delivery to target cells, its effectiveness still encounters some challenges. For instance, the binding affinity and the specificity of ligand-bearing nanoparticles could be affected upon entering blood circulation due to protein corona formation (Monopoli *et al.*, 2012; Van Hong Nguyen, 2017). To date, various active targeting ligands have been utilised and investigated for selectively delivering therapeutic agents to cancer cells. These include folic acid, albumin, aptamers, biotin, hyaluronic acid, monoclonal antibodies, peptides, and proteins such as lactoferrin, which was selected as a targeting ligand in this study (Bertrand *et al.*, 2014; Lim *et al.*, 2015).

1.5. Gold nanoparticles

Gold is a precious golden-yellow colour metal. It is an inert and chemically unreactive metal; therefore, its colour can remain unchanged for thousands of years. Currently, of all newly produced gold, 50% is used for jewellery, 40% for investment, and only 10% for industrial purposes. However, small-sized gold particles exhibit different properties compared to the bulk form (Yang *et al.*, 2015). Small-sized gold particles display a red ruby colour, different from the golden yellow colour of bulk gold. For that, small-sized gold particles have been widely used in painting window glass.

Gold nanoparticles exhibit unique optical and physicochemical properties that differ from those of bulk gold and other nanoparticles. Their size can range from 1 nm to 8 μm, and they can display various shapes, such as nanorods, nanospheres, nanoshells, nanocubes, nanocages and nanoclusters (Figure 1-5). Owing to their

tunable sizes, they preferably accumulate in tumours and enter cells via various mechanisms, much faster than that observed for other small molecules. Furthermore, the ability of gold nanoparticles to convert light into heat makes them ideal agents for efficient thermal therapy of diseased or cancerous tissue. Also, gold nanoparticles can absorb large amounts of X-ray radiation for enhancing cancer radiation therapy or improving imaging contrast in diagnostic CT scans. They can be used to deliver challenging compounds, such as unstable or poorly hydro-soluble drugs, and promote their efficient delivery into target tissues. Hence, they have been widely used in diagnostics, biomedical and therapeutic applications. Most notably, the advantages of gold nanoparticles in biomedicine can be combined in a single platform, providing simultaneous targeting, diagnostic and therapeutic capabilities that can be chemically customised for a specific patient or condition (Dreaden *et al.*, 2011).

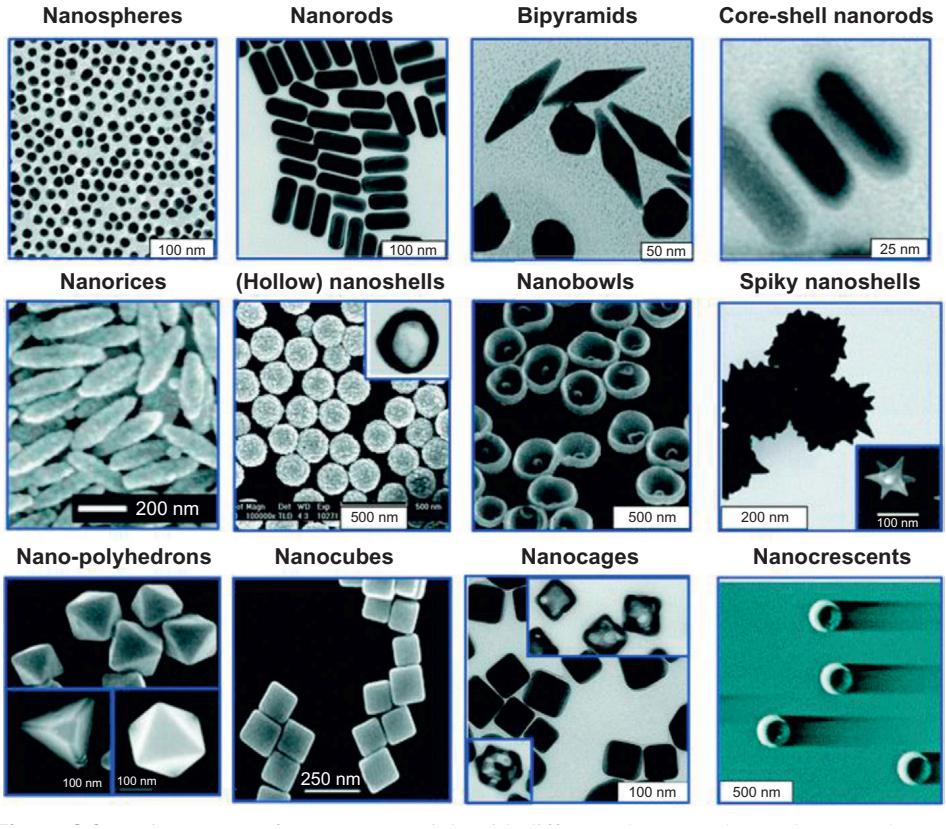

Figure 1-5: Various types of gold nanoparticles with different shapes (Adapted from Ebara and Uto, 2016).

1.5.1. Optical features of gold nanoparticles

Gold nanoparticles exhibit unique optical properties, such as scattering and/or absorbing specific wavelengths of light, compared to bulk gold. These optical properties are based on a phenomenon called localised surface plasmon resonance (LSPR) (Cobley *et al.*, 2011). This phenomenon occurs when incident light interacts with gold nanoparticles, and the free electrons of the nanoparticles will detect the electromagnetic field and begin to oscillate collectively relative to the lattice of positive ions at the same frequency as the incident light (Yang *et al.*, 2015). The LSPR frequency strongly depends on the size, shape, composition and morphology

of the nanoparticles. The LSPR peaks of conventional gold colloids are around 500–600 nm, which explains the ruby-red colour of a gold colloid solution (Kelly *et al.*, 2003). However, the LSPR peaks of gold nanoparticles should be tuned to the near-infrared region (NIR, 700–900 nm) for biomedical applications. In the NIR region, also known as the transparent window, light can penetrate soft tissues deeply owing to the low ability of blood and water to absorb light with NIR wavelengths alongside the low scattering ability of soft tissues. Only gold nanoparticles having non-spherical morphologies (e.g. rod, plate and star) or hollow structures (e.g. shell, box and cage) can exhibit LSPR peaks in the NIR region.

1.5.2. Physicochemical properties essential for biomedical applications

In addition to its optical properties, gold nanoparticles have various physicochemical characteristics that make them an attractive platform for biomedical applications. Gold (Au) is one of the less reactive metals with remarkable resistance against both oxidation and corrosion; therefore, it can be stored for many years under atmospheric conditions without being destroyed (Yang *et al.*, 2015). This non-reactive and hence bio-inert property of Au therefore makes it an ideal candidate for *in vitro* and *in vivo* applications. In addition, the low cell toxicity of Au nanoparticles makes them an attractive platform for *in vivo* applications and clinical biocompatibility (Cobley *et al.*, 2011; Dreaden *et al.*, 2012). Through surface modification, Au nanoparticles can be utilised to deliver therapeutic agents. Drug molecules can be loaded onto the surface of gold nanoparticles via different linkages and conjugation methods. Amine ($-NH_2$) and thiol (-SH) functional groups are widely used to attach drug molecules to the surface of gold nanoparticles owing to the strong affinity between gold and both

sulphur and nitrogen (Cheng *et al.*, 2008). Some studies have demonstrated that the Au-N bond between drugs and the surface of gold nanoparticles is more efficient than the Au-S bond for releasing drugs at the tumour site (Cheng *et al.*, 2009; Cheng *et al.*, 2011). However, the thiol functional group is the most common linker used to attach molecules to gold nanoparticles due to its stability in biological environments (Flynn *et al.*, 2003). The use of the van der Waals force, hydrogen bonding, electrostatic interactions and drug grafting to capping ligands are other strategies for loading drugs on the surface of gold nanoparticles (Funkhouser *et al.*, 1995; Giljohann *et al.*, 2009; Brown *et al.*, 2010; Han *et al.*, 2012). In addition, active targeting capabilities can also be introduced to gold nanoparticles through surface modification. Gold nanoparticles can be conjugated with targeting moieties, such as antibodies, folate and peptides, that can bind to specific receptors on the target cells, resulting in enhancing the gold nanoparticle cell internalisation (Yang *et al.*, 2015).

1.5.3. Synthesis of gold nanoparticles

In 1857, Michael Faraday first reported a scientific procedure for producing colloidal gold nanoparticles. Faraday described that 'fine particles' could be formed by reducing a gold chloride ($HAuCl_4$) aqueous solution with phosphorus in the presence of carbon disulphide as a stabilising agent. Hence, an aqueous suspension of 'fine particles' with a ruby-red colour was formed (Faraday, 1857). Most gold nanoparticles are synthesised using similar methods by reducing gold salts in the presence of surface-capping ligands or stabilising agents that prevent particle aggregation (Yang *et al.*, 2015).

1.5.4. Gold nanoparticles in gene delivery

Gold nanoparticles have been used to deliver nucleic acids (DNA and RNA) via various techniques, such as covalent and non-covalent approaches.

1.5.4.1. Covalent attachment

This loading method leverages the high affinity of the sulphur (S) atom to the gold (Au) surface. Therapeutic molecules that have thiols in their structures, or that have been modified with thiol groups without affecting their activity, can be attached to the surface of gold nanoparticles via the Au-S bond (Ding *et al.*, 2014). Both drugs and nucleic acids (DNA or RNA) can be attached to the surface of gold nanoparticles using this concept. The covalent approach offers some advantages, such as protecting the attached nucleic acid from enzymatic degradation and allowing the use of negatively charged nanocarriers for gene delivery (Ding *et al.*, 2014). For instance, Markin and colleagues developed polyvalent nucleic acid AuNPs (pNA–AuNPs) by covalently conjugating AuNPs with thiol-modified oligonucleotides and utilising them in siRNA-based gene silencing (Seferos *et al.*, 2009). Despite the strong negative charge of the AuNPs, which would be expected to limit cellular uptake, the pNA–AuNPs demonstrated high stability against enzymatic degradation and showed increased cellular uptake in various cell lines. The density of oligonucleotides attached to the AuNPs surface influenced the cellular uptake, with higher densities of oligonucleotides resulting in higher cellular uptake and more effective gene delivery.

The nucleic acid payload can be released differently from the surface of gold nanoparticles. The intercellular release of nucleic acid can be applied by sulphur atom exchange using thiol-containing compounds, such as glutathione. External

stimuli, such as light, can also be used through photothermal ablation to trigger payload release, either by breaking the bonds of sulphur-gold and/or heating the nanoparticles until reaching the melting point, thereby dissociating the attached drugs (Figure 1-6). Internal stimuli such as thiol exchange or external light are critically important to release thiolated drugs or nucleic acids from the nanoparticles due to the strength of sulphur-gold bonds that may prevent the drugs from being released by simple diffusion (Cheng *et al.*, 2009).

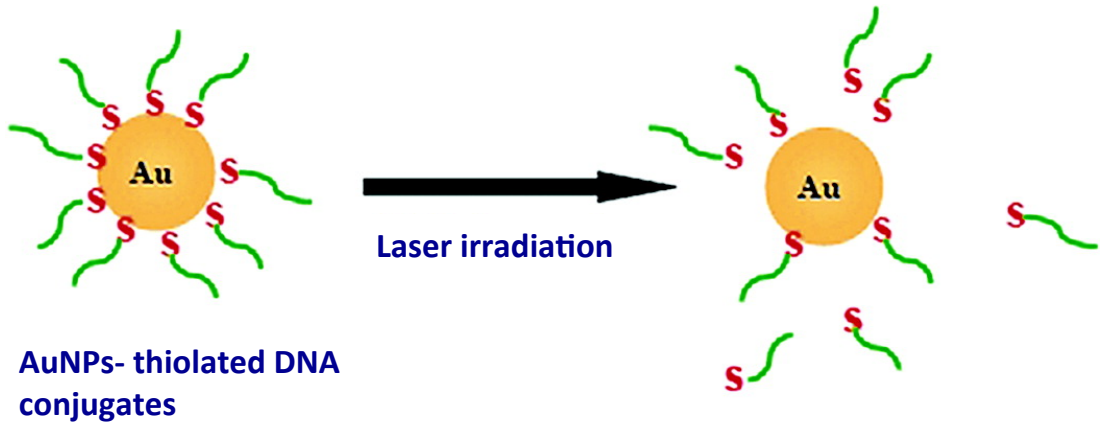

Figure 1-6: Schematic illustration of laser photothermal effect on thiolated-DNA-modified gold nanoparticles (Adapted from Jain *et al.*, 2006).

1.5.4.2. Non-covalent attachment

The non-covalent approach is another efficient technique utilising nanocarriers, such as gold nanoparticles, for gene delivery. Gold nanoparticles prepared in water display a strong charge due to the presence of charged functional groups or capping agents on their surface. Therefore, charged drugs can be loaded onto the gold nanoparticles by non-covalent approaches, such as electrostatic interactions or relevant layer-by-layer (LbL) coatings to the surface of the nanoparticles (Murphy *et al.*, 2010; Ding *et al.*, 2014). Nucleic acids can be non-covalently attached to the gold nanoparticle surface through charge complexation between the negative charges of the nucleic acids and the positive charges of the gold nanoparticles. The major advantages of this non-covalent approach are the ability to use unmodified nucleic acids for gene delivery and gene silencing, adding to promoting their endosomal escape via the proton sponge effect of the gold nanoparticles (Ghosh *et al.*, 2008b; Ding *et al.*, 2014). For example, Thomas and Klibanov developed cationic polymer-AuNP conjugates by modifying AuNPs with thiolated polyethyleneimine with a low molecular weight (2 kDa; PEI) (Thomas and Klibanov, 2003). This PEI-AuNPs conjugates could electrostatically complex the plasmid DNA and showed transfection efficacy six times higher than their unmodified PEI counterpart in monkey kidney cells. Some studies have demonstrated that cetyltrimethylammonium bromide (CTAB)-stabilised gold nanoparticles were successfully customised as a platform for delivering single-stranded RNA (ssRNA) and siRNA due to the interactions between the positively charged gold nanoparticles and the negatively charged nucleic acid (Bonoiu *et al.*, 2009). Indeed, the nucleic acid molecules could be readily attached to the surface of gold nanorods, thereby causing the system to

produce a gene silencing effect with no noticeable cell cytotoxicity. The layer-by-layer assembly method can also be used based on the electrical interactions between the negatively and positively charged species generated by adding multiple polymer layers onto the surface of the nanoparticles (Figure 1-7).

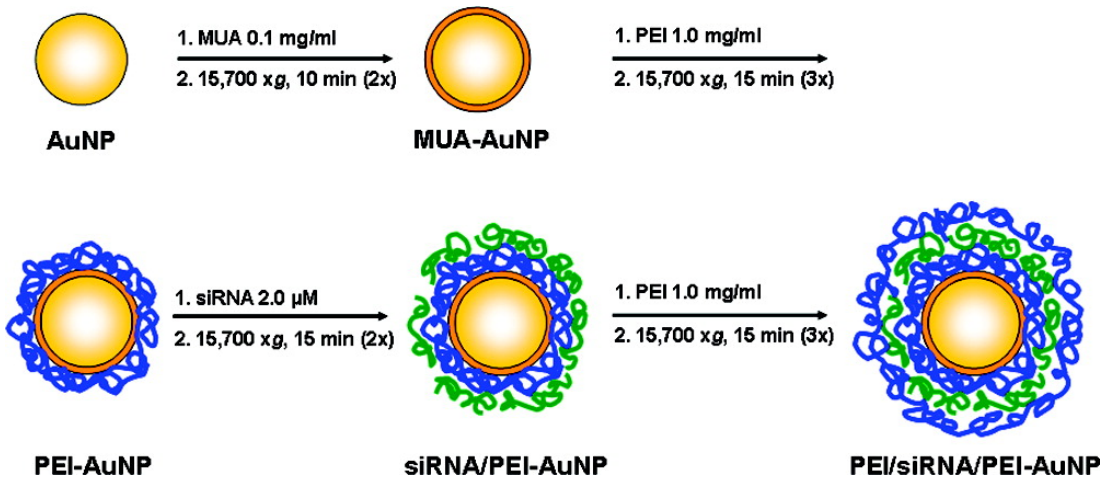

Figure 1-7: Schematic illustration of the layer-by-layer assembly process of PEI/siRNA/PEI-AuNP complexes (Adapted from Elbakry *et al.*, 2009).

1.6. Gold nanocages

Gold nanocages are a novel class of gold nanomaterials with hollow interiors and porous walls developed by the Xia group in 2002. The unique optical, physical and chemical properties make gold nanocages appropriate candidates for nanomedicine applications. Compared to solid Au nanoparticles, the hollow interiors and porous walls of Au nanocages make them suitable for controlled release and drug delivery since the drugs or biomolecules can be loaded in the nanocages, which prevents their release before usage. Also, the LSPR peaks of Au nanocages range from 600 to 1200 nm, which makes them tunable to the near infrared (NIR) region to leverage the so-called 'transparent window' of soft tissues, enabling Au nanocage utilisation in optical imaging and therapeutic applications. Furthermore, Au nanocages are ideal for cancer theranostics because they can be formed in large quantities and in high quality, with flexible sizes ranging from 20 to 500 nm, which is required for optimising their biodistribution and tissue permeation. Au nanocages are suitable for labelling biomolecules and ligands because of their atomically flat surfaces. The inert nature of Au provides high biocompatibility and stability to Au nanocages for *in vivo* applications (Bertrand *et al.*, 2014).

1.6.1. Gold nanocages in photothermal therapy

Gold nanostructures have unique optical features called LSPR, which allow them to absorb and scatter light at specific wavelengths. The absorbed light is converted to heat and applied to the desired tissue. Consequently, irreversible damage occurs to the exposed tissue when heated above the hyperthermia temperature (42 °C) (Desai *et al.*, 2006). This process of transforming light into heat is known as the

photothermal effect, which can be used in drug release strategies and for destroying cancer cells (Cobley *et al.*, 2010). Hence, the ability of Au nanostructures to absorb light highly in the NIR region, where light penetrates deeply into the tissue, makes Au nanoparticles attractive for photothermal therapy in cancer and other diseases.

Gold nanocages significantly destroy cancer cells *in vitro* and *in vivo* with the photothermal effect. *In vitro*, Xia and co-workers demonstrated the ability of Au nanocages conjugated with anti-EGFR to kill SK-BR-3 breast cancer cells with a photothermal effect (Chen *et al.*, 2007b). The same group tested the photothermal effect of Au nanocages *in vivo* on tumour-bearing mice (Chen *et al.*, 2010a). Compared with saline-injected mice, gold nanocages-injected mice showed a significant decrease in tumour size by 70% after the laser treatment. This result indicates the beneficial use of Au nanocages' photothermal effect in cancer therapy.

1.6.2. Gold nanocages in delivery applications

Gold nanocages also represent a novel class of delivery systems. Their large surfaces and hollow interiors allow them to load drugs. Also, the optical photothermal properties of Au nanocages can be used to monitor the drug release. Initially, the controlled drug release system of Au nanocages was developed to fill their hollow interiors with drug molecules and cover their exterior surface with thermo-sensitive polymer (Yavuz *et al.*, 2009). The drug molecules were then released from the Au nanocages in response to light/thermal stimulation. Gold nanocages can absorb light in the NIR region and then convert it into heat that melts the thermo-sensitive polymer shells and allows the release of stored drugs. Thereafter, Xia and co-workers filled the interiors of Au nanocages with a mixture of both drugs and thermo-

responsive materials, known as drug-doped phase change materials (PCMs) (Moon *et al.*, 2011). These materials, such as 1-tetradecanol, have a melting point of 38 °C to 39 °C and surfactant-like features that make them compatible with hydrophobic and hydrophilic drugs. The payload was released from the Au nanocages after heating the drug-PCM mixture by NIR irradiation or high intensity focused ultrasound (HIFU) upon the melting points. Consequently, the drugs were released from the Au nanocages via diffusion, with their release controlled by adjusting the intensity and duration of HIFU exposure.

1.7. Aim and objectives

Gold nanocages have previously been reported as potential platforms for drug and gene delivery alongside photothermal agents for cancer therapy. However, their potential as gene delivery systems for cancer treatment has only been reported in combination with chemotherapeutics and photothermal therapy, but not in isolation so far. We hypothesised that conjugating targeting ligand lactoferrin and various cationic polymers on gold nanocages complexed to plasmid DNA could enhance cellular uptake, gene expression and anti-proliferative activity in PC-3 prostate cancer cells, without assistance of external stimulation.

Therefore, the aims and objectives of this study are as follows:

- to synthesise and characterise gold nanocages
- to synthesise and characterise lactoferrin-bearing gold nanocages conjugated with various cationic polymers: polyethylenimine (PEI), diaminobutyric polypropylenimine (DAB) and poly-L-lysine (PLL), alongside polyethylene glycol (PEG)
- to assess the gene expression efficacy and cellular uptake of the gold nanocages conjugates complexed with plasmid DNA, and to evaluate their therapeutic efficacy following complexation with therapeutic DNA in PC-3 prostate cancer cells.

Chapter 2: Synthesis and characterisation of gold nanocages

2.1. Introduction

Gold nanocages can be produced by a galvanic replacement reaction between silver nanocubes and chloroauric acid ($HAuCl_4$) aqueous solution. This reaction can be conducted through simple titration techniques via the careful addition of $HAuCl_4$ solution to a boiling suspension of silver nanocubes. During the reaction, Ag atoms are gradually oxidised and dissolved, while Au atoms are simultaneously formed on the surface of the Ag nanocubes, eventually inducing AuNC generation. As the reaction proceeds, the silver nanocubes undergo several changes in their structures and morphology until the nanocage shape is achieved at the end of the reaction (Figure 2-1) (Skrabalak *et al.*, 2008). By adding $HAuCl_4$ solution to the heated suspension of Ag nanocubes, the associated LSPR peak position shifted from the visible to the NIR region, indicating the initiation of the galvanic replacement reaction and the conversion of Ag nanocubes into Au nanocages. Accordingly, several colour changes will also be observed, from yellow at the beginning of the reaction to blue and nearly colourless at the end (Skrabalak *et al.*, 2007).

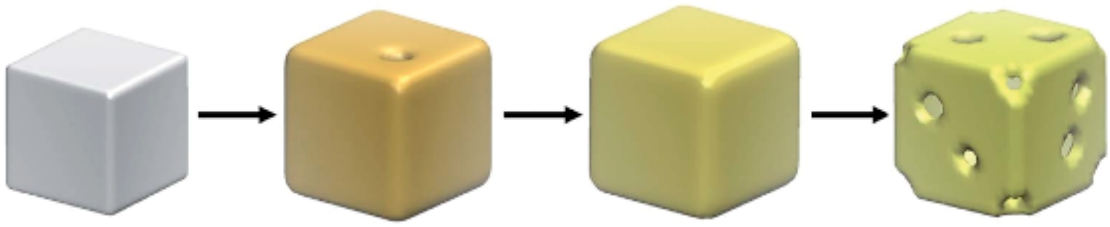

Figure 2-1: Schematic illustration of the structural changes of silver nanocubes during the galvanic replacement reaction with $HAuCl_4$ solution (Adapted from Qiu *et al.*, 2020).

2.1.1. Aims and objectives

The aims of this chapter are as follows:

1) to optimise gold nanocage synthesis and to develop a method for preparing a large amount of gold nanocages with ideal optical and physicochemical properties, enabling us to perform further studies using the same batch.

2) to characterise the gold nanocages synthesised via modified protocols. The physicochemical characteristics of the as-synthesised gold nanocages were evaluated using transmission electron microscopy, UV-vis spectrophotometry and photon correlation spectroscopy.

2.2. Materials and methods

2.2.1. Materials

Materials	Suppliers
Acetone	Sigma-Aldrich, UK
Aqueous hydrochloric acid solution (HCl, 37%)	Sigma-Aldrich, UK
Deionized (DI) water	Sigma-Aldrich, UK
Diethylene glycol (DEG)	Sigma-Aldrich, UK
Ethylene glycol (EG)	Sigma-Aldrich, UK
Hydrogen tetrachloroaurate (III) hydrate ($HAuCl_4$)	Sigma-Aldrich, UK
Polyvinyl pyrrolidone (PVP)	Sigma-Aldrich, UK
Silver nitrate ($AgNO_3$)	Sigma-Aldrich, UK
Silver trifluoroacetate (CF_3COOAg)	Sigma-Aldrich, UK
Sodium chloride (NaCl)	Sigma-Aldrich, UK
Sodium hydrosulphide hydrate (NaSH)	Sigma-Aldrich, UK
Sodium sulphide (Na_2S)	Sigma-Aldrich, UK

2.2.2. Methods

2.2.2.1. Preparation of silver nanocubes

Silver nanocubes were prepared via sulphide-mediated polyol synthesis, using ethylene glycol (EG) and diethylene glycol (DEG) as both reducing and solvent agents, as established by the Xia group (Skrabalak *et al.*, 2007; Wang *et al.*, 2013b).

2.2.2.1.1. Preparation of silver nanocubes in ethylene glycol

Silver nanocubes were synthesized via polyol reduction in ethylene glycol (EG), as previously reported (Skrabalak *et al.*, 2007). Briefly, an oil bath containing a magnetic stir bar was heated to 150 ^{o}C for around 1 hour at a spin rate of 330 rpm. Six mL of EG were then added to two 24 mL-glass vials with a clean stir bar and heated in the oil bath at 150 ^{o}C for 1 hour. Each vial was closed with a loose cap throughout the entire process, except for when adding the reagents. After the EG reaction vials had boiled for 1 hour, 90 and 100 μL of Na_2S solution (3 mM) dissolved in EG were added to Vials 1 and 2, respectively. After 10 minutes, 0.03 g of polyvinyl pyrrolidone (PVP) dissolved in 1.5 mL EG was transferred to each reaction vial. $AgNO_3$ solution (0.5 mL, 48 mg/mL in EG) was added to each vial. The cap was loosely placed back on top of the vials until the end of the reaction process. The reaction subsided after 90 minutes and the vials were cooled in a water bath at 22 ^{o}C. The reaction mixtures were then transferred to 15 mL centrifuge tubes and vortexed with ~ 6 mL of acetone. The mixtures were then centrifuged at 9 000 rpm (16 000 g) for 30 minutes. The supernatant was then removed and the silver nanocubes were transferred to 1.5 mL centrifuges tubes and mixed with DI water. The mixtures were centrifuged again at 9 000 rpm (16 000 g) for 10 minutes and

the supernatant was discarded; this process was repeated a further three times. The final silver nanocubes were stored in 2 mL of DI water at 4 °C for further use.

2.2.2.1.2. Preparation of silver nanocubes in diethylene glycol

Silver nanocubes were synthesized via polyol reduction in diethylene glycol (DEG) as previously reported (Wang *et al.*, 2013b). Briefly, 5 mL of DEG was added to 24 mL glass vial containing a magnetic stir bar and was heated in an oil bath at 150 ^{o}C for 30 minutes. The following reagents were prepared in DEG and then added separately to the reaction vials. Initially, NaSH solution (0.06 mL, 3 mM) was pipetted to the vials. After 4 minutes, HCL solution (0.5 mL, 3 mM) was added, followed by 1.25 mL of PVP solution (20 mg/mL). After 2 minutes, CF_3COOAg solution (0.4 mL, 282 mM) was added. The vials were closed loosely throughout the entire process, except for the addition of the reagents. The reaction was stopped after 90 minutes by placing the vials in an ice water bath. Then, the mixtures were transferred to 15 mL centrifuge tube and mixed with 6 mL acetone, followed by centrifugation at 9 000 rpm (16 000 g) for 30 minutes. The supernatant was removed and the remaining products were washed with 2 mL of DI water and sonicated using a bath sonicator for 10 minutes. The products were transferred to 1.5 mL centrifuge tube and centrifuged at 9 000 rpm (16 000 g) for 10 minutes, followed by the discarding of the supernatant and the sonication of the remaining products with DI water for 2 min; this process was repeated a further three times. The final products were then dispersed in 2 mL of DI water and stored at 4 °C for further use.

2.2.2.1.3. Large-scale synthesis of silver nanocubes

Briefly, 60 mL of DEG was added into a 250-mL round-bottom flask containing a magnetic stir bar and heated in an oil bath at 150 ^{o}C for 30 minutes. The reagents were then prepared in DEG and added separately to the reaction flask. Initially, NaSH solution (0.72 mL, 3 mM) was pipetted to the flask. After 4 minutes, HCL solution (6 mL, 3 mM) was added, followed by 15 mL of PVP solution (20 mg/mL). After 2 minutes, CF_3COOAg solution (4.8 mL, 282 mM) was added. The flask was closed loosely throughout the entire process, except for the addition of the reagents. The reaction was stopped after 90 min by placing the flask in an ice water bath for 30 min. Then, 25 mL of the mixture was transferred to 50 mL centrifuge tube and mixed with 20 mL acetone, followed by centrifugation at 9 000 rpm (16 000 g) for 30 min. After removing the supernatant, 20 mL of DI water was added to the remaining products then sonicated for 10 minutes using ultrasound bath sonicator. Next, the products were centrifuged at 9 000 rpm (16 000 g) for 10 minutes, followed by the discarding of the supernatant and the sonication of the remaining products with 20 mL of DI water; this process was repeated a further three times. The final products were then dispersed in 20 mL of DI water and stored at 4 °C.

2.2.2.2. Synthesis of gold nanocages using standard methods

2.2.2.2.1. Synthesis of gold nanocages according to Xia group's method

Gold nanocages (AuNCs) were synthesized based on a previously published method (Skrabalak *et al.*, 2007). Briefly, 5 mL of polyvinyl pyrrolidone (PVP) solution (1 mg/mL in DI water) was added to a 24-mL glass vial containing a magnetic stir bar.

Then, 100 μL of as-prepared Ag nanocubes were added to the vial and heated at 90 ^{o}C for 10 minutes. An aqueous solution of $HAuCl_4$ (5 mL, 0.1 mM) was added to the reaction vial via a syringe pump at rates of 10 and 45 mL/h with magnetic stirring. The reaction was stopped when the reaction sample attained dark orange, purple and grey colours. Then, the reaction was heated for another 10 minutes until the reaction colour becomes stable. After cooling down the flask to 25 °C, 10 mL of NaCl-saturated solution (0.36 g/mL) was added to remove the AgCl. The products were then centrifuged at 9 000 rpm (16 000 g) for 30 minutes and washed with 10 mL DI water after discarding the supernatant; this process was repeated three times. Finally, the final products were stored in 3 mL of DI water, at 4 °C until further use.

2.2.2.2.2. Synthesis of gold nanocages according to Qu group's method

Gold nanocages were synthesized based on a previously reported method (Shi *et al.*, 2014). Briefly, 500 μL of Ag nanocubes was added to 5 mL of polyvinyl pyrrolidone (PVP) solution (1 mg/mL in DI water) in a 24-mL glass vial and heated at 90 ^{o}C for 10 minutes. Then, various amounts (starting from 0.2 up to 2.5 mL) of 0.5 mM $HAuCl_4$ aqueous solution were added to the vials with a syringe pump at a rate of 45 mL/h. After obtaining different colours of the gold nanocages, the reaction mixtures were heated for a further 10 minutes until the colour stabilises. The reaction vials were cooled at 25 °C, and then 10 mL of NaCl-saturated solution (0.36 g/mL) was added to dissolve and remove the AgCl. The products were then centrifuged at 9 000 rpm (16 000 g) for 30 minutes and washed with 10 mL DI water after discarding the supernatant; this process

was repeated three times. Finally, the final products were stored in 3 mL of DI water, at 4 °C until further use.

2.2.2.2.3. Large-scale synthesis of gold nanocages

Briefly, 600 mL of polyvinyl pyrrolidone (PVP) solution (1 mg/mL in water) was added to a 1-L round-bottom flask containing a magnetic stir bar. Then, 60 mL of as-prepared silver nanocubes was added to the flask and heated at 100 °C, while stirring for 30 minutes. An aqueous solution of 1 mM $HAuCl_4$ (140 mL) was added to the reaction flask via a syringe pump at a rate of 45 mL/h. The reaction was stopped when the reaction sample attained a blue colour and exhibited UV-vis absorption spectrum at 740 nm. The mixture was heated at 100 ^{o}C for another 15 minutes until the reaction colour became stable. After cooling down the flask to 25 °C, 20 mL of NaCl-saturated solution (0.36 g/mL) was mixed with each 25 mL aliquots of the mixture to remove AgCl. The products were then centrifuged at 9 000 rpm (16 000 g) for 30 minutes and washed with 20 mL of DI water after discarding the supernatant. This process was repeated three times. The final products were added to 20 mL of DI water and stored at 4 °C until further use.

2.2.2.3. Characterisation of silver nanocubes

2.2.2.3.1. Scanning electron microscopy (SEM) imaging

The Ag nanocubes sample was prepared for SEM by dispersing 10 µL of the stored Ag nanocubes suspension onto a silicon substrate and allowing it to air-dry at 30 °C overnight. SEM imaging was carried out on the following day.

2.2.2.3.2. Size measurement of silver nanocubes

The size of Ag nanocubes was measured using a Malvern Zetasizer Nano-ZS (Malvern Instruments, Malvern, UK) at room temperature (25 ^{o}C). In the standard process, 10 μL of as-stored Ag nanocubes suspension was diluted with 990 μL of DI water and then transferred to a cuvette for measurement. All size measurements were performed three times.

2.2.2.4. Characterisation of gold nanocages

2.2.2.4.1. Scanning electron microscopy imaging

The gold nanocages sample was prepared for SEM by dispersing 5 μL of the stored Au nanocages suspension onto a silicon substrate and left to dry overnight at a temperature of 30 ^{o}C. SEM imaging was carried out on the following day.

2.2.2.4.2. Size and zeta potential measurement of gold nanocages

The size and zeta potential of gold nanocages were measured using a Malvern Zetasizer Nano-ZS (Malvern Instruments, Malvern, UK) at 25 °C. In the standard process, 10 μL of as-stored gold nanocages suspension was diluted with 990 μL of DI water and then transferred to a cuvette for measurement. All size and zeta potential measurements were performed three times.

2.2.2.4.3. Quantification of gold nanocages

The concentrations of gold nanocages samples were obtained via inductively coupled plasma mass spectrometry (ICP-MS). Briefly, 20 μL of AuNCs in DI water was digested in 180 μL *aqua regia* at 20 °C for 1 h. The mixture was further diluted with DI water to

a final *aqua regia* concentration of 2%. The Au concentration (µg/L) within the samples was measured using the ^{197}Au isotope and the ^{175}Lu isotope used as an internal standard for all measurements. All ICP-MS measurements were performed in triplicate using an Agilent 7700X instrument (Agilent technologies, Santa Clara, US).

2.2.2.4.4. UV-Vis- spectrometry analysis

All UV–Vis spectra were determined using a Varian Cary® 50 Bio UV-visible spectrophotometer in the wavelength range of 300–1000 nm. The UV-Vis-spectra of DI water was adjusted as baseline prior to the measurement of the samples.

2.2.2.4.5. Transmission electron microscopy imaging

The morphology of gold nanocages was examined using transmission electron microscopy (TEM). Typically, 20 µL of AuNCs samples in DI water were placed in carbon-coated 200-mesh copper grids and left to dry at 20 °C for 1 hour. The samples were then visualized using a JEOL JEM-1200EX® transmission electron microscope (Jeol, Tokyo, Japan) operating at an accelerating voltage of 80 kV.

2.3. Results

2.3.1. Synthesis of silver nanocubes

2.3.1.1. Synthesis of silver nanocubes in EG

After 30 minutes of adding all the reagents to the reaction vials, the sample containing 90 μL of Na_2S solution (3 mM) was amber in colour, while the sample containing 100 μL of the same solution was dark brown in colour (Figure 2-2). The colour of the samples remained unchanged, even after prolonging the reaction for up to 120 minutes. However, the colour of the silver nanocubes samples was supposed to be ruby-red or green-ochre based on the Xia group protocol. During the isolation process of silver nanocubes, it was not possible to collect a sufficient amount of Ag nanocubes, with only dark black spots stuck to the bottom of the centrifugation tube. The same result was observed in synthesising the Ag nanocubes using different volumes (70 and 80 μL) of Na_2S solution (3 mM).

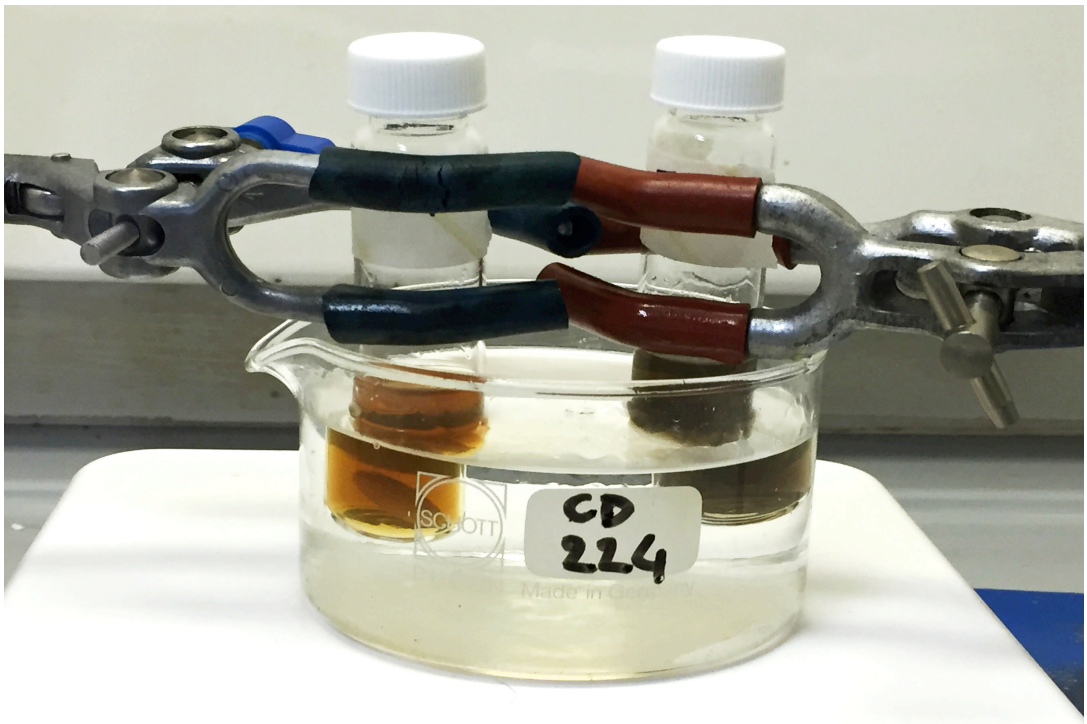

Figure 2-2: Silver nanocubes sample containing 90 μL of Na_2S appeared in amber colour (left vial) and silver nanocubes sample containing 100 μL of Na_2S appeared in dark brown colour (right vial).

2.3.1.2. Synthesis of silver nanocubes in DEG

The Ag nanocubes samples appeared in green-red colour 15 minutes after adding the reaction reagents. In the final stage of the reaction (90 minutes), the samples appeared in a ruby-red colour (Figure 2-3).

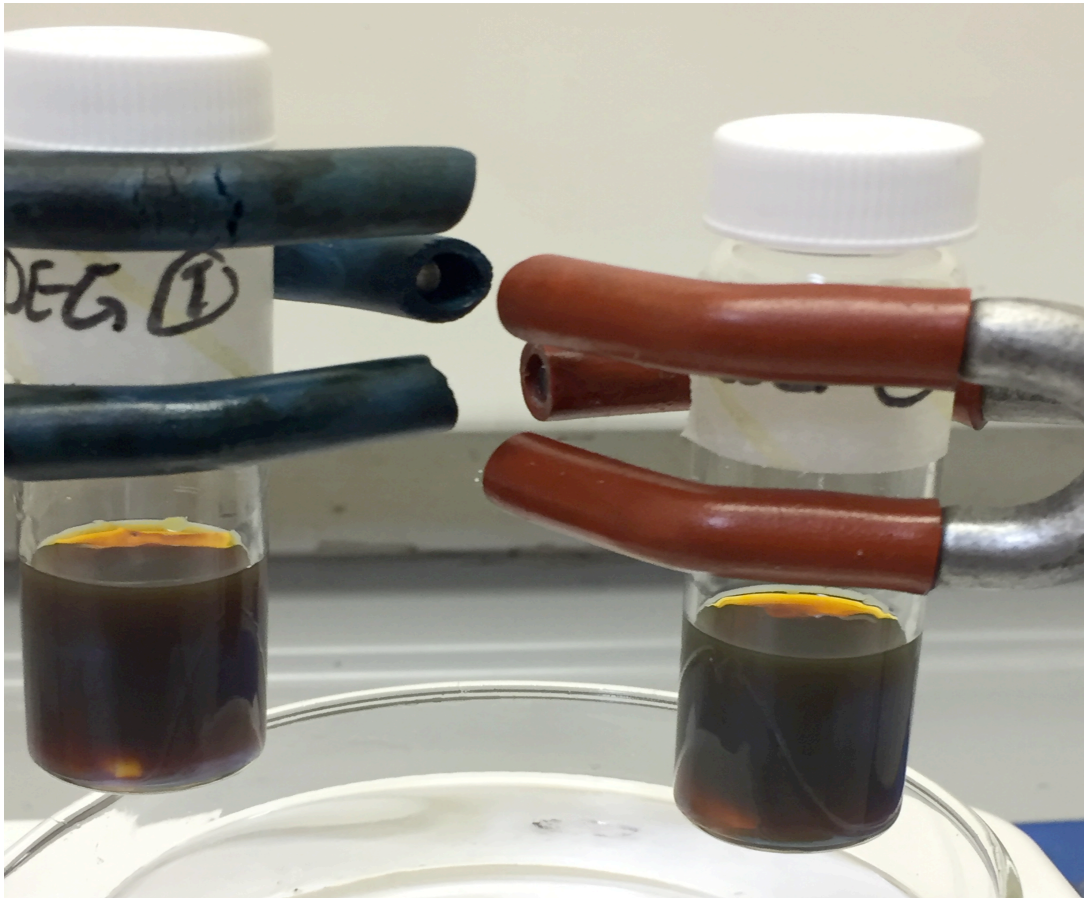

Figure 2-3: Silver nanocubes samples prepared in DEG having a ruby-red colour and green-ochre tone on top of the sample medium after stopping the reaction.

2.3.2. Characterisation of silver nanocubes

SEM imaging revealed that silver nanoparticles had a cubic shape with an average edge length of 38.37 ± 0.96 nm (Figure 2-4). Also, the size measurement using the Zetasizer showed that Ag nanocubes had an average size of 58.5 ± 1.30 nm.

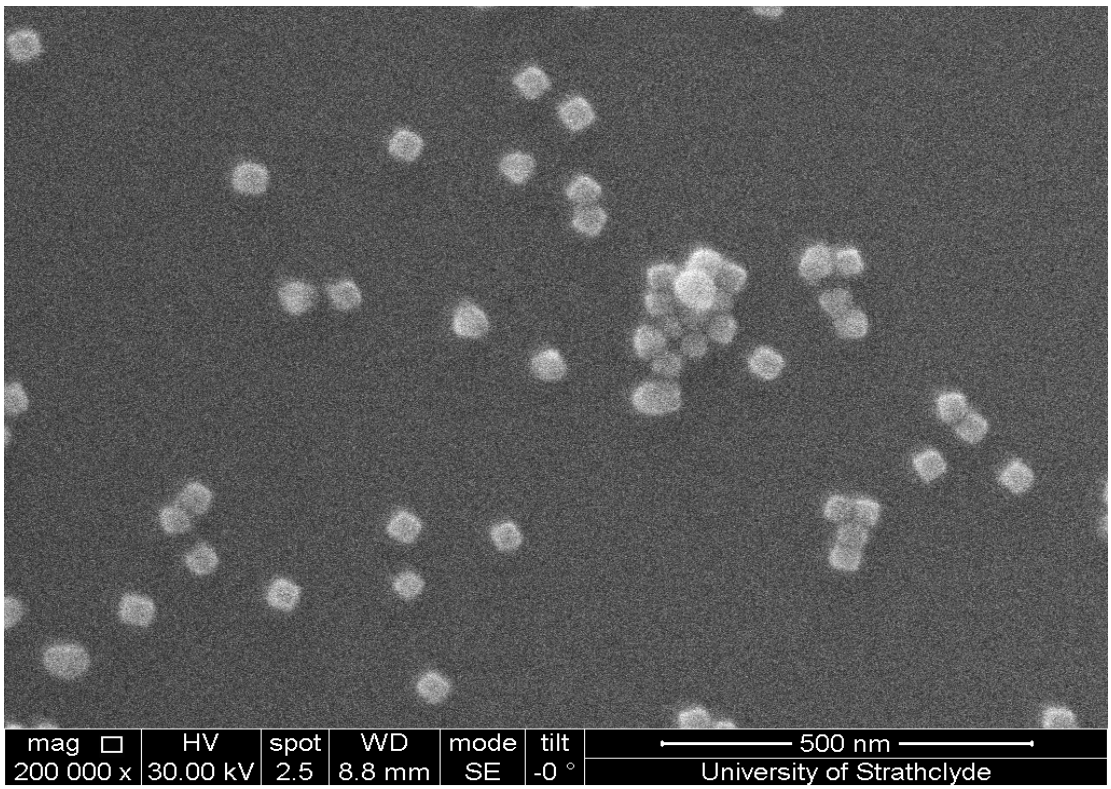

Figure 2-4: Scanning electron microscope (SEM) image of Ag nanocubes.

2.3.3. Synthesis and characterisation of gold nanocages

2.3.3.1. Synthesis of gold nanocages using standard methods

The gold nanocages were produced via a galvanic replacement reaction between the prepared Ag nanocubes and $HAuCl_4$ aqueous solution based on two protocols, following Xia and Qu groups' methods (Skrabalak *et al.*, 2007; Wang *et al.*, 2013b; Shi *et al.*, 2014). While the process and procedure were quite similar in both protocols, different concentrations of Ag nanocubes and $HAuCl_4$ solution were used. The galvanic replacement reaction process was monitored by visualising the colour changes from dark yellow to grey colour.

First, the Xia group's method was used, where the galvanic replacement was accomplished by adding 0.1 mM of $HAuCl_4$ solution to Ag nanocubes vials using a syringe pump at a rate of 10 mL/h. However, no changes in the Ag nanocubes colour were observed after adding 5 mL of $HAuCl_4$ solution. Therefore, the syringe-pumping rate was adjusted from 10 to 45 mL/h. Hence, AuNC samples with three colours were obtained by adding various volumes of $HAuCl_4$ solution (0.1 mM). The dark orange sample was observed after adding 1 mL, the purple sample after adding 2 mL, and the grey sample after adding 2.6 mL of $HAuCl_4$ solution (0.1 mM) (Figure 2-5). However, we could not isolate a sufficient amount of AuNCs from all the three samples.

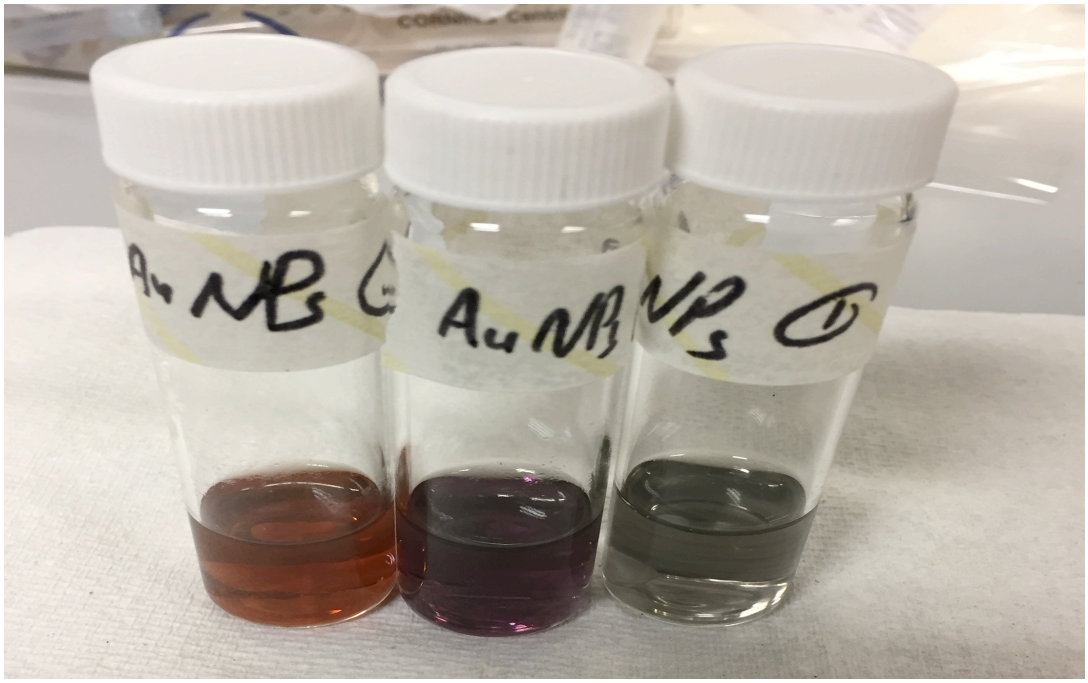

Figure 2-5: Photographs of vials containing AuNCs samples in dark orange, purple and grey colour prepared via galvanic replacement between AgNCs and $HAuCl_4$ solution (0.1 mM).

Therefore, the concentrations of AgNCs and $HAuCl_4$ solution were adjusted based on the Qu group's method. Specifically, 500 μL of as-synthesised AgNCs was dispersed in 5 mL of PVP aqueous solution (1 mg/mL) and boiled under magnetic stirring for 10 minutes. $HAuCl_4$ solution (0.5 mM) was then added with a syringe pump at a rate of 45 mL/h into 24-mL glass vials. Consequently, various colours of gold nanocage samples were obtained after adding different amounts of $HAuCl_4$ solution to each sample (Figure 2-6). However, the volume of gold nanocages isolated from each vial was around 3 mL, which was insufficient for further studies. In addition, the synthesised AuNC samples exhibited a UV-vis spectrum peak less than 700 nm. The last two AuNC samples (blue and grey) obtained from this method were selected for optical and physical characterisations. First, blue AuNCs (AuNCs-B) exhibited a UV-vis spectrum peak at 688 nm, while grey AuNCs (AuNCs-G) exhibited two UV-vis spectrum peaks at 637 and 444 nm (Figure 2-7). Further, SEM and TEM images revealed the cage shapes of both AuNCs-B and AuNCs-G (Figure 2-8). Finally, the DLS measurements showed that AuNCs-G had an average size of 43.08 ± 1.51 nm, while AuNCs-B had an average size of 42.00 ± 2.49 nm. The zeta potential of the AuNCs-G was −38.42 ± 1.60 mV, and −31.73 ± 8.80 mV for the AuNCs-B. Based on these results, gold nanocages with a blue colour were chosen for further investigation.

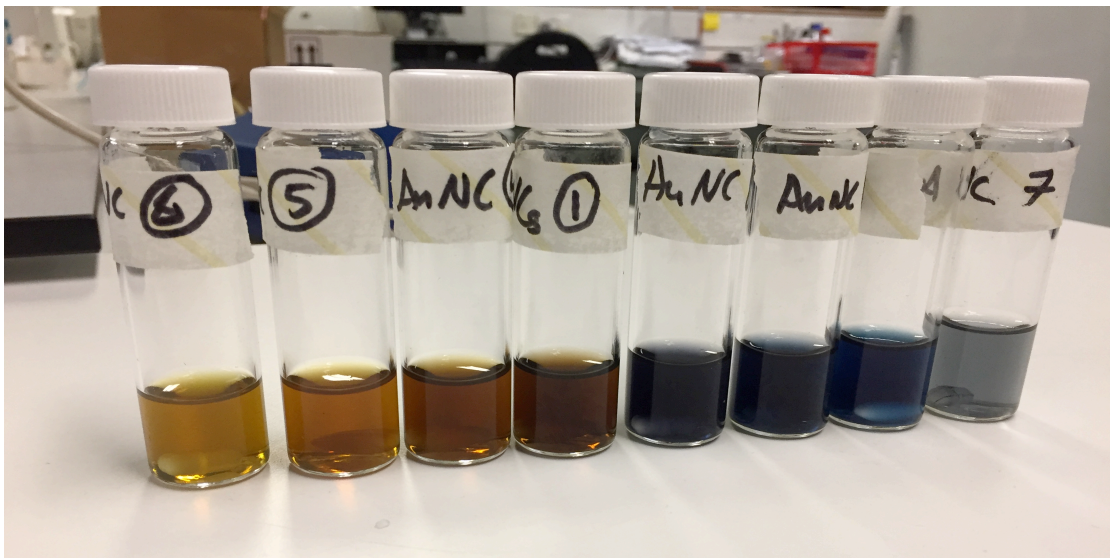

Figure 2-6: Photographs of vials containing gold nanocages showing the changes in the nanocage colour by adding different volumes of $HAuCl_4$ solution (0.5 mM) (from left to right: 0.2, 0.3, 0.4, 0.5, 0.6, 0.8, 1 and 2.5 mL).

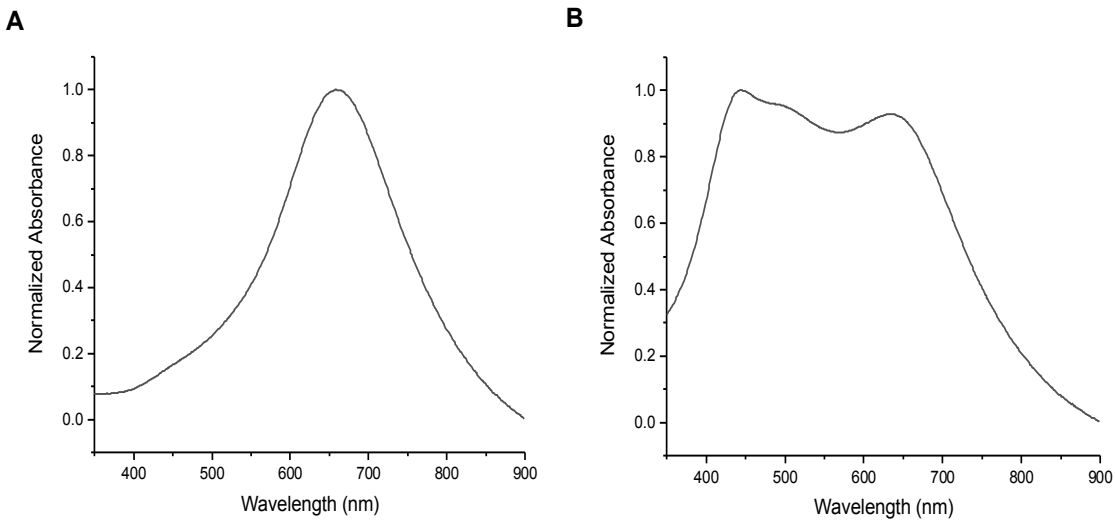

Figure 2-7: UV-vis spectra of blue AuNCs (A) and grey AuNCs (B).

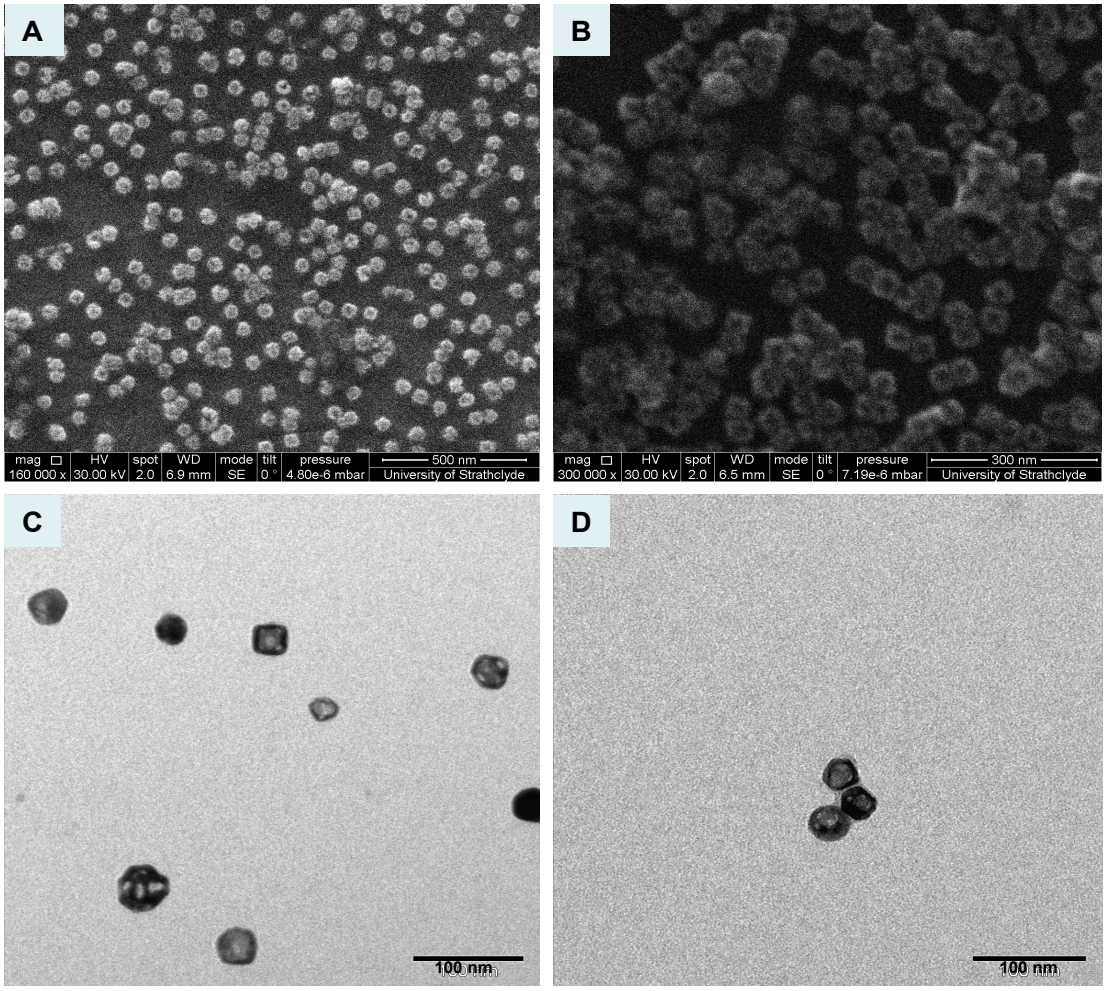

Figure 2-8: Scanning electron microscopy (SEM) images of blue AuNCs (A), grey AuNCs (B) and transmission electron microscope (TEM) images of blue AuNCs (C) and grey AuNCs (D).

2.3.3.2. Synthesis of gold nanocages using modified methods

The concentration of $HAuCl_4$ solution was further increased from 0.5 to 1 mM to scale up the synthesis process. Also, synthesising large quantities of gold nanocages required a vast amount of Ag nanocubes that necessitated the use of large glassware, such as flasks, replacing small vials. Therefore, synthesising gold nanocages using Ag nanocubes prepared in round-bottom flask and in vial was examined. Hence, two batches of AuNCs were obtained: blue gold nanocages synthesised from Ag

nanocubes prepared in a round-bottom flask (AuNCs-BF) and blue gold nanocages synthesised from Ag nanocubes prepared in a vial (AuNCs-BL) via titration with $HAuCl_4$ solution (1 mM). TEM images show the cage shapes of AuNCs-BL and AuNCs-BF (Figure 2-9). The physical characteristics showed that AuNCs-BF had an average size of 80.00 ± 0.41 nm and displayed a UV-vis spectrum peak at 671 nm like AuNCs-BL, which had an average size of 77.45 ± 0.02 nm, and a UV-vis spectrum peak of 692 nm (Figure 2-10). Therefore, preparing Ag nanocubes in a round-bottom flask was chosen for large-scale synthesis of gold nanocages.

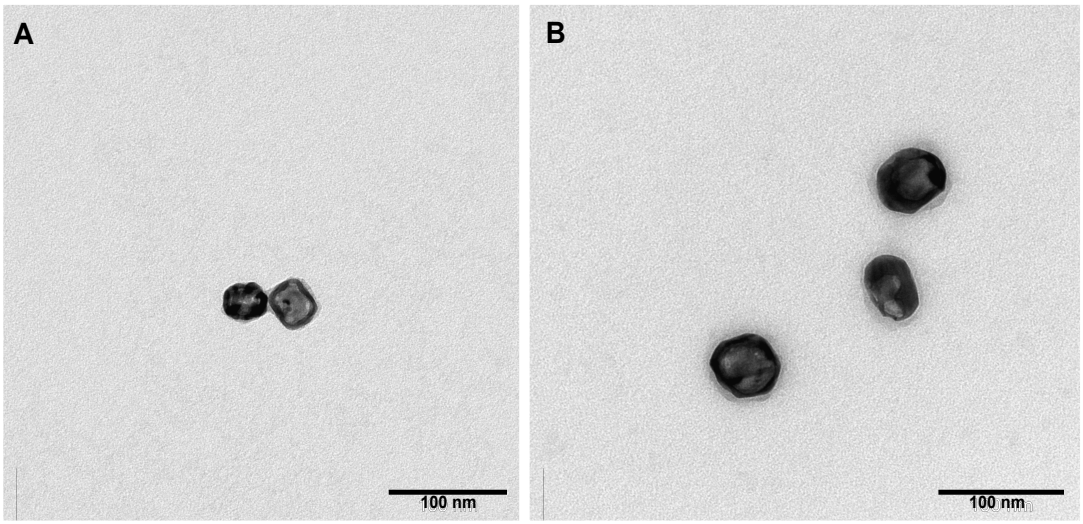

Figure 2-9: Transmission electron microscopic image of (A) blue gold nanocages synthesised from Ag nanocubes prepared in a vial and (B) blue gold nanocages synthesised from Ag nanocubes prepared in a round-bottom flask.

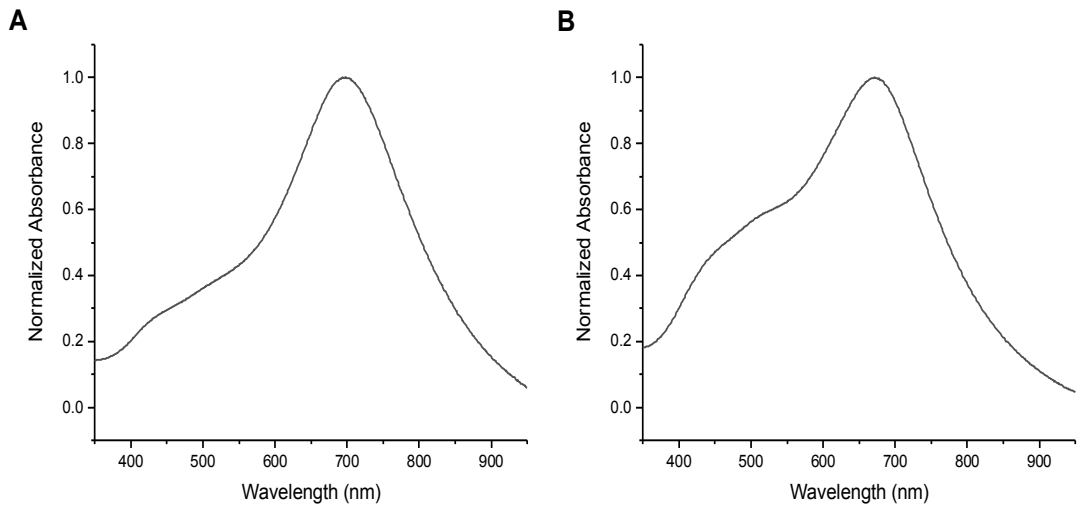

Figure 2-10: UV-vis spectra of (A) blue gold nanocages synthesised from Ag nanocubes prepared in a vial and (B) blue gold nanocages synthesised from Ag nanocubes prepared in a round-bottom flask.

2.3.3.3. Large-scale synthesis of gold nanocages

A large batch of gold nanocages (AuNCs-BR) was synthesised using a galvanic replacement reaction between Ag nanocubes prepared in 250-mL round-bottom flask and $HAuCl_4$ solution (1 mM). AuNCs-BR had a volume of 800 mL with an Au content of 597.93 μg/L based on ICP-MS analysis. TEM image confirmed the cage-shape, hollow interior and thin wall of AuNCs-BR, with an outer-edge length of 30 nm, inner-edge length of 50 nm and wall thickness of 6 nm (Figure 2-11). AuNCs-BR had an average size of 88.69 ± 0.66 nm and a UV-vis spectrum peak at 715 nm (Figure 2-12). Table 2-1 shows the optical and physical properties of the gold nanocages.

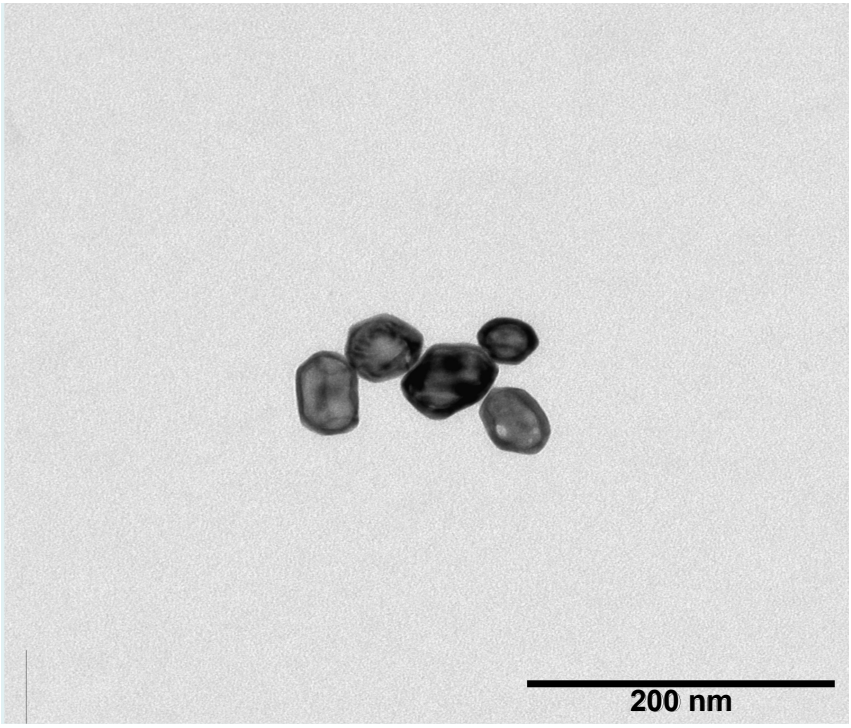

Figure 2-11: Transmission electron microscopy (TEM) image of gold nanocages (AuNCs-BR) produced by scale-up synthesis.

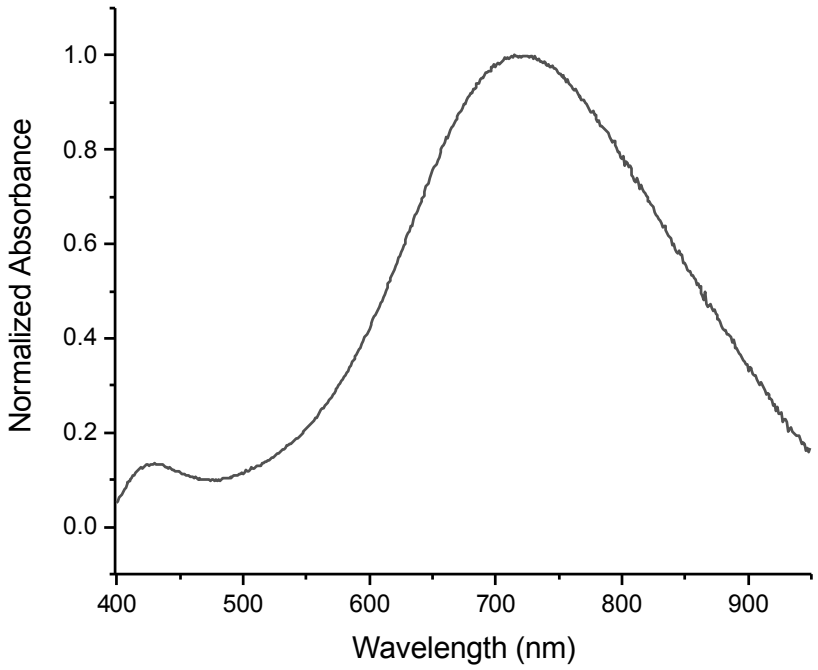

Figure 2-12: UV-vis spectrum of AuNCs produced by scale-up synthesis.

Table 2-1: Summary of the optical and physical properties of synthesised gold nanocages

Sample	Colour	Size (nm)	PDI	Zeta potential (mV)	UV-Vis wavelength (nm)
AuNCs-B	Blue	42.14 ± 2.40	0.47	−31.73 ± 8.80	688
AuNCs-G	Grey	43.08 ± 1.50	0.50	−38.42 ± 1.60	637
AuNCs-BL	Blue	77.45 ± 0.02	0.22	−25.20 ± 3.37	692
AuNCs-BF	Blue	80.00 ± 0.41	0.22	−24.70 ± 0.81	671
AuNCs-BR	Blue	88.69 ± 0.66	0.20	−20.50 ± 0.38	715

PDI = Polydispersity index

2.4. Discussion

Gold nanocages are a novel class of gold nanomaterial with cage shape, hollow interior and porous wall. Their unique optical and physicochemical properties make them appropriate candidates for nanomedicine applications. They can be synthesised by a galvanic replacement reaction between silver nanocubes and chloroauric acid solution. However, only small amounts of gold nanocages can be prepared using the method described in the standard protocol (Skrabalak *et al.*, 2007). Also, one of the key challenges that hamper the use of this type of nanomaterial in medicine is the ability to produce large quantities of nanoparticles, alongside uniform size and shape (Pang *et al.*, 2016). The purpose of this chapter, therefore, is to optimise the synthesis of gold nanocages and to develop an appropriate synthesis procedure to obtain large quantities of gold nanocages. As silver nanocubes are used as sacrificial templates for the galvanic replacement reaction to generate the gold nanocages, most of the published reports focused on scaling-up the synthesis of Ag nanocubes to achieve large quantities of gold nanocages (Sun *et al.*, 2002; Pang *et al.*, 2016). For example, Skrabalak and colleagues performed the synthesis of silver nanocubes simultaneously in 12 different vials as a suggested approach to scale up the production of the nanocubes, which induced some variations in the shape and concentration of the produced silver nanocubes, thereby affecting AuNCs synthesis (Skrabalak *et al.*, 2007). In this study, the large synthesis of silver nanocubes was conducted in a single round-bottom flask to overcome silver nanocubes batch variations from one preparation to another that could impact the AuNCs synthesis. Also, it is important to scale-up the synthesis of gold nanocages to enable us to conduct all the experiments, such as surface modifications and *in vitro* evaluation

using the same batch of gold nanocages. In this study, we considered some steps that successfully helped in scaling-up gold nanocage synthesis. For instance, the glassware was cleaned with *aqua regia* before the synthesis process to remove any trace elements that could affect the syntheses of AgNCs and AuNCs. Furthermore, the concentration of the chloroauric solution was increased from 0.1 to 1 mM to boost gold nanocage formation during the galvanic replacement reaction with a large quantity of silver nanocubes. Large synthesis of gold nanocages also required a large volume of chloroauric solution, which should be added to the reaction flask at a low flow rate (45 mL/h). However, the chloroauric acid solution is light–sensitive, which would impact the uniformity of synthesised gold nanocages regarding size and shape. To avoid this, small quantities of chloroauric acid solution (10 mL) were freshly prepared concurrently and injected into the reaction using a syringe pump in the dark, and this process was repeated until the end of the reaction. Finally, the galvanic replacement reaction was conducted in an oil bath at 100 ^{o}C instead of 90 ^{o}C as mentioned in the standard procedure, and mixed at a spin rate of 700 rpm to prevent the precipitation of AgCl during the reaction (Chen *et al.*, 2010b). Therefore, the gold nanocages obtained using our modified protocol were similar to those synthesised via the conventional method but produced in larger quantities. This large production of gold nanocages ensured the elimination of batch-to-batch variations that could significantly impact the surface conjugation, the characterisation and *in vitro* experiments because of using different gold nanocage batches (Avvakumova *et al.*, 2019). The morphology, particle size and uniformity of the gold nanocages produced by scale-up synthesis and modified protocols were confirmed by TEM and DLS analysis. TEM images revealed the cage-shape, hollow interior and thin wall of

the synthesised gold nanocages. Furthermore, the difference between the inner-and outer-edges of the nanocages length is 20 nm, which represents the uniform shape and structure of the synthesised gold nanocages. The shape and morphology produced by our modified protocol are like those synthesised by the standard protocol. The as-prepared gold nanocages had an average size lower than 90 nm and exhibited a UV-Vis spectrum in the NIR region, which made them appropriate for drug delivery applications and photothermal therapy.

Chapter 3: Synthesis and characterisation of PEG-, PEI-, PLL- and DAB- conjugated, lactoferrin-bearing gold nanocages

3.1. Introduction

Gold nanoparticles have been widely used in biomedicine due to their low toxicity, tunable size, unique physicochemical properties and ease of surface modification with targeting moieties, such as proteins, peptides and antibodies, to specifically target cancer cells (Chen *et al.*, 2007a; Sun *et al.*, 2014; Beik *et al.*, 2019). In addition to these properties, gold nanoparticles have been particularly attractive for gene delivery owing to their ability to condense nucleic acids via electrostatic interactions or by conjugating nucleic acids to their surface via thiol linkages (McIntosh *et al.*, 2001; Oishi *et al.*, 2006; Rosi *et al.*, 2006; Fitzgerald *et al.*, 2016). Among these nanoparticles, gold nanocages are a novel class of gold nanomaterial with a cage shape, hollow interior and porous wall. Furthermore, their ability to convert light into heat at the NIR region (700–900 nm) has made them suitable candidates for biomedical applications and photothermal cancer therapy (Skrabalak *et al.*, 2008; Chen *et al.*, 2010a; Xia and Xia, 2014). Their unique structure allows drugs to be loaded into their hollow interior before the nanocage is coated with a thermo-sensitive polymer (Yavuz *et al.*, 2009; Li *et al.*, 2011). The polymer shell prevents the drug from being released until an external thermal stimulus, such as NIR light or high-intensity-focused ultrasound, is presented. However, the recent advances in gold nanocage utilisation in controlled drug delivery and photothermal cancer therapy have led to the need to explore the possibility of using gold nanocages for targeted gene delivery for cancer treatment, without the assistance of external stimulation or in combination with chemotherapeutics. DNA can be attached covalently to the surface of gold nanoparticles using thiol linkage. However, external triggers, such as laser irradiation, are required to facilitate the release of the attached

DNA by breaking the strong Au-S bond or heating the nanoparticles until their melting point is reached, resulting in payload release (Jain *et al.*, 2006). Also, electrostatic charge repulsions between the negatively charged DNA and negatively charged gold nanoparticles would prevent DNA adsorption to the surface of gold nanocages (Zamora-Justo *et al.*, 2019).

Therefore, we propose to conjugate the surface of gold nanocages with targeting moieties, such as lactoferrin (Lf), for targeting cancer and to functionalise their surface with cationic polymers to promote DNA binding through electrostatics interactions. We also investigated whether the gold nanocages could condense the DNA on their surface, facilitate gene expression and enhance the anti-proliferative effect in prostate cancer cells *in vitro*. Recent research has shown that the cancer-targeting ligand lactoferrin (Lf), whose receptors are overexpressed in most cancers, is highly promising in enhancing the therapeutic efficacy of gene cancer therapy as a result of significant increase in gene expression in tumours after intravenous administration (Lim *et al.*, 2015; Altwaijry *et al.*, 2018b). Cationic polymers, such as polyethylenimine (PEI), diaminobutyric polypropylenimine (DAB) and poly-L-lysine (PLL), have been widely used to generate positively charged nanoparticles due to their capacity to complex DNA or RNA and their high transfection efficacy (Sullivan *et al.*, 2003; Aldawsari *et al.*, 2011a; Shan *et al.*, 2012; Fitzgerald *et al.*, 2016). Conjugating polyethylene glycol (PEG) to nanoparticles is another approach that has recently contributed to enhanced transfection efficacy while reducing the cytotoxicity associated with nanoparticles by shielding their charges and preventing their interaction with plasma proteins (Kong *et al.*, 2009; Ping *et al.*, 2011; Somani *et al.*, 2018).

3.1.1. Aims and objectives

The main objective of this chapter is to study the effect of surface modification of gold nanocages with Lf and cationic polymers on their physicochemical properties, such as size, surface charge and morphology, alongside their DNA condensation efficacy.

This chapter focuses on the synthesis and characterisation of gold conjugates (lactoferrin-bearing gold nanocages, PEG-conjugated, PEI-conjugated, PLL-conjugated and DAB-conjugated lactoferrin-bearing gold nanocages). Hence, the physicochemical characteristics of these gold conjugates were evaluated using transmission electron microscopy, UV-vis spectrophotometry, MALDI-TOF spectroscopy, circular dichroism and Fourier-transform infrared **(**FTIR) spectroscopy to confirm the conjugation of the Lf and polymers onto the nanocages. Also, the DNA condensation efficacy of the gold conjugates was investigated following complexation with plasmid DNA using photon correlation spectroscopy and gel retardation assay.

3.2. Materials and methods

3.2.1. Materials

Materials	Suppliers
2-iminothiolane (Traut's reagent)	Sigma-Aldrich, UK
Acetone	Sigma-Aldrich, UK
Aqueous hydrochloric acid solution (HCl, 37%)	Sigma-Aldrich, UK
Branched polyethyleneimine (PEI) (0.8 kDa)	Sigma-Aldrich, UK
Deionized (DI) water	Sigma-Aldrich, UK
Dialysis tubing, benzoylated	Sigma-Aldrich, UK
Ethylenediaminetetraacetic acid (EDTA)	Sigma-Aldrich, UK
EndoFree Plasmid Giga Kit	Qiagen, UK
Ethidium bromide	Sigma-Aldrich, UK
Generation 3- Diaminobutyric polypropylenimine hexadecaamine dendrimer (DAB)	Sigma-Aldrich, UK
Lactoferrin, bovine colostrum	Sigma-Aldrich, UK
Na_2HPO_4	Sigma-Aldrich, UK
NaH_2PO_4	Sigma-Aldrich, UK
Passive lysis buffer	Promega, UK
PCMVsport β-galactosidase plasmid DNA	Life Technologies, UK

Materials	Suppliers
Phosphate buffered saline (PBS) tablets	Sigma Aldrich, UK
PicoGreen® dsDNA reagent	Life Technologies, UK
Poly-L-lysine (PLL)	Sigma-Aldrich, UK
Sodium chloride (NaCl)	Sigma-Aldrich, UK
Thiol-PEG3.5K-amine (HS-PEG3.5K-NH2)	JenKem Technology, USA

3.2.2. Methods

3.2.2.1. Synthesis of lactoferrin-bearing gold nanocages and PEG-, PEI-, PLL- and DAB- conjugated, lactoferrin-bearing gold nanocages

The experiments in this chapter all used the large-scale batch of gold nanocages (AuNCs-BR) which was prepared as described in Chapter 2.

3.2.2.1.1. Synthesis of lactoferrin-bearing gold nanocages (AuNCs-Lf)

The conjugation of Lf to gold nanocages (AuNCs) was performed with modifications from a previously reported method (Johnsen *et al.*, 2018). Briefly, 8 mg of Lf was dissolved in 2 mL of 50 mM sodium phosphate and 0.15 M sodium chloride buffer (pH 7.5). This was then reacted with 5-fold mole excess of 2-iminothiolane (Traut's reagent, 1 mg/mL in distilled water, 7.26 mM, 61.2 µL) for 75 min at 20 ^{o}C. The modified Lf was purified using a Vivaspin-6® centrifuge tube with a molecular weight cut-off (MWCO) of 5 000 Da for 20 minutes at 8 000 rpm (14 000 g). Each 100 µL of thiolated Lf (8 mg/mL) was added to 1 mL of AuNCs, then vortexed and incubated at 25 °C for 24 hours. The final product was purified twice with 1 mL of DI water using Vivaspin-6® centrifuge tubes with a MWCO of 100 000 Da for 20 minutes at 8 000 rpm (14 000 g) to remove any unreacted AuNCs, before being freeze-dried.

3.2.2.1.2. Synthesis of lactoferrin-bearing PEGylated gold nanocages

3.2.2.1.2.1. Preparation of PEGylated gold nanocages (AuNCs-PEG)

Thiol-PEG3.5K-amine aqueous solution (100 µL, 2 mM) was added to 1 mL of AuNCs suspension and vortexed for 10 seconds before incubating the mixture at 25

°C for 48 hours. Afterwards, the samples were purified by centrifugation at 14 000 rpm (18, 300 g) for 10 minutes and washed twice with 1 mL of DI water after discarding the supernatant. The final products were dispersed in 1 mL of DI water and stored at 4 °C.

3.2.2.1.2.2. Preparation of lactoferrin-bearing PEGylated gold nanocages (AuNCs-PEG-Lf)

As-prepared thiolated Lf (8 mg/mL, 100 µL) was added to each 1 mL of AuNCs-PEG. The reaction mixture was then vortexed and incubated at 25 °C for 24 hours. The final products were purified twice with 1 mL of DI water using a Vivaspin-6® centrifuge tube with a MWCO of 100 000 Da for 20 minutes at 8 000 rpm (14 000 g) to remove any unreacted AuNCs-PEG, before being freeze-dried.

3.2.2.1.2.3. Synthesis of PEG-conjugated, lactoferrin-bearing gold nanocages (AuNCs-Lf-PEG)

Thiol-PEG3.5K-amine aqueous solution (100 µL, 2 mM) was added to 1 mL of lactoferrin-bearing AuNCs (AuNCs-Lf) suspension and vortexed for 10 seconds. The mixture was then incubated at 25 °C for 24 hours. The final product was purified twice with 1 mL of DI water using Vivaspin-6® centrifuge tubes with a MWCO of 100 000 Da for 20 minutes at 8 000 rpm (14 000 g) to remove any unreacted PEG, before being freeze-dried.

3.2.2.1.2.4. Synthesis of 2xPEG-conjugated, lactoferrin-bearing gold nanocages (AuNCs-Lf-2xPEG)

Thiol-PEG3.5K-amine aqueous solution (200 µL, 2 mM) was added to 1 mL of lactoferrin-bearing AuNCs (AuNCs-Lf) suspension and vortexed for 10 seconds. The

mixture was then incubated at 25 °C for 24 hours. The final product was purified twice with 1 mL of DI water using Vivaspin-6® centrifuge tubes with a MWCO of 100 000 Da for 20 minutes at 8 000 rpm (14 000 g) to remove any unreacted PEG, before being freeze-dried.

3.2.2.1.3. Synthesis of PEI-conjugated, lactoferrin-bearing gold nanocages (AuNCs-Lf-PEI)

3.2.2.1.3.1. Preparation of thiolated polyethyleneimine

The thiolation of polyethyleneimine (PEI) was performed with modifications of a previously reported method (Kang *et al.*, 2011). The formation of thiolated PEI was carried out by reacting the PEI with 2-fold moles excess of 2-iminothiolane (Traut's reagent). PEI was dissolved in PBS at a concentration of 10 mg/mL (12.5 mM). In a separate container, a stock solution of Traut's reagent was prepared by dissolving 3.44 mg in 1 mL of PBS. Traut's reagent (3.44 mg/mL in PBS, 25 mM, 4.28 mL) was added to PEI solution (10 mg/mL in PBS, 12.5 mM, 4.28 mL) and vortexed for 5 seconds. The reaction mixture was then incubated at 25 ^{o}C for 24 hours. The final compound was purified using benzoylated dialysis tubing with a molecular weight cut-off of 2000 Da at room temperature (20-22 ^{o}C) against 2 L of distilled water and this was changed twice during dialysis. After 24-hour dialysis, the solution was freeze-dried for 48 hours using Christ Epsilon 2–4 LSC® freeze dryer (Osterode am Harz, Germany).

3.2.2.1.3.2. Preparation of polyethyleneimine-conjugated, lactoferrin-bearing gold nanocages

Thiolated PEI (10 mg/mL in PBS, 400 μL) was added to each 1 mL of as-prepared AuNCs-Lf. The mixture was then vortexed for 5 seconds and incubated at 25 ^{o}C for 24 hours. AuNCs-Lf-PEI was then purified twice with 1 mL of DI water using a Vivaspin-6® centrifuge tube with a MWCO of 5 000 Da for 20 minutes at 8 000 rpm (14 000 g). The purified AuNCs-Lf-PEI conjugate was freeze-dried using a Christ® freeze dryer for 48 hours.

3.2.2.1.4. Synthesis of lactoferrin-bearing dendrimer-conjugated gold nanocages

3.2.2.1.4.1. Preparation of thiolated dendrimer

A thiolated dendrimer was prepared with modifications from a previously reported method (Liu and Chiu, 2013). The process of thiolation was carried out by mixing the DAB dendrimer with 2-fold moles excess of 2-iminothiolane (Traut's reagent). DAB was dissolved in PBS at a concentration of 21.08 mg/ml (12.5 mM). In a separate container, a stock solution of 2-iminothiolane (Traut's reagent) was prepared by dissolving 3.44 mg in 1 mL of PBS. Traut's reagent with 2-fold mole excess (3.44 mg/mL in PBS, 25 mM, 3.44 mL) was added to DAB solution (21.08 mg/mL in PBS, 12.5 mM, 3.44 mL) and vortexed for 5 seconds. The reaction mixture was then incubated at 25 ^{o}C for 24 hours. The final compound was purified using benzoylated dialysis tubing with a MWCO of 2000 Da at room temperature (20-22 ^{o}C) against 2 L of distilled water, changed twice during dialysis. After a 24-hour dialysis, the solution was freeze-dried using Christ® freeze dryer for 48 hours.

3.2.2.1.4.2. Preparation of lactoferrin-bearing dendrimer-conjugated gold nanocages

Thiolated-DAB (7.26 mg/mL in PBS, 240 μL) was added to each 1 mL of as-prepared AuNCs-Lf or bare AuNCs, vortexed for 5 seconds then incubated at 25 ^{o}C for 24 hours. AuNCs-Lf-DAB and AuNCs-DAB were then purified twice with 1 mL of DI water using a Vivaspin-6® centrifuge tube with a MWCO of 5 000 Da for 20 minutes at 8 000 rpm (14 000 g). Lactoferrin was then added to AuNCs-DAB to prepare AuNCs-DAB-Lf conjugates using the same method as for making AuNCs-Lf described above. The purified AuNCs-DAB-Lf conjugate was freeze-dried using Christ® freeze dryer for 48 hours.

3.2.2.1.5. Synthesis of lactoferrin-bearing, polylysine-conjugated gold nanocages

3.2.2.1.5.1. Preparation of thiolated polylysine

The thiolation of polylysine was achieved by reacting the polylysine with 2-fold moles excess of 2-iminothiolane (Traut's reagent). To do so, Traut's reagent (1.1 mg/mL in PBS, 8 mM, 125 μL) was added to PLL solution (14.3 mg dissolved in 2 mL PBS, 0.5 mM) and vortexed for 5 seconds. The reaction mixture was then incubated at 25 ^{o}C for 24 hours. The modified PLL was purified using a Vivaspin-6® centrifuge tube with a molecular weight cut-off (MWCO) of 5 000 Da for 20 minutes at 8 000 rpm (14 000 g). After 24-hour dialysis, the solution was freeze-dried using Christ® freeze dryer for 48 hours.

3.2.2.1.5.2. Preparation of lactoferrin-bearing, polylysine-conjugated gold nanocages

Thiolated-PLL (8 mg/mL in PBS, 100 µL) was added to each 1 mL of as-prepared AuNCs-Lf or bare AuNCs and vortexed for 5 seconds, then incubated at 25 ^{o}C for 24 hours. AuNCs-Lf-PLL and AuNCs-PLL were then purified twice with 1 mL of DI water using a Vivaspin-6® centrifuge tube with a MWCO of 5 000 Da for 20 minutes at 8 000 rpm (14 000 g). Lactoferrin was then added to AuNCs-PLL to prepare AuNCs-PLL-Lf conjugates, using the same method as for making AuNCs-Lf described above. The purified AuNCs-PLL-Lf conjugate was freeze- dried using Christ® freeze dryer for 48 hours.

3.2.2.2. Characterisation of gold nanocages conjugates

3.2.2.2.1. Transmission electron microscopy imaging

The morphology of gold nanocages was examined using transmission electron microscopy (TEM). Typically, 20 µL of AuNCs samples in DI water were placed in carbon-coated 200-mesh copper grids and left to dry at 20 °C for 1 hour. The samples were then visualized using a JEOL JEM-1200EX® transmission electron microscope (Jeol, Tokyo, Japan) operating at an accelerating voltage of 80 kV.

3.2.2.2.2. Size and zeta potential measurement

The size and zeta potential of gold nanocages in DI water were measured by photon correlation spectroscopy and laser Doppler electrophoresis using a Malvern Zetasizer Nano-ZS® (Malvern Instruments, Malvern, UK) at 25 °C. All size and zeta-potential measurements were conducted in triplicate with a He–Ne laser operating at 632.8 nm and with a scattering angle of 173°.

3.2.2.2.3. UV-Vis- spectrometry analysis

All UV–Vis spectra were determined using a Varian Cary® 50 Bio UV-visible spectrophotometer in the wavelength range of 300–1000 nm. The UV-Vis spectrum of DI water was adjusted as a baseline prior to the measurement of the samples.

3.2.2.2.4. Quantification of gold nanocages

The concentrations of gold nanocages samples were obtained by using inductively coupled plasma mass spectrometry (ICP-MS). In summary, 20 µL of AuNCs in DI water was digested in 180 µL *aqua regia* at 20 °C for 1 hour. The mixture was further diluted with DI water to a final *aqua regia* concentration of 2% v/v. The Au concentration (in µg/L) in the samples was measured using the ^{197}Au isotope, and the ^{175}Lu isotope was used as an internal standard for all measurements. All ICP-MS measurements were performed in triplicate using an Agilent® 7700X instrument (Agilent technologies, Santa Clara, US).

3.2.2.2.5. Circular dichroism spectrometer

CD spectra of Lf-bearing AuNCs and PEG-AuNCs samples were recorded using circular dichroism spectrometer (Chirascan® V100, Applied Photophysics, Leatherhead, UK). All samples were prepared at a concentration of 2 mg/mL in DI water. CD spectra were recorded using a quartz cuvette with a path length of 10 mm over a range of 190-900 nm with a scan speed of 70 nm/min and a bandwidth of 1 nm.

3.2.2.2.6. Fourier-transform infrared spectrophotometer

The infrared spectra of Lf-bearing AuNCs and PEG-AuNCs were carried out using a FTIR spectrophotometer equipped with an attenuated total reflectance (ATR) probe

(IRSpirit® QATR-S, Shimadzu, Kyoto, Japan). They were collected over a range of 4000–400 cm^{-1} at a resolution of 4 cm^{-1} and analysed using the LabSolutions IR® software (Shimadzu, Kyoto, Japan).

3.2.2.2.7. Matrix assisted laser desorption/ionisation-time of flight mass spectroscopy (MALDI-TOF)

The molecular weights of Lf-bearing AuNCs and PEG-AuNCs were measured using MALDI-TOF mass spectrometry (Axima® CFR, Kratos, Shimadzu, Kyoto, Japan). The samples were prepared by mixing 10 µL of Lf-bearing AuNCs (2mg/mL, dissolved in DI water) with 10 µL of matrix solution (sinapinic acid). One µL of this mixture was then transferred to the MALDI sample plate and left to dry before the measurement.

3.2.2.3. Complexation of DNA with gold nanocages conjugates

3.2.2.3.1. Gel retardation assay

The ability of AuNCs conjugates to condense DNA was assessed by agarose gel retardation assay. AuNCs conjugate complexes were prepared at various AuNCs conjugate:DNA weight ratios from 0.5:1 to 40:1, with a constant DNA concentration of 20 µg/mL. After mixing with the loading buffer, the samples (15 µL) were loaded on to a 1X Tris-Borate-EDTA (TBE) (89 mM Tris base, 89 mM boric acid, 2 mM Na_2-EDTA, pH 8.3) buffered 0.8% (w/v) agarose gel containing ethidium bromide (0.4 µg/mL), with 1x TBE as a running buffer. The DNA size marker was HyperLadder I. The gel was run at 50 V for 1 hour and then photographed under UV light.

3.2.2.3.2. Size and zeta potential of the complexes

The size and zeta potential of the complexes in glucose solution (5% w/v) were measured for various AuNCs conjugates:DNA weight ratios of 0.5:1, 1:1, 5:1, 10:1, 20:1 and 40:1, by photon correlation spectroscopy and laser Doppler electrophoresis at 37 °C, using a Malvern Zetasizer Nano-ZS® (Malvern Instruments, Malvern, UK). The DNA concentration (1 μg/mL) remained constant throughout the experiment.

3.3. Results

3.3.1. Synthesis of lactoferrin-bearing gold nanocages and PEG-, PEI-, PLL- and DAB- conjugated, lactoferrin-bearing gold nanocages

3.3.1.1. Transmission electron microscopy imaging

TEM imaging revealed the cage-shape, hollow interior and thin wall of the lactoferrin-bearing gold nanocages, PEGylated gold nanocages and lactoferrin-bearing, PEGylated gold nanocages (Figure 3-1 A–D). These findings indicated that the surface conjugation did not change the shape or impact the morphology of the nanocages.

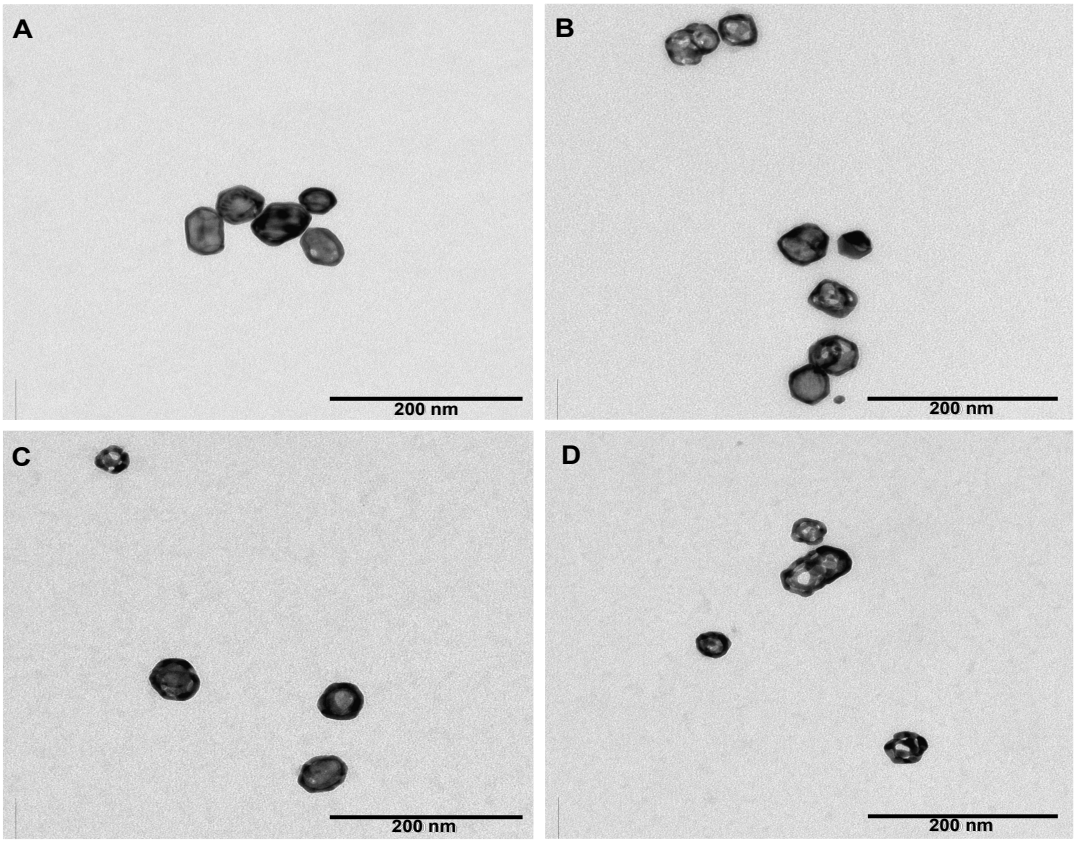

Figure 3-1: Transmission electron microscopic images of gold nanocages (A), lactoferrin-bearing gold nanocages (B), PEGylated gold nanocages (C) and lactoferrin-bearing, PEGylated gold nanocages (D) (Bar size: 200 nm).

3.3.1.2. Circular dichroism spectrometer

Conjugating Lf to AuNCs was confirmed using CD (Figure 3-2). The CD spectrum of Lf exhibited distinctive negative ellipticity peaks at 244 nm and 283 nm and a positive ellipticity peak at 309 nm. These peaks were visible in the CD spectrum of AuNCs-Lf, unlike that of unmodified AuNCs, indicating that Lf was successfully conjugated to the surface of AuNCs. The highest molar ellipticity values for the lactoferrin protein and conjugates at identical wavelengths, such as 244 nm and 283 nm, indicated that there was no significant conformational change in the protein folding upon grafting to the nanocages.

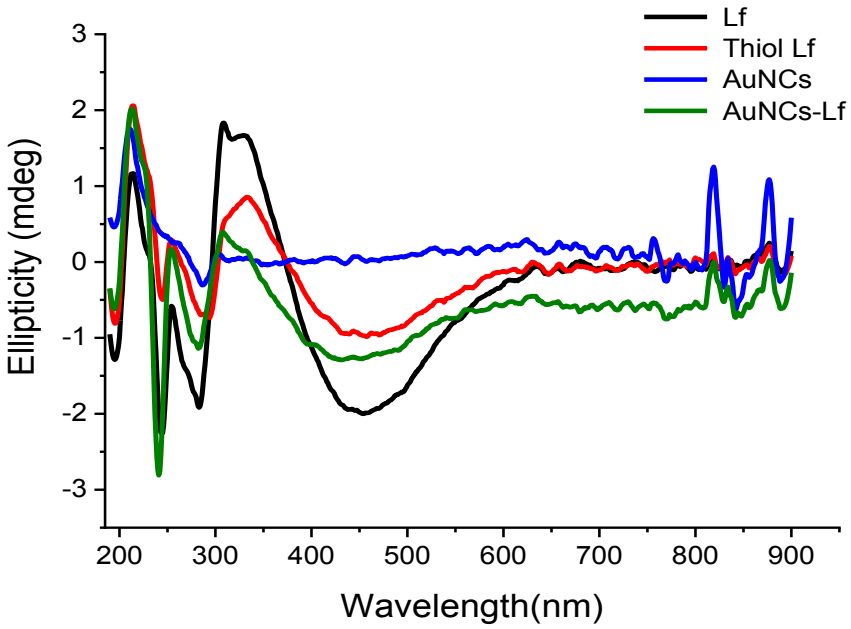

Figure 3-2: CD spectra of lactoferrin (Lf), thiolated lactoferrin (Thiol Lf), non-conjugated gold nanocages (AuNCs) and lactoferrin-bearing gold nanocages (AuNCs-Lf).

3.3.1.3. Fourier-transform infrared spectrophotometry

The FTIR spectrum of AuNCs-Lf demonstrated the presence of characteristic peaks at 1645.01 and 1534.86 cm^{-1} (corresponding to amide-I and amide-II of bare lactoferrin) and the absence of peaks at 1049.94 cm^{-1} and 1398.97 cm^{-1}, respectively, corresponding to the sulfoxide and sulphate groups of thiolated lactoferrin, compared with the starting materials (Figure 3-3). These findings confirm the successful conjugation of Lf to gold nanocages via an Au-S bond and demonstrate the absence of significant changes in the protein secondary structure. This was consistent with the data obtained from the CD.

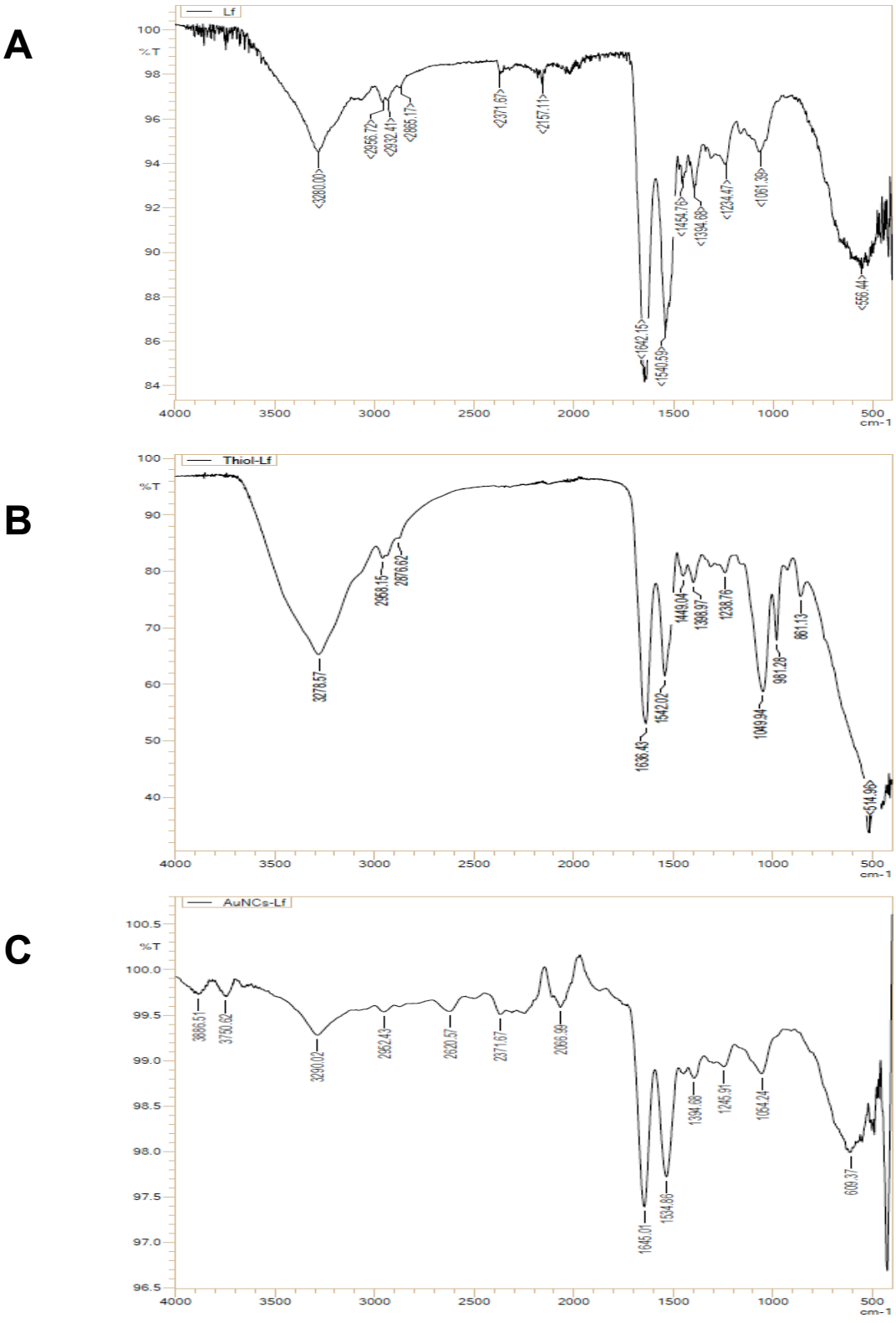

Figure 3-3: FTIR spectra of A) Lf, B) Thiol-Lf and C) AuNCs-Lf.

3.3.1.4. MALDI-TOF spectroscopy

The conjugation of Lf to AuNCs and AuNCs-PEG was assessed using MALDI-TOF spectroscopy (Figure 3-4). The average molecular weights of AuNCs-Lf and AuNCs-PEG-LF were 83797.04 and 83911.91 *m/z*, respectively. However, the bare Lf had an average molecular weight of 83499.79 *m/z*. Therefore, this difference between the AuNCs-Lf samples and bare Lf supports the conjugation of Lf protein onto AuNCs or AuNCs-PEG, while indicating that the conjugation ratio of Lf per AuNCs or AuNCs-PEG was nearly 1.

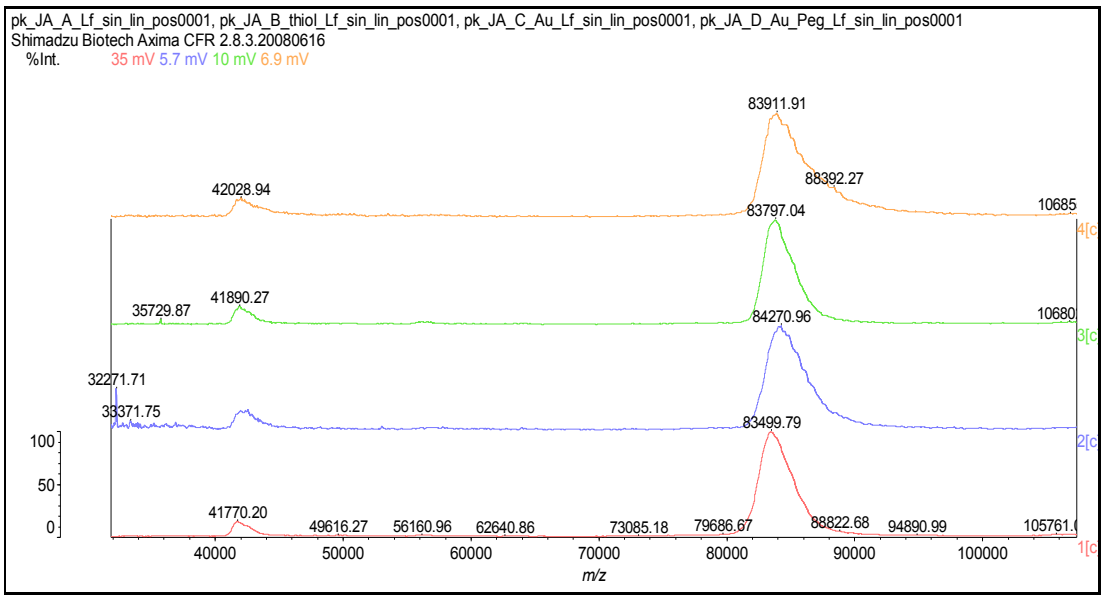

Figure 3-4: MALDI-TOF spectra of Lf (red), Thiol-Lf (blue), AuNC-Lf (green) and AuNC-PEG-Lf (orange).

3.3.1.5. UV-Vis spectrometry

The conjugation of Lf to the surface of AuNCs was further confirmed by UV-Vis-spectrometry analysis (Figure 3-5). AuNCs and AuNCs conjugates exhibited UV-vis spectrum peaks in the NIR regions (715 nm, 750 nm, 745 nm, 813 nm, 746 nm, 757 nm, 768 nm, 771 nm and 757 nm respectively for AuNCs, AuNCs-PEG, AuNCs-DAB-Lf, AuNCs-Lf-PEI, AuNCs-Lf-PLL, AuNCs-DAB, AuNCs-Lf-PEG, AuNCs-Lf and AuNCs-PEG-Lf). The red-shift in the UV-vis spectra of AuNCs-PEG, AuNCs-DAB and AuNCs-Lf compared to the unmodified AuNCs confirmed the surface modification of AuNCs with PEG, DAB and Lf. Further, it indicated the efficient formation of AuNCs conjugates.

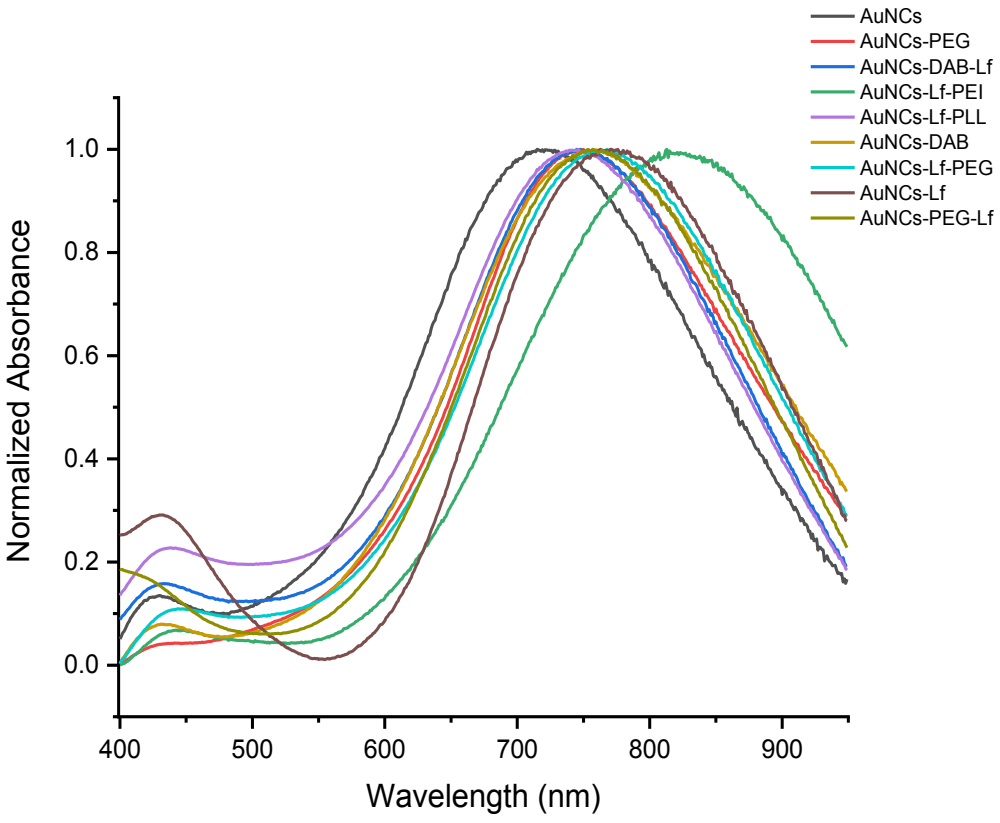

Figure 3-5: UV-vis spectra of AuNCs, AuNCs-PEG and AuNCs-DAB before and after conjugation with Lf.

3.3.1.6. Size and zeta potential measurements

The size and zeta potential of the unmodified AuNCs and AuNCs conjugates were measured to assess the formation of AuNCs conjugates. The conjugation of Lf, PEG, PEI, PLL and DAB onto the surface of the AuNCs induced a slight increase in the hydrodynamic size of AuNCs-Lf (105.40 ± 0.43 nm), AuNCs-PEG-Lf (89.31 ± 2.16 nm), AuNCs-Lf-PEG (103.30 ± 1.31 nm), AuNCs-Lf-2xPEG (142.70 ± 0.92 nm), AuNCs-PLL-Lf (120.40 ± 1.30 nm), AuNCs-Lf-PLL (118.80 ± 0.69 nm), AuNCs-Lf-PEI (127 ± 1.62 nm) and AuNCs-DAB-Lf (92.65 ± 0.57 nm) compared to that of AuNCs (88.69 ± 0.66 nm), as determined by DLS measurements (Table 3-1).

Zeta potential measurements revealed a change in AuNCs surface charge upon conjugation with Lf, PEG, PLL and DAB. The net surface charge of AuNCs changed from a highly negative potential (−20.50 ± 0.38 mV) for unmodified AuNCs, to slightly negative potentials (−8.04 ± 2.56 mV and −12.50 ± 0.16 mV) for AuNCs-PEG-Lf and AuNCs-Lf-2xPEG, and to positive potentials (3.05 ± 0.18 mV, 4.11 ± 0.38 mV, 14.10 ± 0.14 mV, 17 ± 0.45 mV, 6.39 ± 0.11 mV and 13.80 ± 0.18 mV) for AuNCs-Lf, AuNCs-Lf-PEG, AuNCs-Lf-PEI, AuNCs-Lf-PLL, AuNCs-PLL-Lf and AuNCs-DAB-Lf, respectively (Table 3-1).

Table 3-1: Size and zeta potential characterisation of various gold nanocage formulations

Formulation	Size (nm)	Zeta potential (mV)	Polydispersity index
AuNCs	88.69 ± 0.66	−20.50 ± 0.38	0.204
AuNCs-Lf	105.40 ± 0.43	3.05 ± 0.18	0.233
AuNCs-Lf-PEG	103.30 ± 1.31	4.11± 0.38	0.220
AuNCs-Lf-2xPEG	142.70 ± 0.92	−12.50 ± 0.16	0.373
AuNCs-Lf-PEI	127 ± 1.62	14.10 ± 0.14	0.309
AuNCs-Lf-PLL	118.80 ± 0.69	17 ± 0.45	0.221
AuNCs-PLL-Lf	120.40 ± 1.30	6.39 ± 0.11	0.228
AuNCs-PEG-Lf	89.31 ± 2.16	−8.04 ± 2.56	0.231
AuNCs-PEG	104.80 ± 0.44	24.30 ± 0.52	0.225
AuNCs-DAB-Lf	92.65 ± 0.57	13.80 ± 0.18	0.261
AuNCs-DAB	112.90 ± 2.45	25 ± 0.52	0.266

3.3.2. Characterisation of the formation of AuNCs-Lf-DNA complex

3.3.2.1. Size and zeta potential

3.3.2.1.1. AuNCs-Lf

AuNCs-Lf complexed with DNA displayed an average hydrodynamic size lower than 250 nm at AuNCs-Lf:DNA weight ratios exceeding 1:1 (Figure 3-6). The average size of AuNCs-Lf complexes decreased with increasing weight ratios (from 0.5:1 to 5:1), and then reached a plateau at a 10:1 weight ratio. At a weight ratio of 0.5:1, AuNCs-Lf exhibited the largest complex size of 464 ± 37.37 nm. However, AuNCs-Lf displayed a smaller complex size at a AuNCs-Lf:DNA weight ratio of 40:1, with an average size of 155.60 ± 1.94 nm, compared with the complex size at a weight ratio of 0.5:1. Zeta potential experiments demonstrated that the AuNCs-Lf complex had a slightly negative surface charge of −5.84 ± 0.53 mV at a AuNCs-Lf:DNA weight ratio of 0.5:1, indicating that the negatively charged DNA was not fully complexed with AuNCs-Lf at this ratio. The zeta potential then increased as the weight ratios of the AuNCs-Lf complexes increased to reach the final maximum positive charge of 19.90 ± 0.45 mV at a AuNCs-Lf:DNA weight ratio of 40:1 (Figure 3-6).

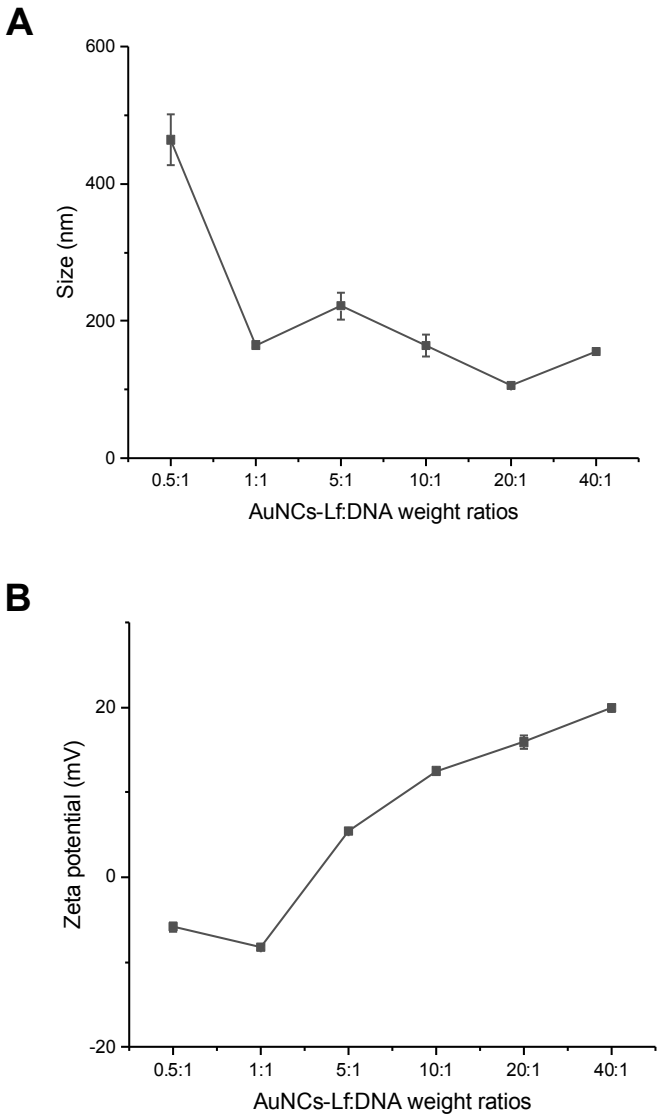

Figure 3-6: Size (A) and zeta potential (B) for AuNCs-Lf complexed with DNA at various AuNCs-Lf:DNA weight ratios. Results are expressed as mean ± SEM (*n = 9*) (error bars smaller than symbols when not visible).

3.3.2.1.2. AuNCs-PEG-Lf and AuNCs-Lf-PEG

To investigate the effect of the PEG and Lf conjugation procedures on the DNA condensation efficacy of gold conjugates, the size and zeta potential of AuNCs-PEG-Lf (in which the nanocages were conjugated to PEG first, then to Lf) and AuNCs-Lf-

PEG (in which the nanocages were conjugated to Lf first, then to PEG) complexes were examined. Both AuNCs-PEG-Lf and AuNCs-Lf-PEG displayed complex sizes less than 250 nm at conjugate:DNA weight ratios higher than 1:1 (Figure 3-7). Like AuNCs-Lf, the average size of AuNCs-PEG-Lf and AuNCs-Lf-PEG complexes decreased as the weight ratios increased from 0.5:1 to 5:1, before reaching a plateau from a 10:1 weight ratio onwards. At a weight ratio of 0.5:1, AuNCs-PEG-Lf showed a smaller complex size of 270.70 ± 37.43 nm compared to AuNCs-Lf-PEG with a complex size of 520.80 ± 28.48 nm at the same ratio. Similarly, the AuNCs-PEG-Lf complex at a weight ratio of 40:1 had a smaller size of 128 ± 2.44 nm compared with the AuNCs-Lf-PEG complex size of 153 ± 2.38 nm at the same ratio. Zeta potential measurements showed that both AuNCs-PEG-Lf and AuNCs-Lf-PEG complexes had a slight negative charge at a weight ratio of 0.5:1 with zeta potential values of −8.22 ± 0.69 and −7.53 ± 0.60 mV for AuNCs-PEG-Lf and AuNCs-Lf-PEG, respectively. The zeta potential values then increased as the weight ratios of the complexes increased, reaching the highest positive charges of 31.30 ± 0.24 mV and 26.70 ± 0.37 mV for AuNCs-PEG-Lf and AuNCs-Lf-PEG at a weight ratio of 40:1 (Figure 3-7). Hence, AuNCs-PEG-Lf and AuNCs-Lf-PEG had similar DNA complexation efficacy, indicating that the PEGylation procedure of AuNCs-Lf did not affect DNA condensation efficacy.

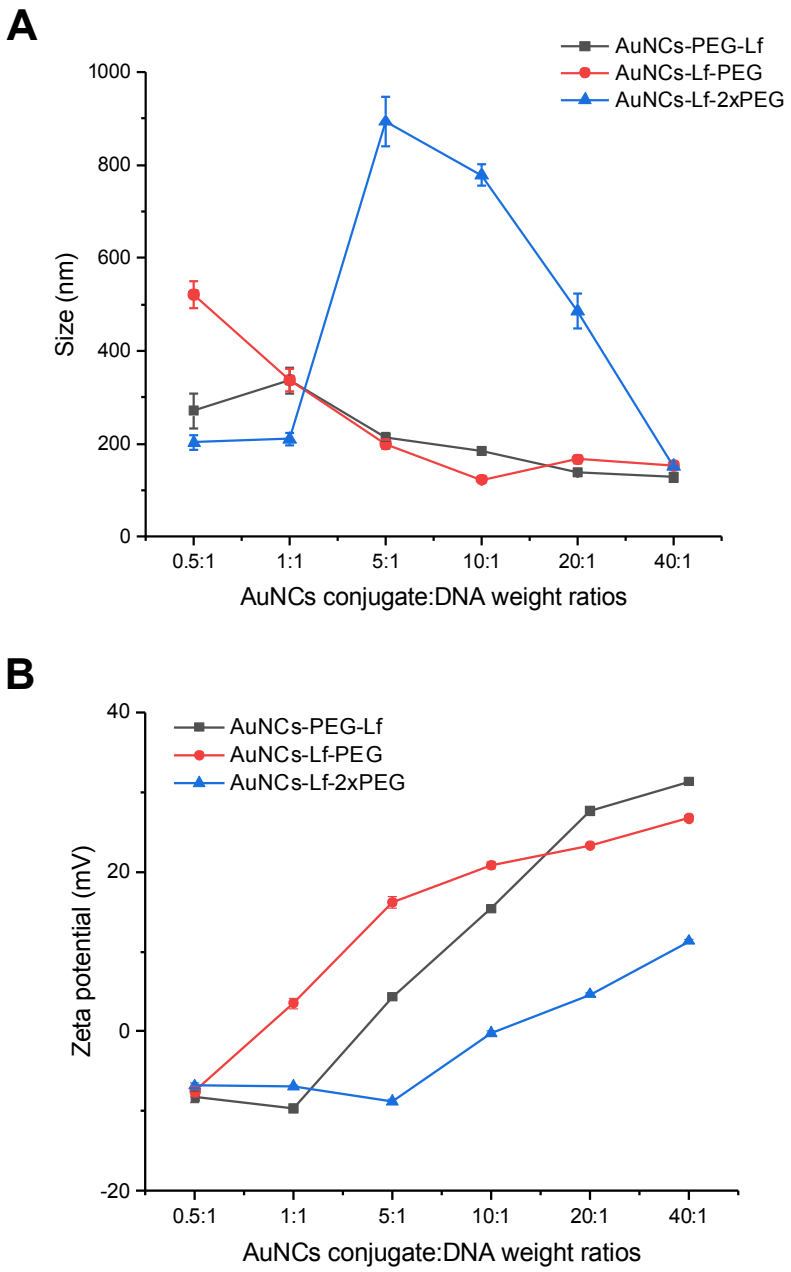

Figure 3-7: Size (A) and zeta potential (B) of gold conjugates complexed with DNA at various AuNCs conjugate:DNA weight ratios. Results are expressed as mean ± SEM (*n* = *9*) (error bars smaller than symbols when not visible).

3.3.2.1.3. AuNCs-Lf-2xPEG

To investigate whether the increase in PEG concentration would enhance the DNA condensation efficacy, AuNCs-Lf-2xPEG complex size and zeta potential were examined (Figure 3-7). Unlike AuNCs-Lf-PEG, AuNCs-Lf-2xPEG displayed a large complex size of 892.7 ± 53.30 nm at a weight ratio of 5:1. However, the AuNCs-Lf-2xPEG complex size decreased as the weight ratio increased to 150.90 ± 2.60 nm at a weight ratio of 40:1. The zeta potential values of AuNCs-Lf-2xPEG complexes had a negative charge starting from weight ratios of 0.5:1 to 10:1. Conversely, the AuNCs-Lf-PEG complex had a negative charge at a weight ratio of 0.5:1 only. AuNCs-Lf-2xPEG showed positive zeta potential values of 4.63 ± 0.17 mV and 11.30 ± 0.2 6 mV at weight ratios of 20:1 and 40:1, respectively (Figure 3-7). Thus, AuNCs-Lf-2xPEG had lower DNA complexation efficacy compared to AuNCs-Lf-PEG and AuNCs-PEG-Lf. These findings indicate that the increase in PEG concentration did not lead to an enhancement of DNA condensation efficacy.

3.3.2.1.4. AuNCs-PLL-Lf and AuNCs-Lf-PLL

AuNCs-PLL-Lf and AuNCs-Lf-PLL complexes displayed an average size of less than 300 nm at all conjugate:DNA weight ratios used for AuNCs-PLL-Lf and at weight ratios exceeding 1:1 for AuNCs-Lf-PLL (Figure 3-8). The average size of AuNCs-PLL-Lf and AuNCs-Lf-PLL complexes decreased with an increase in the weight ratio from 0.5:1 to 5:1, before reaching a plateau from a 10:1 weight ratio onwards. At a weight ratio of 0.5:1, AuNCs-Lf-PLL complex size was the largest, with an average size of 551.60 ± 40.40 nm compared to the AuNCs-PLL-Lf complex with an average size of 205.50 ± 15.14 nm at the same ratio. However, AuNCs-Lf-

PLL complex had the smallest size at a weight ratio of 40:1, with an average size of 159.90 ± 6.68 nm, compared to the AuNCs-PLL-Lf complex with an average size of 208.80 ± 12.41 nm at the same ratio. Zeta potential measurements demonstrated that the AuNCs-Lf-PLL complex had a positive surface charge at all weight ratios tested, while the AuNCs-PLL-Lf complex had a negative surface charge at all weight ratios used (Figure 3-8). The AuNCs-Lf-PLL complex displayed a positive charge of 10.60 ± 1.21 mV at a weight ratio of 0.5:1; thus, the zeta potential increased as the weight ratios of the complex increased. It reached a final maximum positive charge of 46.40 ± 0.66 mV at a weight ratio of 40:1. Moreover, the AuNCs-PLL-Lf complex showed almost steady negative charges from a weight ratio of 0.5:1 to 40:1, with a zeta potential value of −11.60 ± 0.45 mV and −9.87 ± 0.28 mV, respectively. This indicates that the negatively charged DNA was not fully complexed by AuNCs-PLL-Lf at all ratios used. Hence, AuNCs-Lf-PLL had a higher tendency to complex DNA than AuNCs-PLL-Lf. These findings showed that the surface modification of AuNCs with Lf first, followed by PLL, would generate AuNCs conjugate with improved DNA condensation efficacy.

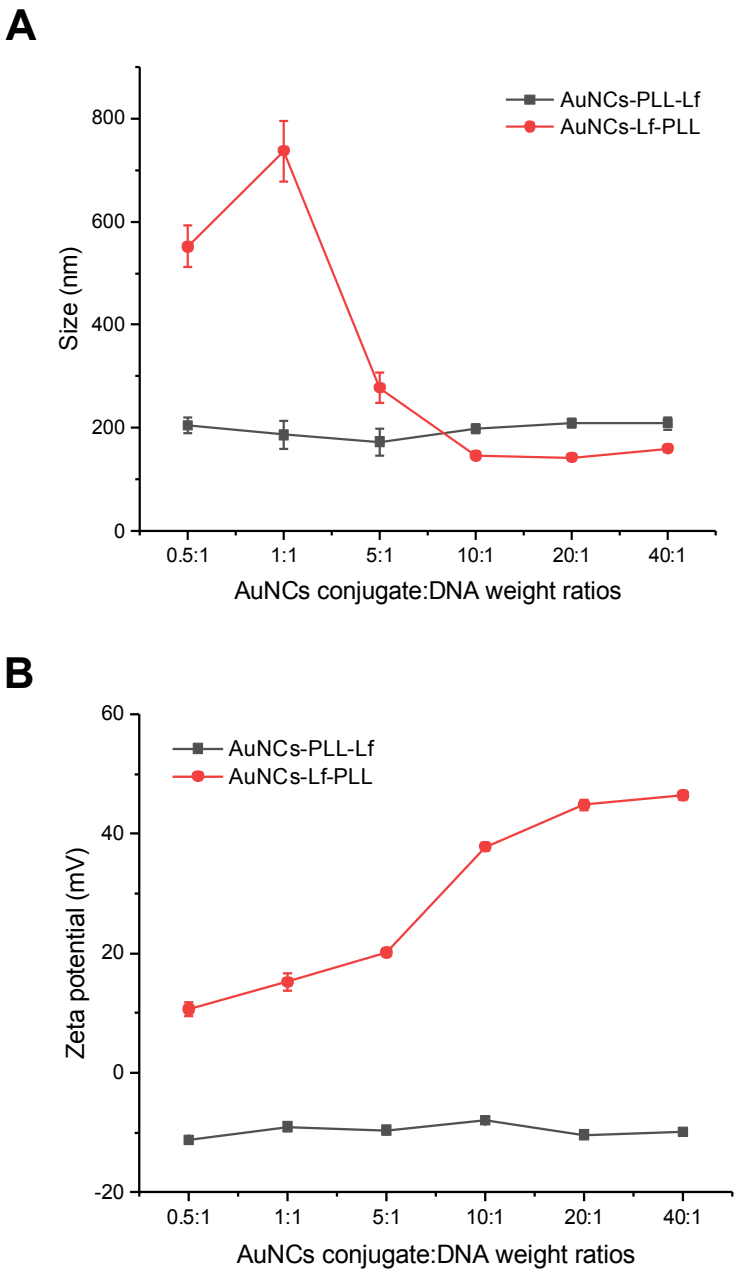

Figure 3-8: Size (A) and zeta potential (B) of gold conjugates complexed with DNA at various AuNCs conjugate:DNA weight ratios. Results are expressed as mean ± SEM (*n* = *9*) (error bars smaller than symbols when not visible).

3.3.2.1.5. AuNCs-Lf-PEI

AuNCs-Lf-PEI complexed with DNA displayed an average hydrodynamic size lower than 250 nm at conjugate:DNA weight ratios higher than 5:1 (Figure 3-9). The average size of the AuNCs-Lf-PEI complexes decreased with increased weight ratios from 0.5:1 to 5:1, before reaching a plateau from a 10:1 weight ratio onwards. At a weight ratio of 0.5:1, AuNCs-Lf-PEI exhibited the largest complex size of 1 503 ± 207 nm. Conversely, AuNCs-Lf-PEI displayed the smallest complex size at a conjugate:DNA weight ratio of 40:1, with an average size of 144.30 ± 6.27 nm. Zeta potential experiments demonstrated that the AuNCs-Lf-PEI complexes had a slightly negative surface charge of −2.17 ± 0.89 mV at an AuNCs-Lf-PEI:DNA weight ratio of 0.5:1, indicating that the negatively charged DNA was not fully complexed with AuNCs conjugates at this ratio. The zeta potential then increased as the weight ratios of the complexes increased to reach a final maximum positive charge of 28.70 ± 0.38 mV at a weight ratio of 40:1 (Figure 3-9).

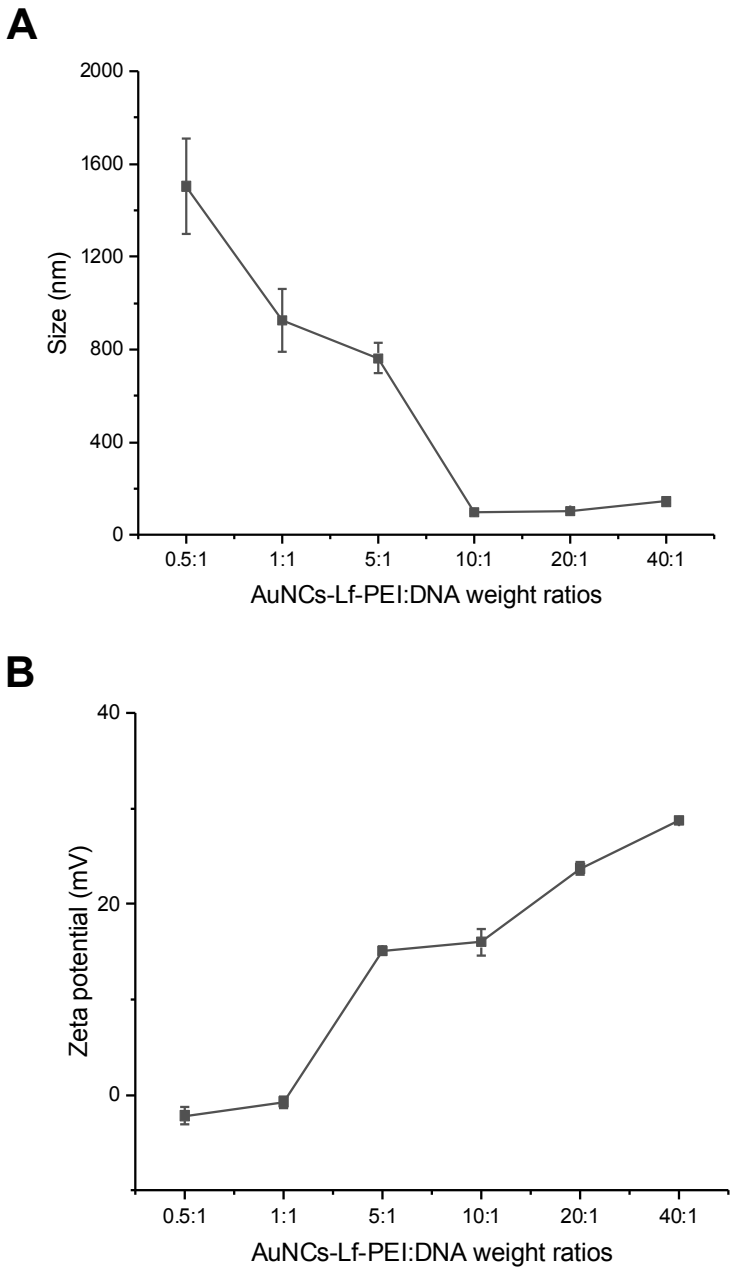

Figure 3-9: Size (A) and zeta potential (B) for AuNCs-Lf-PEI complexed with DNA at various AuNCs-Lf-PEI:DNA weight ratios. Results are expressed as mean ± SEM (*n = 9*) (error bars smaller than symbols when not visible).

3.3.2.1.6. AuNCs-DAB-Lf

AuNCs-DAB-Lf complexed with DNA had an average size lower than 160 nm at all AuNCs-DAB-Lf:DNA weight ratios used (Figure 3-10). The average size of the complexes decreased with an increase in the weight ratios, from 1:1 to 5:1, before reaching a plateau at a weight ratio of 10:1 onwards. AuNCs-DAB-Lf exhibited the largest complex size at a weight ratio of 1:1, with an average size of 152 ± 8.24 nm and showed the smallest size at weight ratio at 5:1 with a complex size of 95.11 ± 4.78 nm. Zeta potential experiments demonstrated that AuNCs-DAB-Lf complexes had a negative surface charge of −9.28 ± 0.72 mV at the minimum weight ratio 0.5:1, indicating that the negatively charged DNA was not yet complexed with AuNCs-DAB-Lf at this ratio. The values of zeta potential were then increased as the weight ratios of the complexes increased to reach final positive charges of 26.80 ± 1.18 mV at the maximum weight ratio of 40:1 (Figure 3-10).

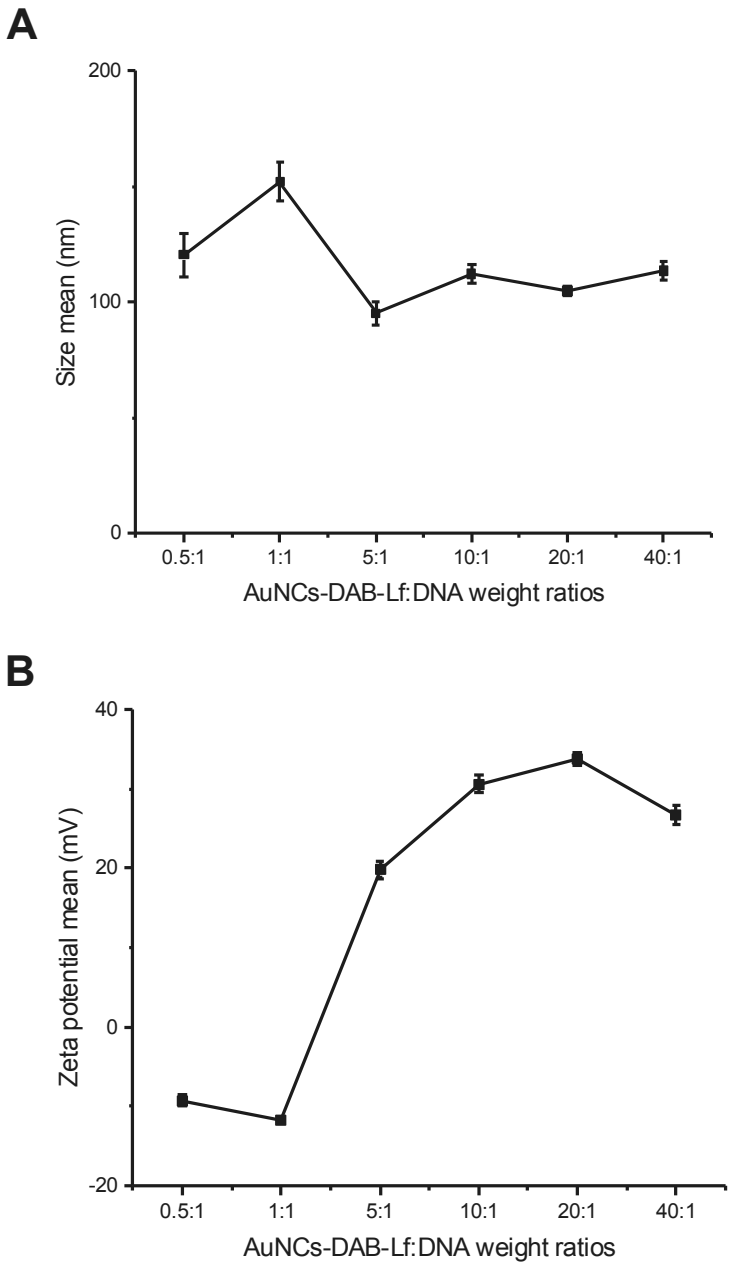

Figure 3-10: Size (A) and zeta potential (B) for AuNCs-DAB-Lf complexed with DNA at various AuNCs-DAB-Lf:DNA weight ratios. Results are expressed as mean ± SEM (*n = 9*) (error bars smaller than symbols when not visible).

3.3.2.2. Gel retardation assay

An agarose gel retardation assay was performed to test the ability of AuNCs conjugates to condense DNA. The concentrations of AuNCs conjugates were prepared at various AuNCs conjugates:DNA weight ratios from 0.5:1 to 40:1, with a constant DNA concentration of 20 µg/mL.

3.3.2.2.1. AuNCs-Lf

Gel retardation assay showed the AuNCs conjugate capability of partially and fully condensing the plasmid DNA (Figure 3-11). At the lowest ratios of 0.5:1 and 1:1, free DNA bands were visible, indicating the low ability of the AuNCs conjugate to condense the DNA at these ratios. Furthermore, the intensity of DNA bands began to decrease from a weight ratio of 5:1 to fully disappear at a weight ratio of 40:1. AuNCs-Lf:DNA therefore exhibited DNA partial complexation at ratios of 5:1, 10:1 and 20:1. However, AuNCs-Lf:DNA completely prevented DNA migration at a weight ratio of 40:1, indicating the complete DNA condensation by AuNCs-Lf at this ratio.

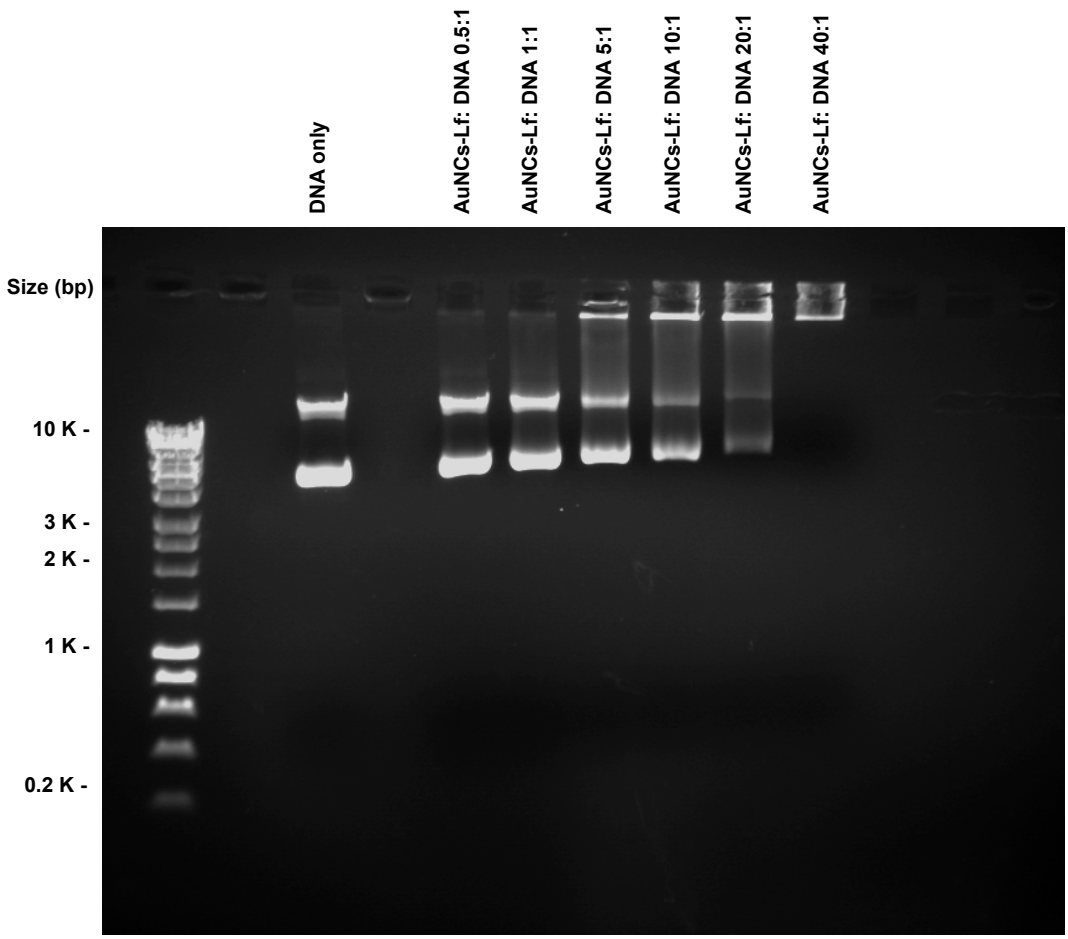

Figure 3-11: Gel retardation assay of AuNCs-Lf complex at various AuNCs-Lf:DNA weight ratios (0.5:1, 1:1, 5:1, 10:1, 20:1 and 40:1) (control: DNA only).

3.3.2.2.2. AuNCs-PEG-Lf

AuNCs-PEG-Lf completely prevented DNA migration at AuNCs-PEG-Lf:DNA weight ratios of 20:1 and 40:1, demonstrating the strong tendency of this gold conjugate to condense the DNA completely at these ratios (Figure 3-12). At ratios of 5:1 and 10:1, some DNA migrated into the gel, indicating partial complexation of the DNA at these ratios. Conversely, most DNA migrated into the gel at ratios 0.5:1 and 1:1, demonstrating the failure of the gold conjugate to condense the DNA at these ratios.

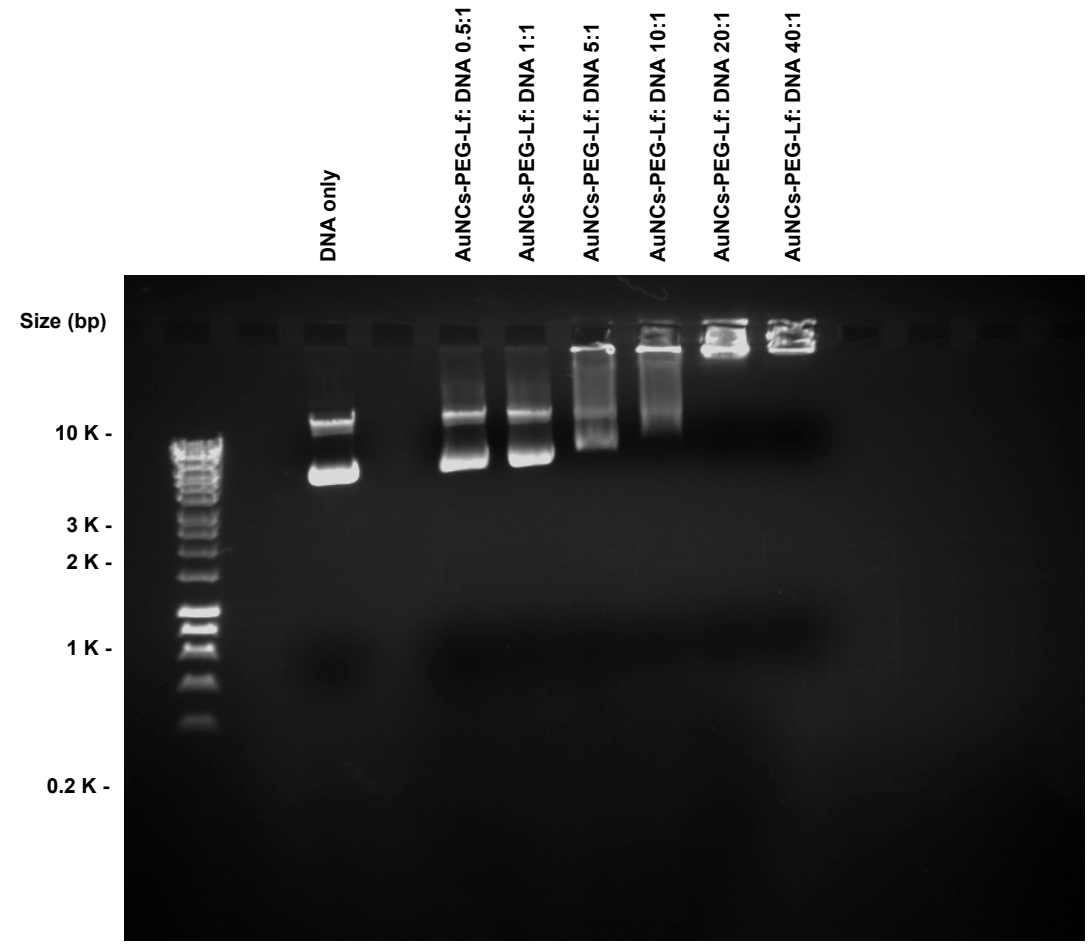

Figure 3-12: Gel retardation assay of AuNCs-PEG-Lf complex at various AuNCs-PEG-Lf:DNA weight ratios (0.5:1, 1:1, 5:1, 10:1, 20:1 and 40:1) (control: DNA only).

3.3.2.2.3. AuNCs-Lf-PEG

The gel in Figure 3-13 revealed partial and complete DNA complexation by AuNCs-Lf-PEG conjugate. At a high ratio of 40:1, the conjugate prevented DNA migration, confirming complete DNA condensation. However, the lowering of the weight ratios induced a gradual decrease in the intensity of DNA condensation. Therefore, ratios of 20:1 and 10:1 showed partial DNA condensation, as some DNA migration was detected through the gel. Minor DNA complexation was shown at a ratio of 5:1 with

more DNA migration. The lower ratios of 1:1 and 0.5:1 exhibited migration bands similar to those of free DNA, indicating the failure of the gold conjugate to complex the DNA at these ratios.

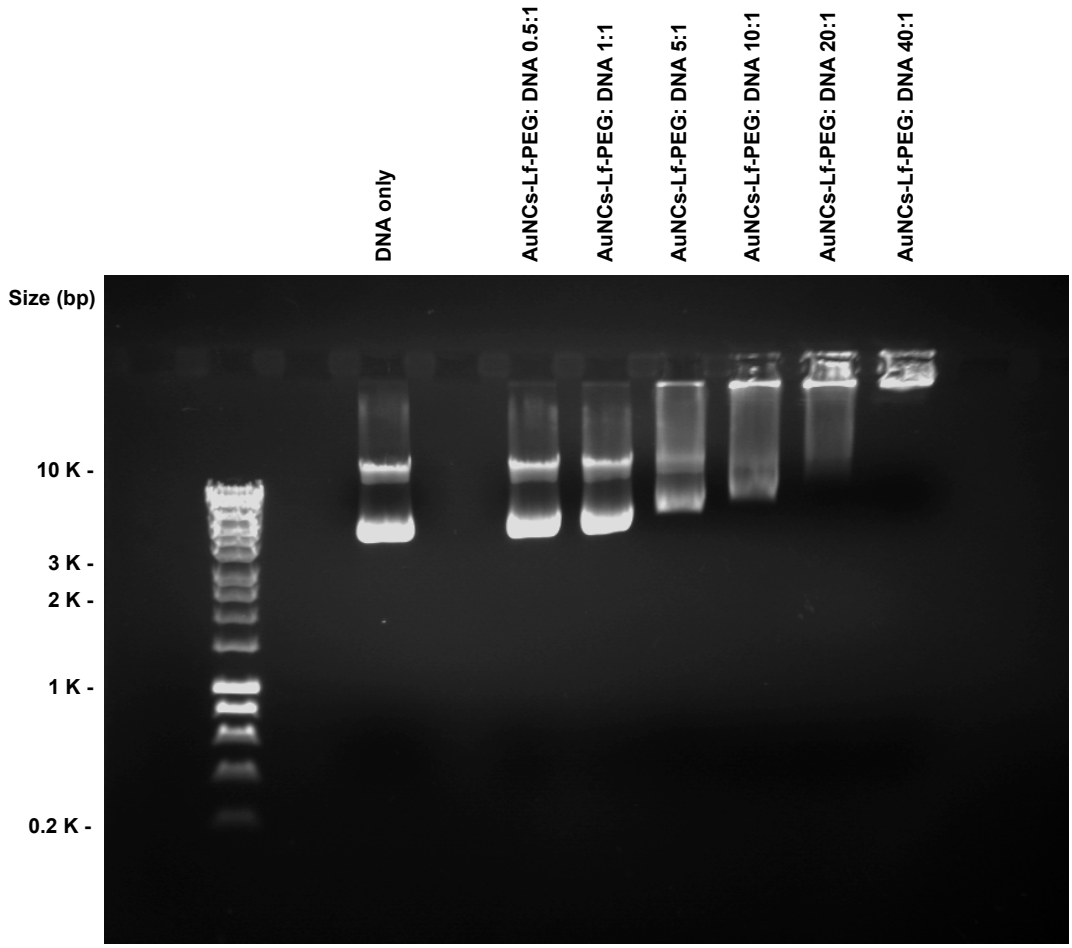

Figure 3-13: Gel retardation assay of AuNCs-Lf-PEG complex at various AuNCs-Lf-PEG:DNA weight ratios (0.5:1, 1:1, 5:1, 10:1, 20:1 and 40:1) (control: DNA only).

3.3.2.2.4. AuNCs-Lf-2xPEG

AuNCs-Lf-2xPEG induced complete DNA complexation at a weight ratio of 40:1, and partial complexation at ratios of 20:1, 10:1 and 5:1 (Figure 3-14). At lower ratios of 1:1 and 0.5:1, bands closely resembling those of the free DNA were visible, indicating that the DNA had not been complexed by the gold conjugate.

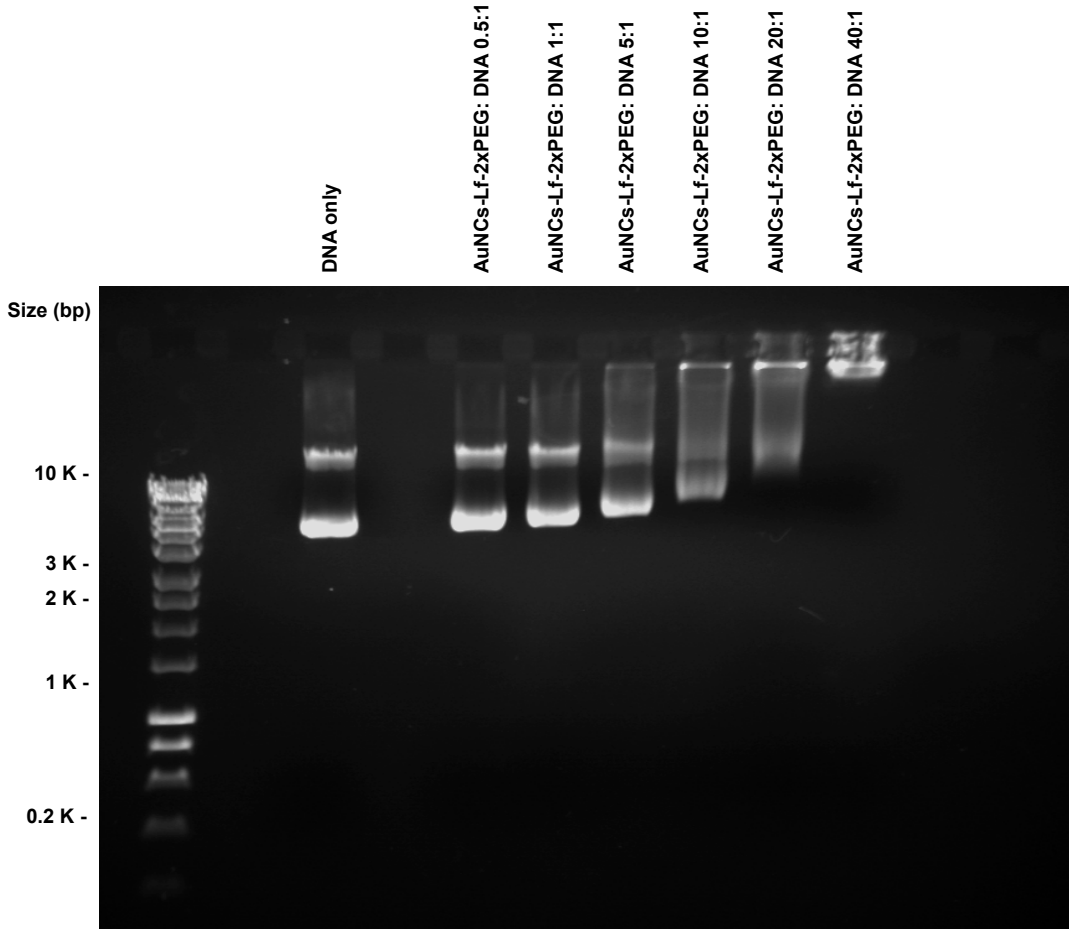

Figure 3-14: Gel retardation assay of AuNCs-Lf-2xPEG complex at various AuNCs-Lf-2xPEG:DNA weight ratios (0.5:1, 1:1, 5:1, 10:1, 20:1 and 40:1) (control: DNA only).

3.3.2.2.5. AuNCs-Lf-PEI

The gel retardation assay confirmed complete or partial DNA condensation by AuNCs-Lf-PEI. DNA was fully condensed at AuNCs-Lf-PEI:DNA weight ratios of 5:1 and above, thus preventing ethidium bromide from intercalating with the DNA. No free DNA was therefore visible at these ratios (Figure 3-15). In contrast, DNA was partially condensed at AuNCs-Lf-PEI:DNA weight ratios of 1:1 and below. Ethidium bromide could therefore intercalate with DNA, and a band corresponding to free DNA was visible.

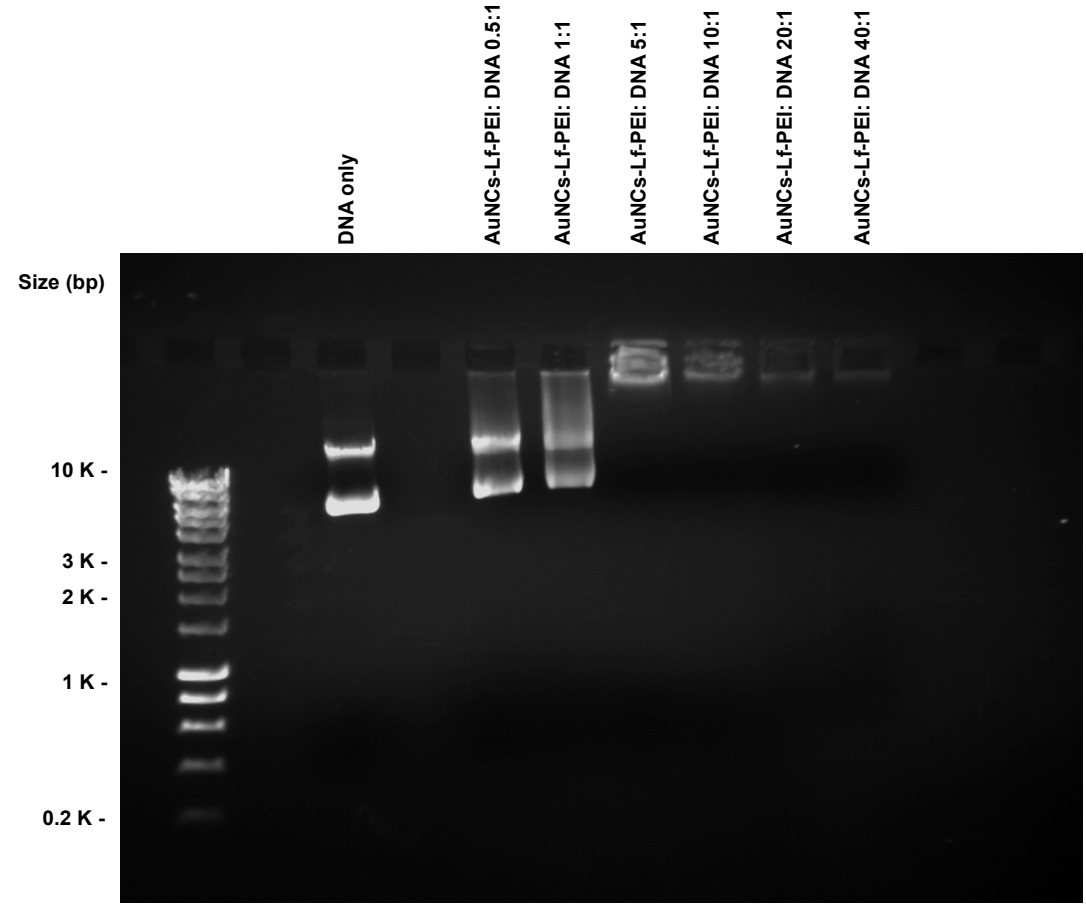

Figure 3-15: Gel retardation assay of AuNCs-Lf-PEI complex at various weight ratios (0.5:1, 1:1, 5:1, 10:1, 20:1 and 40:1) (control: DNA only).

3.3.2.2.6. AuNCs-Lf-PLL

A gel retardation assay demonstrated complete or partial DNA complexation by AuNCs-Lf-PLL. DNA was completely condensed at AuNCs-Lf-PLL:DNA weight ratios of 5:1 and above, as no free DNA was observed at these ratios (Figure 3-16). Conversely, DNA was partially condensed at AuNCs-Lf-PLL:DNA weight ratios of 1:1 and below. Ethidium bromide could therefore intercalate with DNA, and a band corresponding to free DNA was visible.

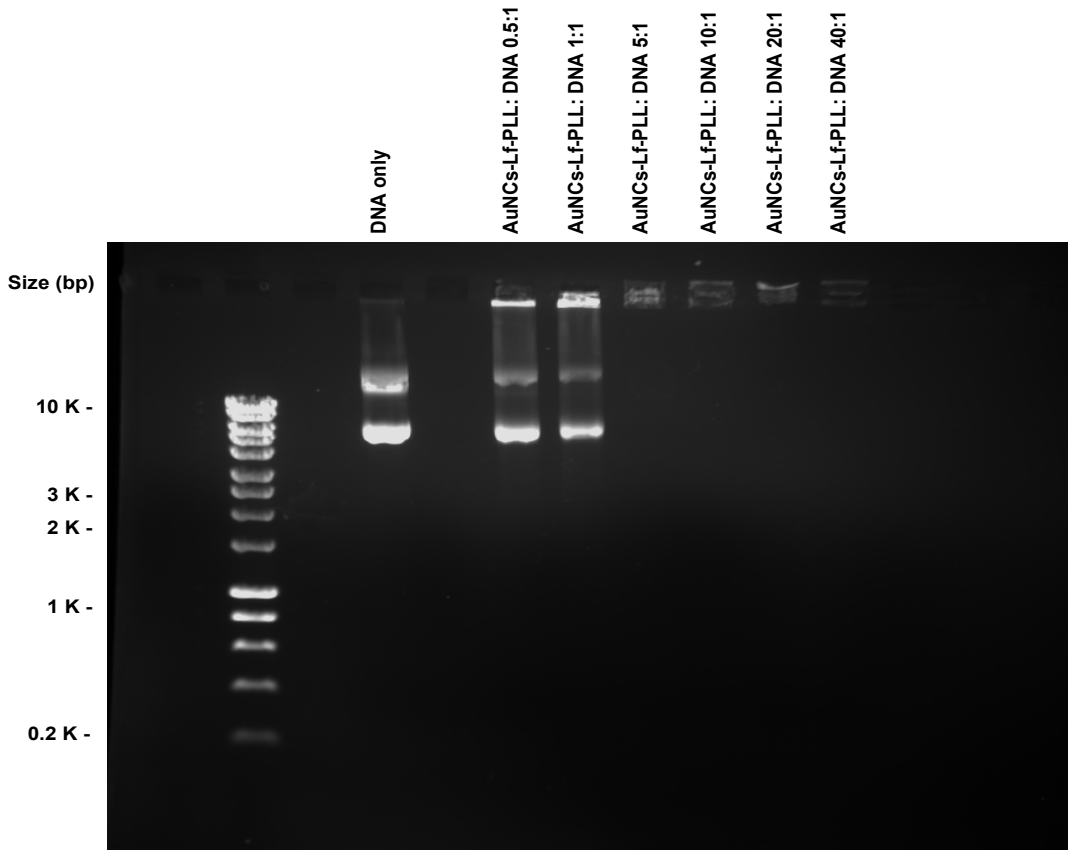

Figure 3-16: Gel retardation assay of AuNCs-Lf-PLL complex at various AuNCs-Lf-PLL:DNA weight ratios (0.5:1, 1:1, 5:1, 10:1, 20:1 and 40:1) (control: DNA only).

3.3.2.2.7. AuNCs-DAB-Lf

A gel retardation assay confirmed complete or partial DNA condensation by AuNCs-DAB-Lf. DNA was fully condensed at AuNCs-DAB-Lf:DNA weights ratios of 5:1 and above. Thus, no visible sign of free DNA was observed at these ratios (Figure 3-17). However, DNA was partially condensed at AuNCs-DAB-Lf:DNA weight ratios of 1:1 and below. Ethidium bromide could therefore intercalate with DNA, and a band corresponding to free DNA was visible.

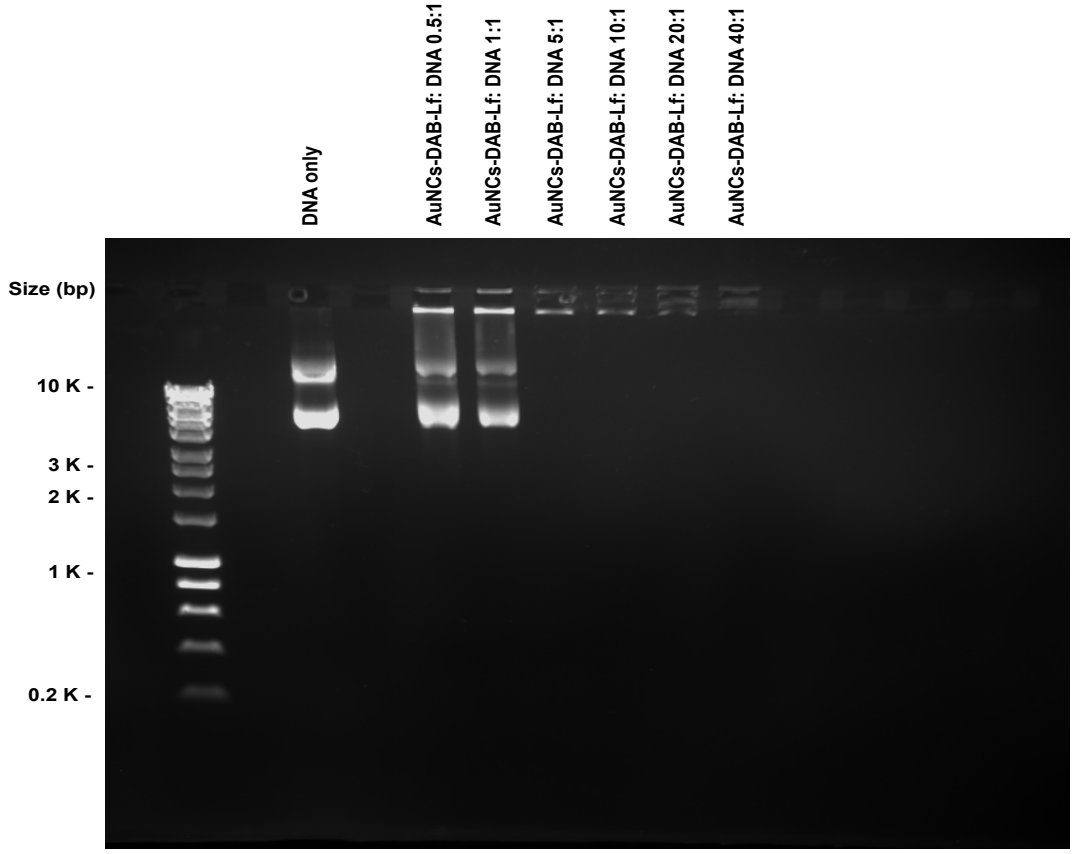

Figure 3-17: Gel retardation assay of AuNCs-DAB-Lf complex at various AuNCs-DAB-Lf:DNA weight ratios (0.5:1, 1:1, 5:1, 10:1, 20:1 and 40:1) (control: DNA only).

3.4. Discussion

Ligand exchange is one of the most common conjugation methods that are generally used for the surface modification of gold nanocages (Yavuz *et al.*, 2009; Chen *et al.*, 2010b). After synthesising gold nanocages via galvanic replacement, the gold nanocage surface was coated with PVP, a biocompatible polymer, to be used as a stabiliser and capping agent during the synthesis reaction. Due to the strong binding affinity of thiolates towards the gold surface, PVP on nanocages can be replaced with thiolated ligands, such as targeting agents or cationic polymers. In this study, targeting ligand Lf and cationic polymers (PEI, PEG, PLL and DAB) were conjugated to the surface of gold nanocages through gold-thiolate (Au-S) bonds. Conjugating these ligands onto the nanocages would generate positively charged gold conjugates that can complex negatively charged DNA plasmids via electrostatic interactions.

First, AuNCs-Lf synthesis was confirmed by FTIR spectroscopy. The FTIR spectrum of Lf was assessed in the presence and absence of gold nanocages to ensure successful conjugation between Lf and AuNCs and to monitor any changes in the secondary structure of the protein. Bare Lf displayed characteristic bands appearing at the amide I region (1600–1690 cm^{-1}) and amide II region (1480–1575 cm^{-1}), in agreement with previous reports (Xavier *et al.*, 2010; Bokkhim *et al.*, 2013). The FTIR spectrum of AuNCs-Lf shows bands at 1645.01 and 1534.86 cm^{-1}, indicating the presence of characteristic amides I and II band peaks assigned to the Lf protein, thereby confirming the successful conjugation between Lf and AuNCs. The amide I band is the most sensitive to protein secondary structures; therefore, the second derivative of FTIR spectra of Lf and AuNCs-Lf were analysed in the range of 1600–

1690 cm^{-1}. After conjugating Lf to AuNCs, there was no significant change in the protein conformation, as AuNCs-Lf displayed bands in the amide I region similar to those observed for the bare Lf, indicating that AuNCs-Lf and Lf had identical secondary structures. The successful formation of AuNCs-Lf was also confirmed by circular dichroism spectroscopy. The CD spectrum peaks of AuNCs-Lf in the 240–290 nm region appeared at an identical wavelength with a similar ellipticity intensity of the bare Lf, unlike unmodified AuNCs. These findings indicate the successful formation of AuNCs-Lf and suggest that the conjugation between Lf and AuNCs does not impact the secondary structures of the protein, in line with the FTIR results. The conjugation of Lf to AuNCs was also demonstrated by MALDI-TOF mass spectrometry analysis. The mass spectra showed the average molecular weight of bare Lf with a peak at 83499 *m/z*, following previously reported values (Xavier *et al.*, 2010). However, after conjugating Lf to AuNCs, the mass spectra of AuNCs-Lf showed an increase in molecular mass compared to bare Lf. The difference in average masses between the peaks in AuNCs-Lf at 83797 *m/z* and bare Lf corresponds to the Au core of AuNCs conjugated with the Lf protein. Thus, the data obtained from MALDI-TOF mass spectrometry supports the successful conjugation of AuNCs with Lf and suggests that AuNCs bind to a single Lf protein molecule.

The surface modification of the gold nanocages with Lf and the polymers was analysed by UV-vis spectroscopy. After surface functionalisation of the gold nanocages with Lf and the polymers, all gold conjugates displayed characteristics of UV-vis NIR absorption peaks at 750–813 nm. The red-shifted absorption peaks of these AuNCs conjugates, compared with the unmodified AuNCs, are attributed to the change in refractive index on the AuNCs surface. This confirms the surface

functionalisation and further indicates that the shape and structure of the nanocages remained the same upon the functionalised conjugation (Huang *et al.*, 2016). These findings are in line with the TEM images that demonstrated the cage shape of AuNCs conjugates. These were consistent with previously published results showing that the surface conjugation of gold nanocages with the polymer and targeting ligands did not change the shape and structure of the nanocages (Suresh *et al.*, 2014). The surface functionalisation of gold nanocages was also validated by DLS size and zeta potential analysis. The DLS measurements showed a slight increase in size diameter by ~14 nm after Lf conjugation with gold nanocages and by ~22 nm after the surface modification with the polymers, indicating AuNCs-Lf formation and supporting the successful grafting of the polymers onto the nanocages.

Also, the zeta potential analysis confirmed the change in the surface charge of the nanocages from negative to positive values upon the surface functionalisation with Lf and the polymers, further confirming the successful generation of positively charged gold conjugates that could complex the negatively charged DNA effectively. Thus, AuNCs conjugates were able to complex the negatively charged DNA by electrostatic interactions, although an excess of conjugate (conjugate:DNA weight ratios of 5:1 and above) was required to ensure efficient DNA condensation. AuNCs conjugate complexes at a weight ratio of above 5:1 displayed a suitable size diameter to allow them to penetrate into cancer cells, as the cut-off size for extravasation was found to be 400 nm for most tumours (Yuan *et al.*, 1995). Also, conjugating AuNCs-Lf with cationic polymers enhanced the DNA complexation efficacy, as AuNCs-Lf-PEG, AuNCs-Lf-PLL, AuNCs-DAB-Lf and AuNCs-Lf-PEI conjugates displayed higher positive charges compared to unmodified AuNCs-Lf, where its positive

charge is mostly due to the presence of the positively charged amino acids within Lf. This could be explained by the presence of amine groups in DAB, PEI, PLL and PEG, and by the hydrophobic nature of the attached PLL rich in hydrophobic amino acids. These positive charges of the amino groups from the polymers, which attached to the gold nanocages surface, electrostatically interacted with the negative charges from the phosphate groups of the DNA, thereby condensing DNA into small complexes, with sizes suitable for gene delivery.

Further, the rigid structure of gold nanocages could be a further explanation for DNA condensation enhancement. Notably, the rigidity of the gold nanoparticles helps to maintain the 3D structure of the attached polymer, such as dendrimers, inducing improved electrostatic interactions between the attached polymer and the DNA (Shan *et al.*, 2012). The conjugation approach of Lf and cationic polymers onto the gold nanocage surface in this study influenced the DNA condensation efficacy. The AuNCs-Lf-PLL showed higher DNA condensation efficacy than its AuNCs-PLL-Lf counterpart. The stronger DNA complexation ability might be attributed to the enhanced positive surface charge of AuNCs-Lf-PLL (17 ± 0.45 mV) compared to AuNCs-PLL-Lf (6.39 ± 0.11 mV), as grafting PLL into AuNCs-Lf could create a more cationic and hydrophobic environment on the conjugate surface, facilitating the complexation of negatively charged DNA.

Overall, the positive zeta potential values of all AuNCs conjugates complexed DNA at weight ratios of 5:1 and above, which confirmed the efficient complexation of the DNA. These findings were in accordance with the gel retardation results of AuNCs conjugates. However, the gel retardation assay evaluation of AuNCs-Lf-PLL, AuNCs-DAB-Lf and AuNCs-Lf-PEI showed better DNA condensation efficacy than

that of AuNCs-Lf-PEG, in which they fully complexed the DNA at weight ratios of 5:1 to 40:1. Complete DNA complexation occurred at 40:1 only for AuNCs-Lf-PEG because of the presence of a higher number of amine groups in PEI, DAB and PLL polymers than in PEG (thiol-PEG-amine), causing the generation of higher positive charges on the conjugate surface, which can attract and complex more DNA.

In conclusion, DNA condensation studies demonstrated that AuNCs conjugates have the required physicochemical properties to be efficient gene delivery systems. Notably, the DNA condensation efficacy of AuNCs conjugates could not be assessed using PicoGreen® assay due to the fluorescence quenching properties of gold nanoparticles and the blue colour of the AuNC samples, which interfered with the fluorescence intensity measurements and so might have induced false positive results (Xia *et al.*, 2011).

Chapter 4: *In vitro* cell culture evaluation of PEG-, PEI-, PLL- and DAB- conjugated, lactoferrin-bearing gold nanocages

4.1. Introduction

Prostate cancer is the second most common cancer and the fifth-leading cause of cancer death in men, with approximately 1.4 million new cases diagnosed and 375,000 deaths recorded globally in 2020 (Sung *et al.*, 2021). Despite the advancements in available treatments for this cancer, current therapy can only provide a short increase in lifespan and offer limited therapeutic effects for patients with recurrent or metastatic diseases (Graff and Chamberlain, 2015). Consequently, new and improved therapeutic approaches are urgently needed for these patients. Among innovative experimental techniques, gene therapy offers promising potential for prostate cancer treatment. However, its use is currently hampered by the lack of safe and efficient delivery systems that can selectively deliver therapeutic genes to tumours without causing secondary effects on healthy tissues.

To examine the efficacy of nanomedicines and anticipate their potential toxicity, several experiments were initially conducted in cell culture, which is mandatory to assess the efficacy of the tested treatments before proceeding to animal studies (Ravi *et al.*, 2015). Since the introduction of the first cancer cell line, HeLa, in the late 19th century, cell culture has become one of the most essential techniques used in preclinical studies of new therapeutics (Jaroch *et al.*, 2018). The major feature of cell culture techniques is the ability to regulate the physicochemical environment of the cells, such as the pH, temperature and carbon dioxide, which is critical for precise and repeatable experimental investigations (Ravi *et al.*, 2015). Also, cell culture experiments provide a better understanding of the cellular physiological environment of the desired organ and the biochemical response to nanoparticles carrying therapeutics. Only with a thorough understanding of

nanoparticle–cell interactions can these nanoparticles be tailored to display suitable characteristics for optimal *in vivo* delivery and effective treatment (Sun *et al.*, 2014). In the field of cancer therapy, *in vitro* study is considered a fundamental stage for evaluating nanomedicines for therapeutic effectiveness, cellular internalisation, cell transfection and proliferation before eventually proceeding to *in vivo* studies (Kura *et al.*, 2014).

4.1.1. Aims and objectives

In the previous chapter, we described the synthesis and characterisation of lactoferrin-bearing gold nanocage conjugates and evaluated their DNA condensation efficacy. The objectives of this chapter, therefore, are to assess the transfection efficacy and cellular uptake of the conjugates complexed with plasmid DNA encoding β-galactosidase while evaluating the therapeutic efficacy of the conjugates complexed with therapeutic DNA in PC-3 prostate cancer cells.

4.2. Materials and methods

4.2.1. Materials

Materials	Suppliers
2-nitrophenyl-β-D-galactopyranoside (ONPG)	Sigma-Aldrich, UK
3-(4,5-dimethylthiazol-2-yl)-2,5-diphenyl tetrazolium bromide (MTT)	Sigma-Aldrich, UK
Bioware® B16-F10-luc-G5 mouse melanoma	Calliper Life Sciences, USA
Dimethyl sulfoxide (DMSO)	Sigma-Aldrich, UK
Foetal Bovine Serum (FBS)	Invitrogen, UK
Isopropanol	Sigma-Aldrich, UK
L-Glutamine	Invitrogen, UK
Label IT® Fluorescein Nucleic Acid Labelling kit	Cambridge Biosciences, UK
Minimum Essential Medium (MEM)	Sigma-Aldrich, UK
Passive lysis buffer	Promega, UK
PC-3M-luc-C6 human prostate cancer cell line	Calliper Life Sciences, USA
Penicillin-Streptomycin	Invitrogen, UK
Phosphate buffered saline (PBS) tablets	Sigma Aldrich, UK
Plasmid encoding TNFα (pORF9-mTNFα)	InvivoGen, USA
Plasmid encoding β-galactosidase (pCMVsport β-galactosidase)	Life Technologies, UK
Triton-X	Sigma-Aldrich, UK

Materials	Suppliers
Trypsin	Invitrogen, UK
Vectashield® 4′, 6-diamidino-2-phenylindole (DAPI)	Vector Laboratories, UK

4.2.2. Methods

4.2.2.1. Cell culture

PC-3 cells were grown as monolayers in Minimum Essential Medium (MEM) supplemented with 10% (v/v) foetal bovine serum, 1% (v/v) L-glutamine, and 0.5% (v/v) penicillin–streptomycin. The cell culture flasks were kept at 37 °C in a 5% carbon dioxide humid atmosphere.

4.2.2.2. *In vitro* transfection

The transfection efficacy of the DNA complexed by AuNCs conjugates was assessed using a plasmid DNA encoding β-galactosidase. PC-3 cells were seeded at a concentration of 10 000 cells/well in 96-well plates and incubated for 24 h at 37 °C in a 5% CO_2 atmosphere. They were then treated with AuNCs conjugates complexes in quintuplicate at various AuNCs conjugate:DNA weight ratios (40:1, 20:1, 10:1, 5:1, 2:1, 1:1 and 0.5:1). Naked DNA was used as a negative control whereas DOTAP-DNA, PEI-DNA, PLL-DNA and DAB-DNA (weight ratio 5:1) served as positive controls. DNA concentration (0.5 μg/well) was maintained constant throughout the experiment. After treatment, the cells were incubated for 72 h before analysis. They were then lysed with 50 μL/well of 1× passive lysis buffer (PLB) for 20 min and then tested for β-galactosidase expression (Zinselmeyer *et al.,* 2002). Briefly, 50 μL of the assay buffer (2 mM magnesium chloride, 100 mM mercaptoethanol, 1.33 mg/mL o-nitrophenyl- β-D-galactosidase, 200 mM sodium phosphate buffer, pH 7.3) was added in each well containing the lysates, before being incubated for 2 h at 37 °C. The absorbance of the samples was subsequently

read at 405 nm using a Multiskan AscentVR® plate reader (MTX Lab Systems, Bradenton, FL).

4.2.2.3. Cellular uptake

4.2.2.3.1. Quantitative analysis

The quantification of the cellular uptake of the AuNCs conjugates complexed with DNA by the prostate cancer cells was carried out by flow cytometry. PC-3 cells were seeded at a density of 3×10^5 cells per well in 6-well plates and grown at 37 °C for 24 h, before being treated with fluorescein-labelled DNA (2.5 μg DNA per well) complexed with the complexes at AuNCs conjugate:DNA weight ratios of 0.5: 1, 10:1 and 40: 1. Other wells were treated with DAB, PEI and PLL polyplexes as positive controls and DNA solution as negative control, respectively. After 24 h of incubation with the treatments, each well was washed with 2 mL of PBS pH 7.4 twice. Single-cell suspensions were then prepared (using 250 μL trypsin per well, followed by 500 μL medium per well once the cells were detached), before being analysed using a FACSCanto® flow cytometer (BD, Franklin Lakes, NJ). Their mean fluorescence intensity was analysed with FACSDiva® software (BD, Franklin Lakes, NJ), counting 10 000 cells (gated events) for each sample.

4.2.2.3.2. Qualitative analysis

The cellular uptake of AuNCs conjugates complexed with fluorescently labelled DNA was qualitatively assessed using confocal microscopy. Labelling of plasmid DNA with the fluorescent probe fluorescein was performed using a Label IT® Fluorescein Nucleic Acid Labelling kit, as described by the manufacturer. PC-3 cells

were seeded on coverslips in 6-well plates at a concentration of 3×10^5 cells per well and grown for 24 h at 37 °C. The cells were then treated with fluorescein-labelled DNA (2.5 μg /well) complexed to AuNCs-Lf-PEI at a conjugate:DNA weight ratio of 40:1, AuNCs-Lf-PLL and AuNCs-DAB-Lf at a weight ratio of 10:1 and DAB at a dendrimer: DNA weight ratio of 5:1 for 24 h at 37 °C. Control wells were also treated with naked DNA or remained untreated. The cells were then washed twice with 3 mL PBS before being fixed with 2 mL methanol for 10 min at 20 °C. They were then washed again with 3 mL PBS. Upon staining of the nuclei with Vectashield® mounting medium containing DAPI, the cells were examined using a Leica TCS SP5 confocal microscope (Wetzlar, Germany). DAPI (which stained the cell nuclei) was excited with a 405 nm laser line (emission bandwidth: 415–491 nm), and fluorescein (which labelled the DNA) was excited with a 514 nm laser line (emission bandwidth: 550–620 nm).

4.2.2.4. Anti-proliferative activity

The anti-proliferative activity of the gold nanocages conjugates (AuNCs-Lf, AuNCs-PEG-Lf, AuNCs-Lf-PEG, AuNCs-Lf-PEI and AuNCs-DAB-Lf) complexed with plasmid DNA encoding TNFα was assessed using a standard MTT assay. PC-3 cells were seeded in quintuplicate at a density of 10 000 cells/well in 96-well plates and incubated at 37 ^{o}C for 24h. The cells were then treated with the AuNCs-Lf complexes at a AuNCs: DNA weight ratio of 10:1 using various DNA concentrations ranging from 80 to 0.31 μg/mL. Naked DNA was used as a negative control, while DAB: DNA 5:1 ratio served as a positive control. The cytotoxicity of the AuNCs-Lf conjugates was also examined by the same method, treating the seeded cells with 800

to 3.12 μg/ml, which is equivalent to the amount of AuNCs-Lf conjugates used in the anti-proliferation assay. For AuNCs-Lf-PLL, PC-3 cells were treated with AuNCs-Lf-PLL: DNA weight ratio of 10:1 using various DNA concentrations ranging from 20 to 0.25 μg/ml, using naked DNA as a negative control, while PLL: DNA 5:1 ratio served as a positive control. The cytotoxicity of AuNCs-Lf-PLL only was also examined by treating the cells with 200 to 2.5 μg/ml of the conjugate, which is equivalent to the amount used in the anti-proliferation assay.

The plates were incubated for 72 h at 37 ºC and 5% CO_2, then 50 μL of 0.5% MTT solution was added to the medium and incubated at 37 ºC protected from light for four hours. The medium was then replaced with 200 μL of DMSO per well to dissolve the precipitated formazan. The absorbance of the complex was measured at 570 nm using a plate reader (Thermo Labsystems, Multiscan Ascent) and the growth inhibitory concentration for 50% of the cells (IC_{50}) was measured. IC_{50} values were obtained by plotting a dose-response curve between the percentage of the cell viability and the logarithm of the DNA concentration.

4.2.2.5. Statistical analysis

Results were expressed as means ± standard error of the mean. Statistical significance was assessed by one-way analysis of variance and Tukey multiple comparison post-test (Minitab® software, State College, PE). Differences were considered statistically significant for P values lower than 0.05.

4.3. Results

4.3.1. Transfection assay

4.3.1.1. Optimisation of transfection duration

AuNCs-Lf and AuNCs-Lf-PEI complexes were used to examine the transfection efficacy after treating PC-3 prostate cancer cells for 4 and 72 h. AuNCs-Lf complexed with DNA induced gene transfection after treatment for 4 and 72 h on PC-3 cancer cells (Figure 4-1). The highest level of transfection of the AuNCs-Lf complex was observed at a conjugate:DNA weight ratio of 0.5:1 (2.31 ± 0.24 mU/mL) for 4 h treatment. At this ratio, the transfection efficacy of the AuNCs-Lf complex was 1.45-fold higher than that obtained with DOTAP (1.59 ± 0.13 mU/mL) and 1.91-fold higher than with DNA (1.21 ± 0.04 mU/mL). Similarly, the highest transfection level for the AuNCs-Lf complex 72 h post-treatment was recorded at a weight ratio of 0.5:1 (2.22 ± 0.24 mU/mL). The gene expression at this ratio was 1.32-fold higher than that treated with DOTAP (1.68 ± 0.09 mU/mL), and higher by 1.9-fold than DNA (1.16 ± 0.01 mU/mL).

Also, the AuNCs-Lf-PEI complex improved gene transfection upon treating PC-3 cells for 4 and 72 h compared with DOTAP and PEI (Figure 3-2). The highest transfection level was observed at a weight ratio of 1:1 for 4 h treatment. Its transfection efficacy was 1.64-fold higher that treated with DNA, 1.39-fold higher than PEI (1.43 ± 0.07 mU/mL) and 1.25-fold higher than DOTAP. However, the highest transfection level was obtained at a weight ratio of 40:1 (2.49 ± 0.10 mU/mL) after 72 h. At this ratio, the transfection efficacy was 1.95-fold higher than that observed with DNA, 1.71-fold higher than PEI (1.46 ± 0.05 mU/mL) and 1.48-

fold higher than DOTAP. According to the described results, a 72-h treatment was chosen to investigate the transfection efficacy of the gold complexes.

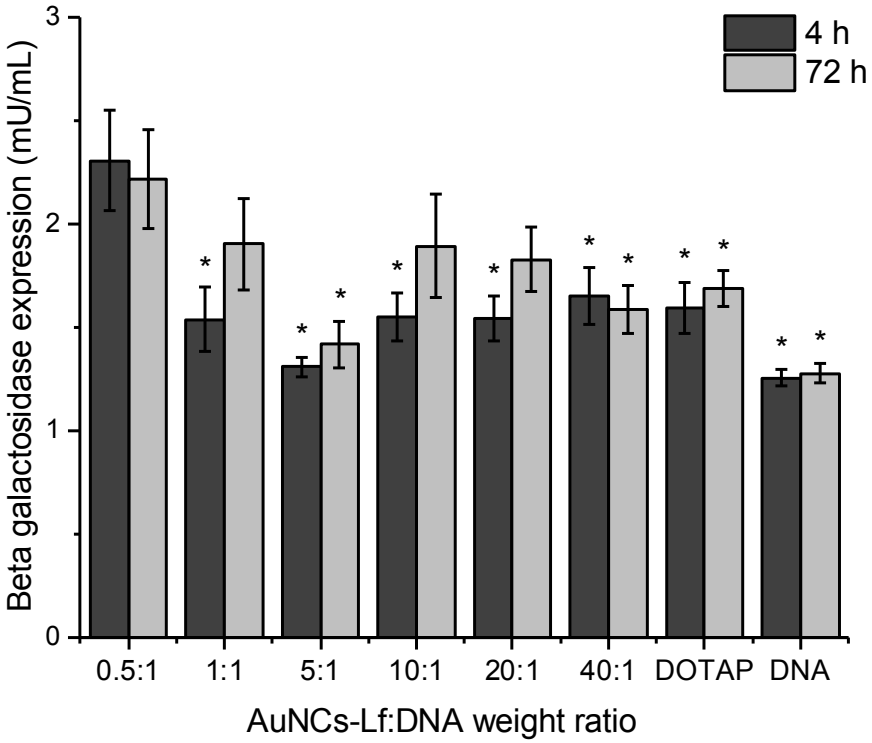

Figure 4-1: Transfection efficacy of lactoferrin-bearing gold nanocages (AuNCs-Lf) in PC-3 cells. The complexes were incubated with the cells for 4 and 72 h. Complexes incubated with the cells for 4 h were removed and replaced with MEM medium until the end of the transfection study (72 h). Results are expressed as the mean ± SEM of three replicates (n = 15). *: $P < 0.05$ versus the highest transfection ratio.

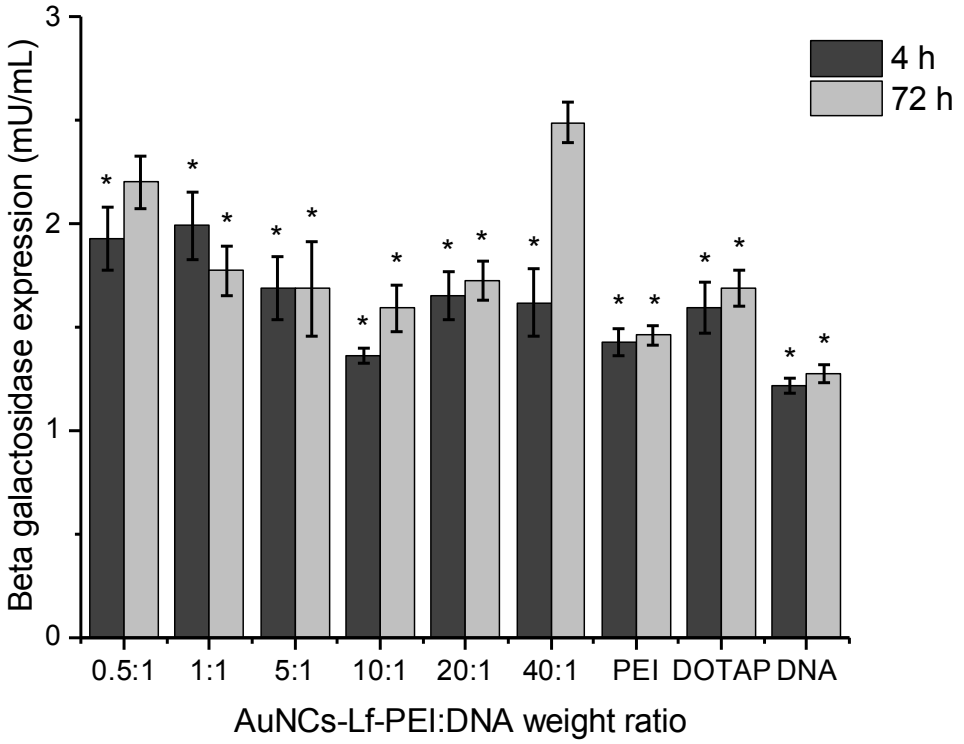

Figure 4-2: Transfection efficacy of AuNCs-Lf-PEI in PC-3 cells. The complexes were incubated with the cells for 4 and 72 h. Complexes incubated with the cells for 4 h were removed and replaced with MEM medium until the end of the transfection study (72 h). Results are expressed as the mean ± SEM of three replicates (n = 15). *: $P < 0.05$ versus the highest transfection ratio.

4.3.1.2. Effect of PEGylation and conjugation procedure on transfection efficacy

4.3.1.2.1. AuNCs-Lf-PEG and AuNCs-PEG-Lf complexes

The transfection efficacy of the AuNCs-Lf-PEG and AuNCs-PEG-Lf complexes was examined to explore the effect of PEGylation of AuNCs conjugates on gene transfection. From Figure 4-3, the highest transfection level was observed following treatment with AuNCs-Lf-PEG complex at a conjugate:DNA weight ratio of 0.5:1

(2.43 ± 0.21 mU/mL), and after treatment with AuNCs-PEG-Lf complex at a ratio of 20:1 (1.61 ± 0.14 mU/mL). The transfection efficacy of the AuNCs-Lf-PEG complex at weight ratio 0.5:1 was 1.89- and 1.45-fold higher than that obtained with DNA (1.16 ± 0.01 mU/mL) and DOTAP (1.68 ± 0.09 mU/mL), respectively. However, the transfection efficacy of the AuNCs-PEG-Lf complex at a weight ratio of 20:1 (1.61 ± 0.14 mU/mL) was only 1.26-fold higher than that obtained with DNA and 1.04-fold lower than that with DOTAP.

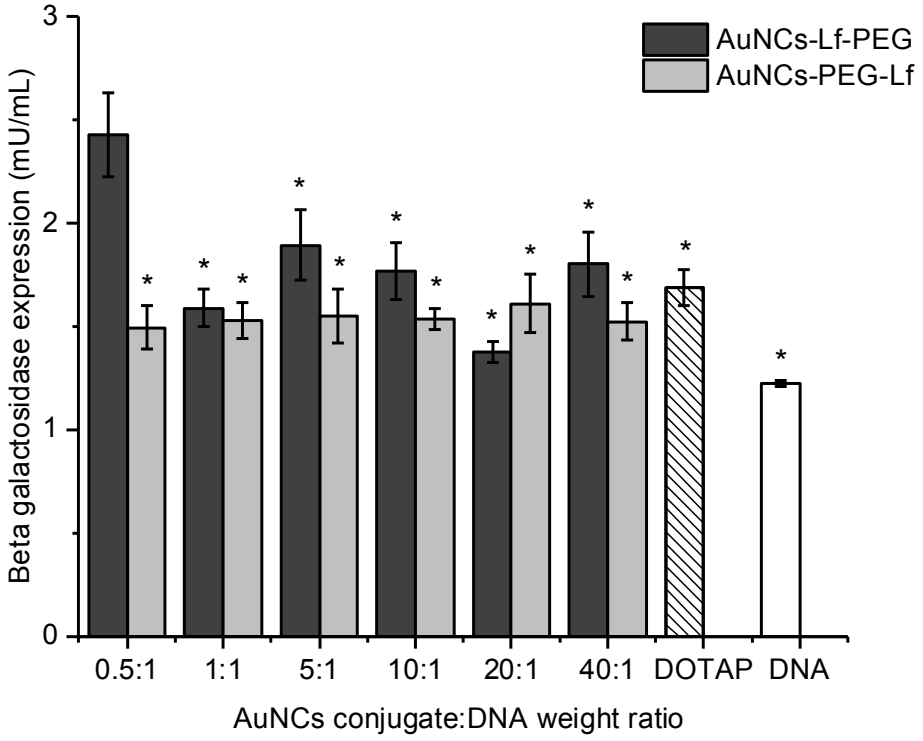

Figure 4-3: Transfection efficacy of AuNCs-Lf-PEG and AuNCs-PEG-Lf in PC-3 cells. Results are expressed as the mean ± SEM of three replicates (n = 15). *: P < 0.05 versus the highest transfection ratio.

4.3.1.2.2. AuNCs-Lf-2xPEG complex

The transfection efficacy of the AuNCs-Lf-2xPEG complex was evaluated to examine whether the increase in PEG concentration would enhance the transfection efficacy of AuNCs-Lf-PEG. From Figure 4-4, the highest transfection level was found at a weight ratio of 20:1 for the AuNCs-Lf-2xPEG complex (1.66 ± 0.12 mU/mL). The transfection efficacy of AuNCs-Lf-2xPEG complex at a weight ratio of 20:1 was 1.43-fold higher than that obtained with DNA (1.16 ± 0.01 mU/mL) and displayed an almost similar transfection level as DOTAP (1.68 ± 0.09 mU/mL). Hence, AuNCs-Lf-2xPEG showed a lower transfection efficacy than AuNCs-Lf-PEG. These findings further indicated that increasing the concentration of PEG grafted to AuNCs-Lf from 200 µM as in AuNCs-Lf-PEG to 400 µM in case of AuNCs-Lf-2xPEG did not enhance gene expression.

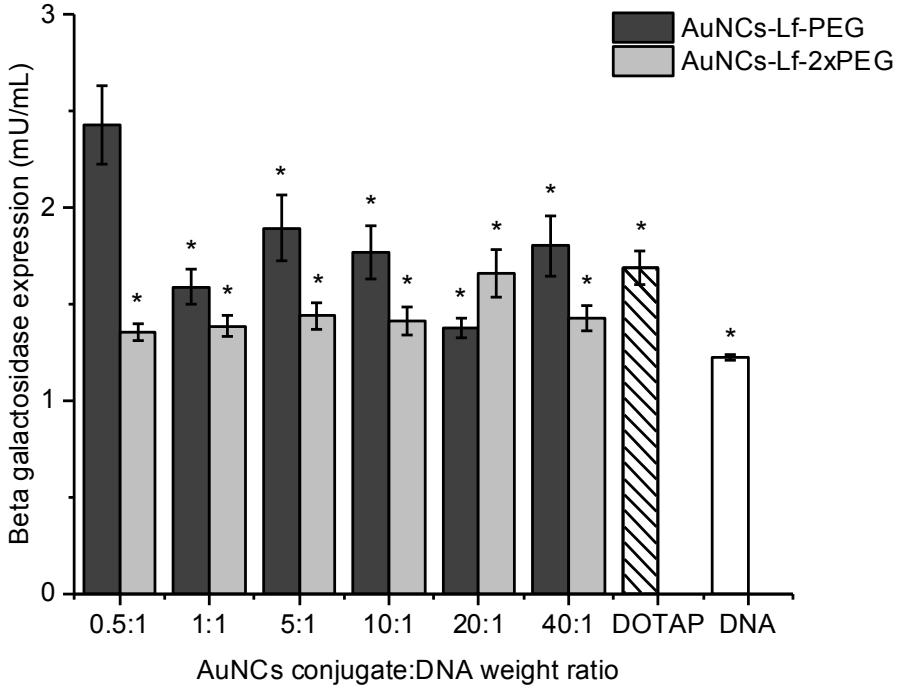

Figure 4-4: Transfection efficacy of AuNCs-Lf-PEG and AuNCs-Lf-2xPEG in PC-3 cells. Results are expressed as the mean ± SEM of three replicates (n = 15). *: $P < 0.05$ versus the highest transfection ratio.

4.3.1.2.3. AuNCs-Lf-PLL and AuNCs-PLL-Lf complexes

The transfection efficacy of AuNCs-Lf-PLL and AuNCs-PLL-Lf complexes was also tested to assess the effect of the conjugation of PLL and Lf of AuNCs on gene transfection (Figure 4-5). The highest transfection level was found at a weight ratio of 20:1 for AuNCs-Lf-PLL complex (2.17 ± 0.07 mU/mL) and at a ratio 40:1 as a result of treatment with AuNCs-PLL-Lf complex (1.98 ± 0.17 mU/mL). The transfection efficacy of the AuNCs-Lf-PLL complex at a weight ratio 20:1 was 1.87-folds higher than that obtained with DNA (1.16 ± 0.01 mU/mL) and 1.29-fold higher than that obtained with DOTAP (1.68 ± 0.09 mU/mL). However, the transfection efficacy of the AuNCs-PLL-Lf complex at weight ratio 40:1 was 1.71- and 1.18-fold higher than that obtained with DNA and DOTAP, respectively.

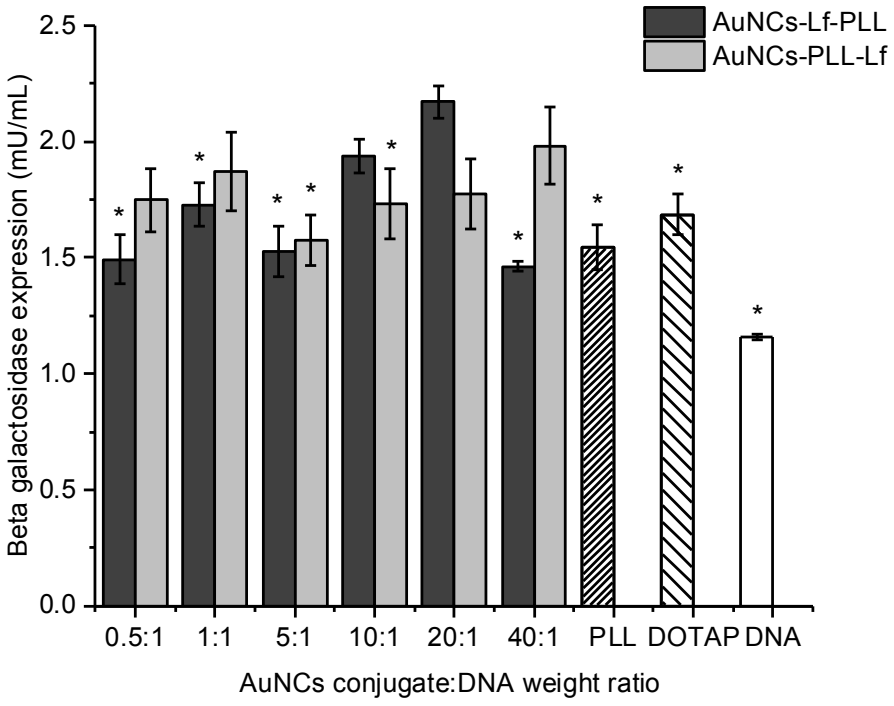

Figure 4-5: Transfection efficacy of AuNCs-Lf-PLL and AuNCs-PLL-Lf in PC-3 cells. Results are expressed as the mean ± SEM of three replicates (n = 15). *: $P < 0.05$ versus the highest transfection ratio.

4.3.1.2.4. AuNCs-DAB-Lf complex

The treatment with AuNCs-DAB-Lf complexed with DNA induced gene transfection at weight ratios of 5:1, 10:1 and 20:1 on PC-3 cells (Figure 4-6). The highest transfection level was observed following treatment with AuNCs-DAB-Lf complex at a weight ratio of 10:1 (3.44 ± 0.23 mU/mL). At this ratio, transfection efficacy was 2.97-fold higher than when treated with DNA (1.16 ± 0.01 mU/mL), 2.05-fold higher than DOTAP (1.68 ± 0.09 mU/mL) and 1.86-fold higher than DAB (1.85 ± 0.08 mU/mL). Notably, AuNCs-Lf-DAB was aggregated during the synthesis process and could therefore not be used to assess transfection efficacy.

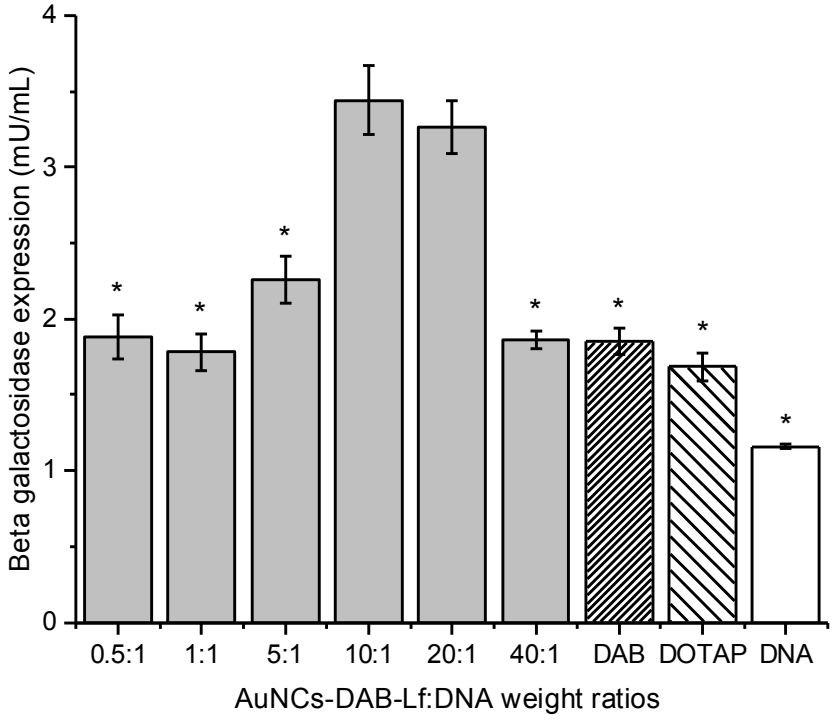

Figure 4-6: Transfection efficacy of AuNCs-DAB-Lf in PC-3 cells. Results are expressed as the mean ± SEM of three replicates (n = 15). *P < 0.05 versus the highest transfection ratio.

4.3.2. Cellular uptake

4.3.2.1. Quantitative analysis

4.3.2.1.1. AuNCs-Lf, AuNCs-PEG-Lf, AuNCs-Lf-PEG and AuNCs-Lf-PEI

The uptake of fluorescence-labelled DNA by PC-3 cells was quantitatively measured using flow cytometry. Based on transfection assay results, the cellular uptake of fluorescence-labelled DNA complexed with AuNCs-Lf, AuNCs-PEG-Lf, AuNCs-Lf-PEG and AuNCs-Lf-PEI by the prostate cancer cells was examined at conjugate:DNA weight ratios of 0.5:1 and 40:1 (Figure 4-7).

For the AuNCs-Lf complex, the highest level of DNA uptake was found at a weight ratio of 40:1 with a fluorescence mean of 725.17 ± 15.72 arbitrary units (a.u.), while the lowest DNA uptake was found at a weight ratio of 0.5:1, with a fluorescence mean of 322.83 ± 33.93 (a.u.). The cellular fluorescence observed following treatment with AuNCs-Lf complex at a weight ratio of 40:1 was 3.64-fold higher than that with DNA (199.50 ± 1.31 a.u.).

For PEGylated AuNCs-Lf complexes, PC-3 cells showed low cellular fluorescence following treatment with AuNCs-PEG-Lf and AuNCs-Lf-PEG complexes. At a weight ratio of 40:1, the highest fluorescence level was observed after treatment with AuNCs-PEG-Lf complex with a fluorescence mean of 388.17 ± 27.69 a.u. compared to that observed with the AuNCs-Lf-PEG complex, with a fluorescence mean of 247.50 ± 3.53 (a.u.). At a weight ratio of 0.5:1, the highest cellular fluorescence was observed following treatment with AuNCs-PEG-Lf complex with a fluorescence mean of 367.17 ± 21.48 a.u., compared to that observed as a result of treatment with AuNCs-Lf-PEG complex, with a fluorescence mean of 242.00 ± 2.27 a.u.

However, the treatment of PC-3 cells with AuNCs-Lf-PEI complexed with fluorescein-labelled DNA at a weight ratio 40:1 induced higher cellular fluorescence (1726.17 ± 49.71 a.u.) than that observed with AuNCs-Lf, AuNCs-PEG-Lf and AuNCs-Lf-PEG complexes (725.17 ± 15.72, 388.17 ± 27.69 and 247.50 ± 3.53 a.u., respectively) at the same ratio. The cellular fluorescence of the AuNCs-Lf-PEI complex was 8.65-fold higher than that observed after treatment with DNA solution (199.50 ± 1.31 a.u.). As expected, the treatment of cells with naked DNA resulted in a weak DNA uptake, indicating the failure of DNA to be taken up by prostate cancer cells without the assistance of a carrier.

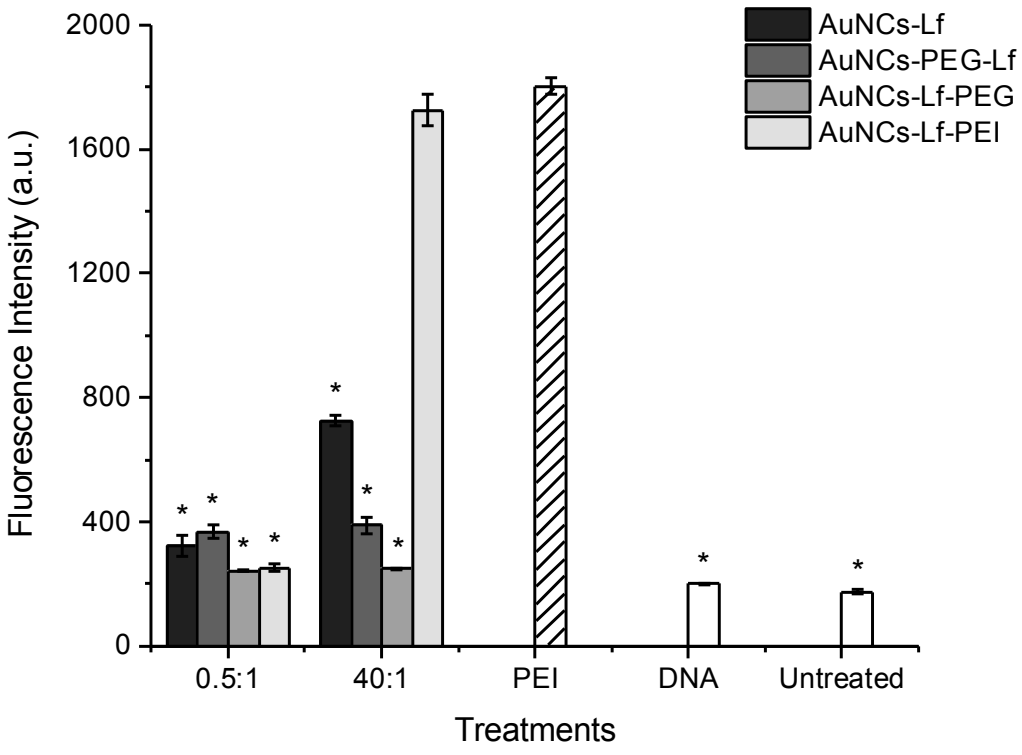

Figure 4-7: Quantification of the cellular uptake of fluorescein-labelled DNA complexed with AuNCs-Lf, AuNCs-PEG-Lf, AuNCs-Lf-PEG and AuNCs-Lf-PEI or left uncomplexed after 24 h incubation with PC-3-Luc cells, using flow cytometry *(n = 6).* *: $P < 0.05$ versus the highest cellular uptake.

4.3.2.1.2. AuNCs-PLL-Lf and AuNCs-Lf-PLL

The cellular fluorescence of AuNCs-PLL-Lf and AuNCs-Lf-PLL complexes was measured to examine the effect of the conjugation process on DNA cellular uptake (Figure 4-8). The highest cellular fluorescence was observed from PC-3 cells treated with AuNCs-Lf-PLL complex at a weight ratio of 10:1 (3116.67 ± 173.41 a.u.), which is 14.7-fold higher than that observed with AuNCs-PLL-Lf at the same ratio (212.33 ± 3.01 a.u.). Similarly, PC-3 cells treated with AuNCs-Lf-PLL complex at a weight ratio of 20:1 showed higher cellular fluorescence (1436.17 ± 16.23 a.u.), which is 6.6-fold higher than that observed from the AuNCs-PLL-Lf complex at the same ratio (218.17 ± 4.74 a.u.). The cellular fluorescence of the AuNCs-Lf-PLL complex at a weight ratio 10:1 was 1.32-fold and 15.62-fold higher than that observed after treatment with PLL (2364.33 ± 181.93 a.u.) and DNA solution (199.50 ± 1.31 a.u.).

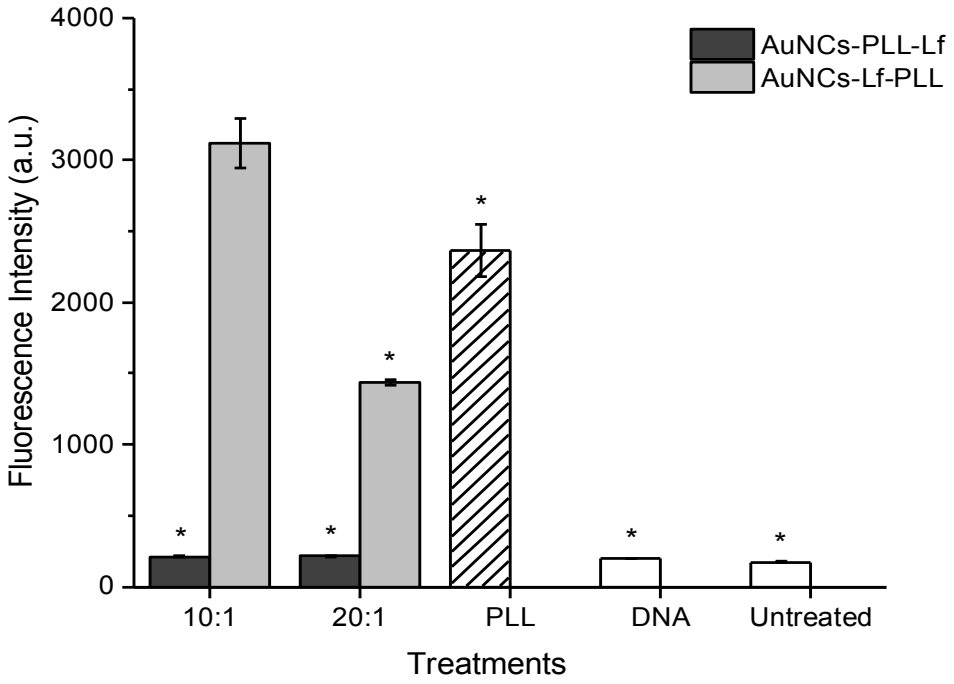

Figure 4-8: Quantification of the cellular uptake of fluorescein-labelled DNA complexed with AuNCs-PLL-Lf, AuNCs-Lf-PLL or left uncomplexed, after 24 h incubation with PC-3 cells, using flow cytometry *(n = 6)*. *: $P < 0.05$ versus the highest cellular uptake.

4.3.2.1.3. AuNCs-DAB-Lf

The highest cellular uptake level of the AuNCs-DAB-Lf complex on PC-3 cells was observed at a weight ratio of 10:1 with a cellular fluorescence of 6896.33 ± 353.48 a.u. compared with cells treated with the same complex at a weight ratio of 20:1 (6038.17 ± 79.83 a.u.) (Figure 4-9). The cellular fluorescence of the AuNCs-DAB-Lf complex at a weight ratio of 10:1 was 1.53-fold and 35.57-fold higher than that observed after treatment with DAB (4517.33 ± 152.27 a.u.) and DNA solution (199.50 ± 1.31 a.u.). Also, the treatment of cells with naked DNA induced weak DNA uptake, indicating the failure of DNA to be taken up by prostate cancer cells without the assistance of a delivery system.

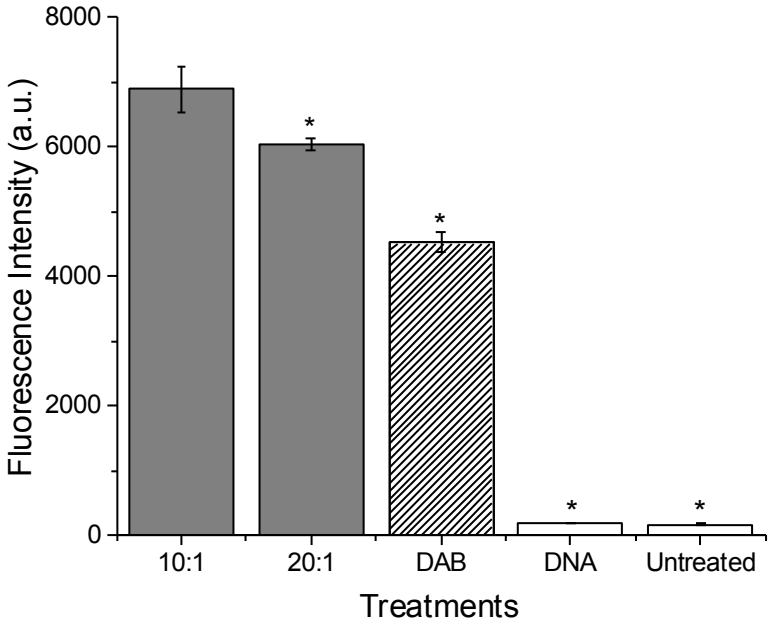

Figure 4-9: Quantification of the cellular uptake of fluorescein-labelled DNA complexed with AuNCs-DAB-Lf or left uncomplexed after 24 h incubation with PC-3 cells, using flow cytometry *(n = 6)*. *: $P < 0.05$ versus the highest cellular uptake.

4.3.2.2. Confocal microscopy

The cellular uptake of fluorescein-labelled DNA complexed with AuNCs-Lf-PEI, AuNCs-Lf-PLL and AuNCs-DAB-Lf by PC-3 cells was qualitatively confirmed using confocal microscopy (Figure 4-10). Fluorescein-labelled DNA was disseminated in the cytoplasm after treatment with the complexes. However, in line with the flow cytometry results, the DNA uptake appeared to be increasingly pronounced in the cells treated with AuNCs-DAB-Lf, then with AuNCs-Lf-PLL, and finally with AuNCs-Lf-PEI complexes. However, cells treated with the DNA solution did not show any fluorescein-derived fluorescence. AuNCs-Lf conjugates therefore enhanced the DNA uptake by PC-3 prostate cancer cells. No co-localisation of DNA in the nuclei was visible after 24 h incubation, leading to the hypothesis that the nuclear uptake of the DNA occurred at a later time.

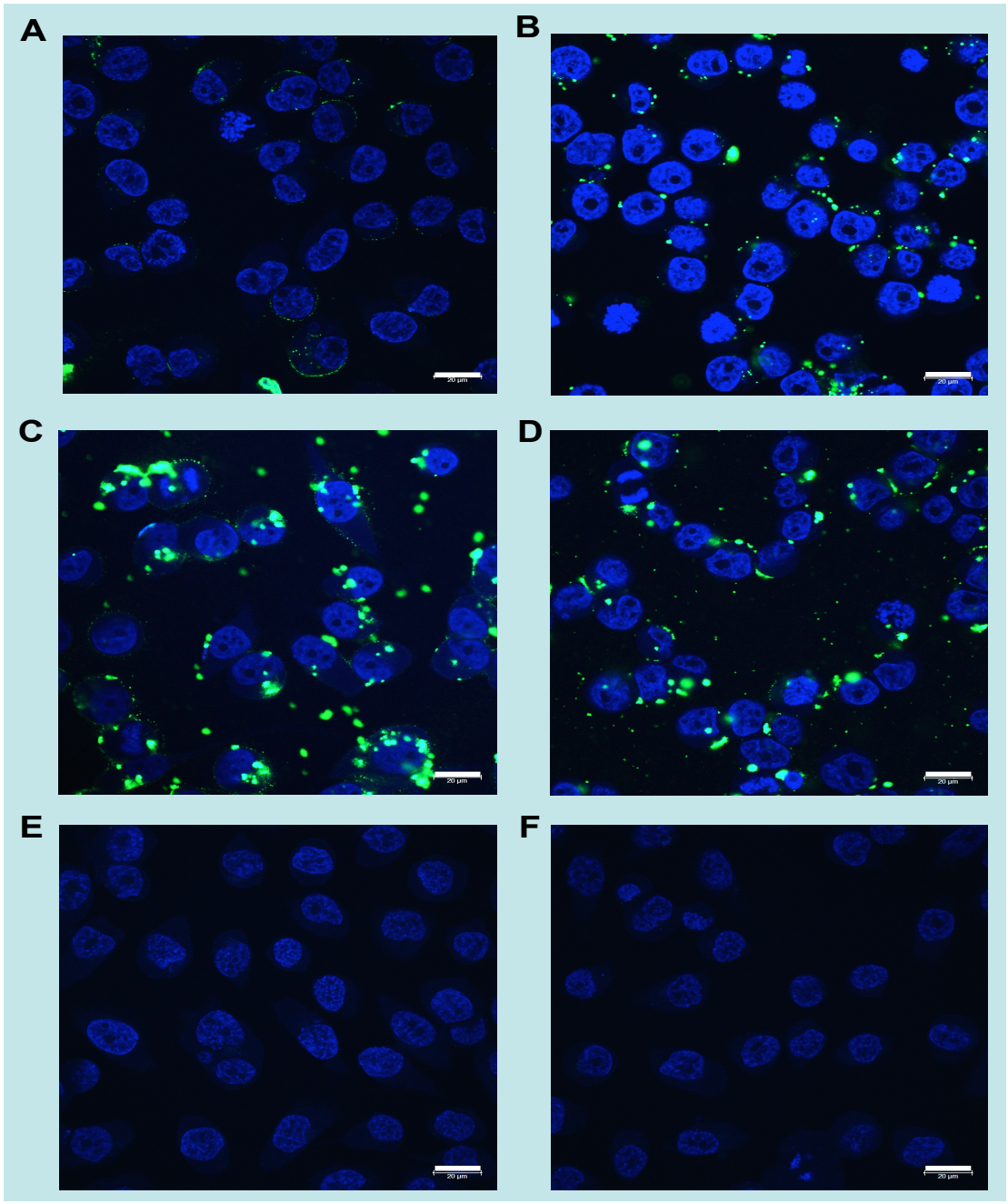

Figure 4-10: Confocal microscopy images of the cellular uptake of fluorescein-labelled DNA (2.5 µg per well), complexed with A) AuNCs-Lf-PEI at conjugate:DNA weight ratio of 40:1, B) AuNCs-Lf-PLL at conjugate:DNA weight ratio of 10:1, C) AuNCs-DAB-Lf at conjugate:DNA weight ratio of 10:1, D) DAB at a weight ratio of 5:1, and E) free in solution (F: untreated cells) after 24 h incubation with PC-3 cells. Blue: nuclei stained with DAPI (excitation: 405 nm laser line; bandwidth: 415–491 nm), green: fluorescein-labelled DNA (excitation: 453 nm laser line; bandwidth: 550–620 nm) (magnification: ×63) (bar: 20 µm).

4.3.3. Anti-proliferative assay: MTT assay

4.3.3.1. AuNCs-DAB-Lf

The treatment of PC-3 cells with AuNCs-DAB-Lf complexed with DNA-encoding TNFα at the weight ratios of 40:1 and 10:1 induced an increase in the *in vitro* anti-proliferative efficacy, respectively, by 9- and 2.4-fold, with an IC_{50} of 1.80 ± 0.31 and 6.66 ± 1.87 μg/mL compared with the positive control DAB dendriplex (IC_{50}: 16.28 ± 1.31 μg/mL) (Figure 4-11 A–B).

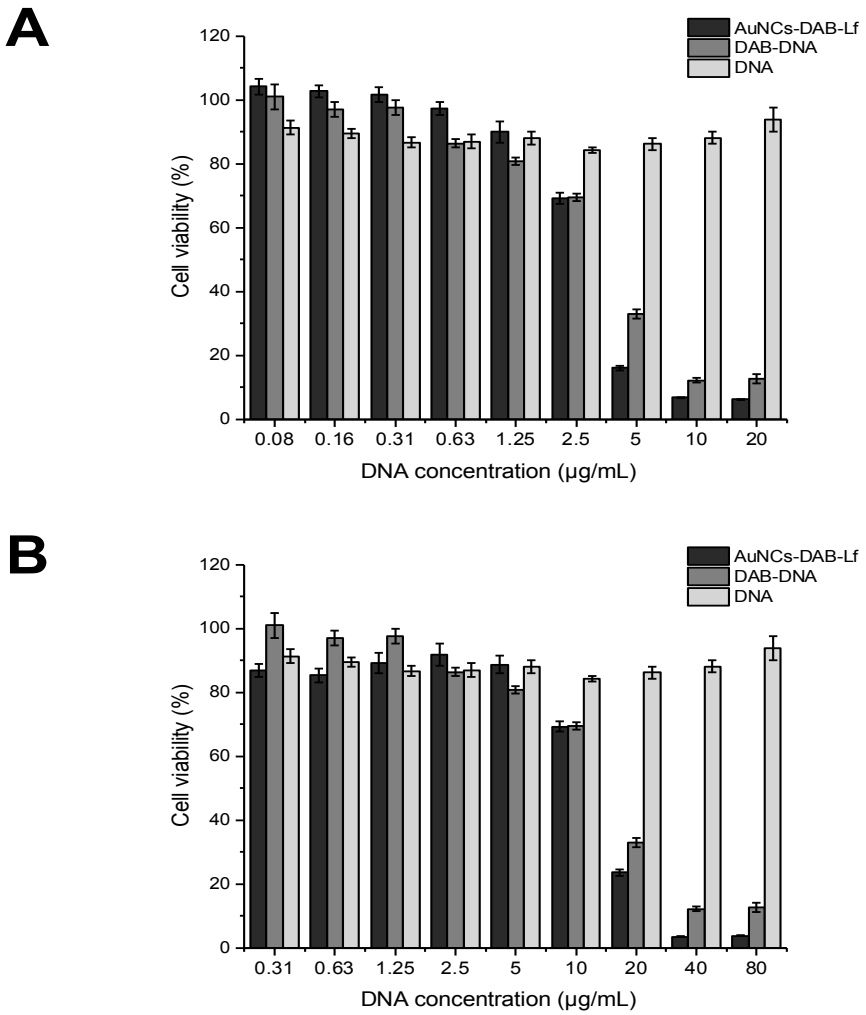

Figure 4-11: Anti-proliferative activity of AuNCs-DAB-Lf complexed with DNA-encoding TNFα at conjugate:DNA weight ratio of 40:1 (A) and 10:1 (B) in PC-3 cells (*n = 15*).

4.3.3.2. AuNCs-Lf-PLL

AuNCs-Lf-PLL complexed to DNA-encoding TNFα increased the anti-proliferative effect by 2.06-fold (IC_{50}: 4.74 ± 0.81 µg/mL) compared to the positive control PLL polyplex, which had an IC_{50} of 9.78 ± 0.56 µg/mL (Figure 4-12).

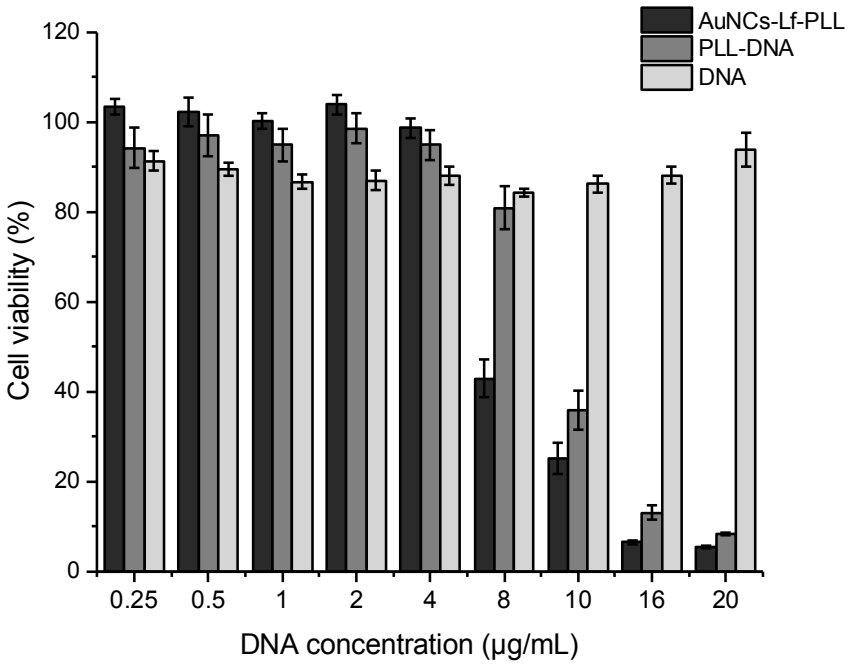

Figure 4-12: Anti-proliferative activity of AuNCs-Lf-PLL complexed with DNA-encoding TNFα at conjugate:DNA weight ratio of 10:1 in PC-3 cells (*n = 15*).

4.3.3.3. AuNCs-Lf-PEI, AuNCs-Lf-PEG and AuNCs-Lf

AuNCs-Lf-PEI, AuNCs-Lf-PEG and unmodified AuNCs-Lf complexed with DNA-encoding TNFα did not show any anti-proliferative activity on PC-3 cells at the tested concentrations compared with AuNCs-DAB-Lf and AuNCs-Lf-PLL

conjugates (Figure 4-13). These results suggest the need to modify the concentration of complexed DNA (Table 4-1).

However, uncomplexed lactoferrin-bearing gold nanocage conjugates did not exert any cytotoxicity on PC-3 cells, demonstrating that the anti-proliferative efficacy of therapeutic DNA complexed to AuNCs-Lf conjugates most probably resulted from DNA internalisation into the cells only.

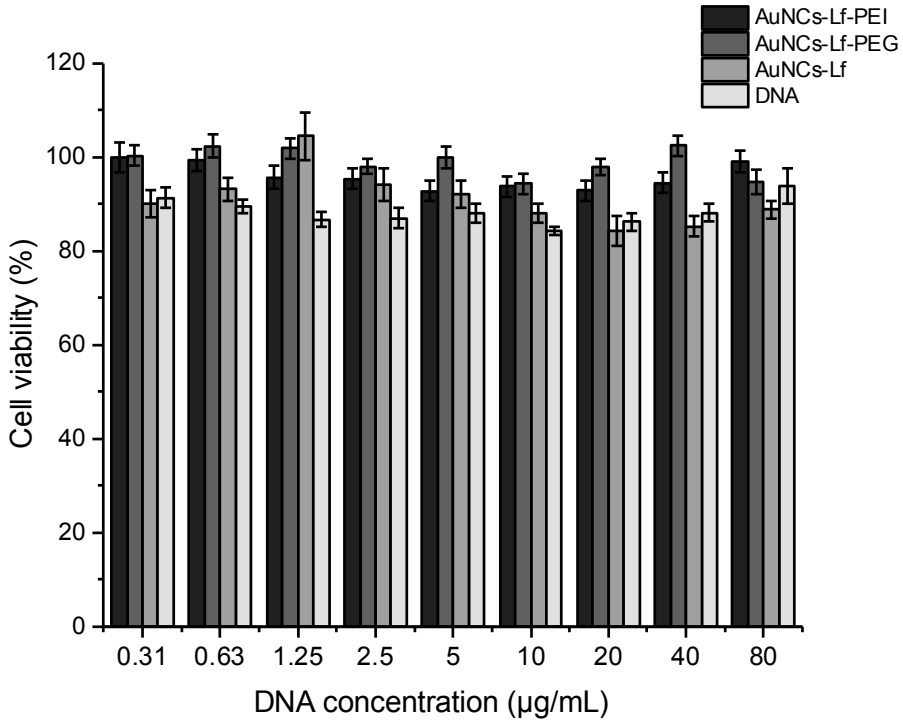

Figure 4-13: Anti-proliferative activity of AuNCs-Lf-PEI, AuNCs-Lf-PEG and unmodified AuNCs-Lf complexed with DNA-encoding TNFα at a weight ratio of 10:1 in PC-3 cells (*n = 15*).

Table 4-1: Anti-proliferative activity of various lactoferrin-bearing gold nanocages formulations complexed to DNA-encoding TNFα in PC-3 cells, expressed as IC_{50} values (*n = 15*).

Formulation	**IC_{50} (μg/mL) (mean ± SEM)**
AuNCs-DAB-Lf-DNA	6.66 ± 1.87
AuNCs-Lf-PLL-DNA	4.74 ± 0.81
AuNCs-Lf-PEI-DNA	>50
AuNCs-Lf-PEG-DNA	>50
AuNCs-Lf-DNA	>50
DAB-DNA	16.28 ± 1.31
PLL-DNA	9.78 ± 0.56
DNA	n.d.

n.d. : not determined

4.4. Discussion

The possibility of using gold nanocages as gene delivery systems for cancer treatment has previously been reported jointly with photothermal therapy and chemotherapeutics but has never been assessed in isolation and without external stimulations so far. To explore this possibility, we hypothesise that the conjugation of a targeting ligand lactoferrin, PEG, PEI, PLL and DAB on gold nanocages complexed to plasmid DNA would induce enhanced gene expression, cellular uptake and anti-proliferative activity in PC-3 prostate cancer cells.

In the previous chapter, we successfully synthesised lactoferrin-bearing gold nanocage conjugates as novel non-viral gene delivery systems and presented their potent DNA condensation efficacy. This chapter therefore is dedicated to *in vitro* evaluation of these conjugates to study the gene expression, cellular uptake and therapeutic efficacy on prostate cancer cells, which are required before undertaking any *in vivo* investigations.

In vitro, the treatment of PC-3 cells with AuNCs-Lf resulted in an enhanced transfection compared to the positive controls PEI and DOTAP. This result is in line with reports that showed that conjugating Lf to various delivery systems significantly improved gene expression in cancer cell lines. For instance, Lim and colleagues demonstrated that conjugating Lf to a generation 3-diaminobutyric polypropylenimine dendrimer (DAB) resulted in a 1.4-fold higher gene expression compared with unconjugated DAB on A431 and B16F10 cells (Lim *et al.*, 2015). Similarly, Altwaijry and colleagues reported that treating PC-3 cells with DAB-Lf dendriplex induced 2-fold higher gene expression compared to unmodified DAB (Altwaijry *et al.*, 2018b). In this study, gene expression following treatment with

AuNCs-Lf complex was 1.5 and 1.3-fold higher than that obtained with PEI and DOTAP, respectively.

Furthermore, the conjugation of AuNCs-Lf with PEG, PLL, PEI and DAB induced a significant enhancement in gene transfection compared with unmodified AuNCs-Lf. Gene expression following treatment with AuNCs-Lf-PEI, AuNCs-Lf-PLL, AuNCs-DAB-Lf and AuNCs-Lf-PEG complexes at their optimal AuNCs conjugate:DNA ratios (40:1 for AuNCs-Lf-PEI, 20:1 for AuNCs-Lf-PLL, 10:1 for AuNCs-DAB-Lf and 0.5:1 for AuNCs-Lf-PEG) was, respectively, 1.6-, 1.2-, 1.8- and 1.1-fold higher than that obtained from unmodified AuNCs-Lf complex. The grafting of PEG onto AuNCs-Lf, which increased the transfection efficacy by 1.5 compared to the positive control DOTAP, has previously been shown to improve the gene transfection of various delivery systems. For example, Somani *et al.* (2018) reported that PEGylated dendrimers showed significantly higher transfection levels compared to non-PEGylated dendrimers in B16F10-Luc, A431, T98G, DU145 and PC-3-Luc cancer cell lines. In the PC-3 cell line, the highest gene expression obtained by PEGylated G3-dendrimers was 2.7-fold higher than with unmodified dendrimers. For gold-based delivery systems, Luan *et al.* (2019) demonstrated that the PEGylation of gold nanoparticles led to significantly increased gene silencing in PC-3 cells compared to Lipofectamine® 2000 (a lipid-based transfection reagent used as a positive control). In another study, the PEGylation of gold nanoparticles induced an increase in transfection efficacy and cellular uptake by more than 45%, with low cytotoxicity, compared with non-PEGylated nanoparticles (Zamora-Justo *et al.*, 2019). Moreover, it has recently been reported that PEGylated gold nanoparticles tested in HeLa cells showed a high level of gene expression similar to those obtained from PEI (Li *et al.*,

2020). In this study, the gene expression after treatment with AuNCs-Lf-PEG was 1.7-fold higher than that obtained with the PEI complex

The grafting of PLL to AuNCs-Lf also induced a significant improvement in transfection efficacy by 1.3- and 1.4-fold compared to DOTAP and PLL polyplex, respectively. This result supports previous reports showing that the grafting of PLL to delivery systems resulted in remarkable enhancement of their gene expression. Aldawsari and colleagues demonstrated that the grafting of PLL to the PEI polyplex induced significant improvement of the transfection level on A431 and T98G cells compared to unmodified PEI polyplex (Aldawsari *et al.*, 2011b). The gene expression observed after treatment with PEI-PLL polyplex was 2.2 and 3-fold higher than that obtained with unmodified PEI polyplex on A431 and T98G cells, respectively. Furthermore, Aldawsari and co-workers also demonstrated that the conjugation of PLL to a DAB polyplex led to an increase in the transfection level compared to an unmodified DAB polyplex (Aldawsari *et al.*, 2011a). The gene expression following treatment with the DAB-PLL polyplex was 1.9-fold higher than that with the unmodified DAB polyplex on both A431 and T98G cells. In this study, the gene expression after treatment with AuNCs-Lf-PLL was 1.2 and 1.5-fold higher than that obtained with unmodified DAB and PEI polyplex, respectively.

The transfection efficacy following treatment with AuNCs-Lf-PEI complex was 1.5-fold higher than that with DOTAP. This result supports previous studies that demonstrated that conjugating gold nanoparticles with PEI improves the transfection efficacy. For example, Kilbanov and Thomas (2003) demonstrated that the gene transfection obtained in COS-7 monkey kidney cells upon treatment with PEI-AuNP conjugates was 12-fold more potent than that of unmodified PEI. In another study,

the enhanced transfection efficacy of Au-PEI conjugates was 3-fold higher than that of unmodified PEI in HeLa cells (Tian *et al.*, 2012). However, it has been reported that the AuNPs-PEI might have transfection efficacy lower than or like unmodified PEI, and their transfection efficacy could be reduced after adding targeting ligand. For example, gold nanoparticles modified with targeting ligand folate (FA) and polyethylenimine (AuNPs-FA-PEI) exhibited transfection efficacy lower than those with both PEI and unmodified AuNPs-PEI in HeLa cells (Li *et al.*, 2019). Furthermore, the transfection efficacy of AuNPs-FA-PEI was less than half that obtained from unmodified AuNPs-PEI. The reduction in gene transfection was explained due to the small amount of PEI modified onto the AuNP surface and due to the presence of folic acid that decreased the buffer capacity of PEI, which, in turn, reduced the transfection efficacy of AuNPs-FA-PEI. In this study, the transfection efficacy following treatment with the AuNCs-Lf-PEI complex was 1.7-fold higher than that with PEI and 1.6-fold higher than that with unmodified AuNCs-Lf.

Conjugating DAB to AuNCs-Lf induced an enhanced transfection level at the optimum weight ratio 10:1 by 2.1- and 1.9-fold compared to DOTAP and DAB dendriplex, respectively, and these results corroborate other reported studies. For instance, Ghosh *et al.* (2008b) demonstrated that lysine dendrimer-functionalised gold nanoparticles efficiently condensed the DNA and significantly enhanced β-gal gene expression by 28-fold in Cos-1 monkey kidney cells compared to that observed following treatment with the positive control polylysine. Kim *et al.* (2012) also demonstrated that dendron-conjugated gold nanoparticles improved gene silencing by 48% at an NP/siRNA ratio of 2, for which the siRNA was fully complexed, and

showed therefore a knockdown efficacy similar to that obtained from positive control Lipofectamine® in SVR-bag4 endothelial cells.

In this study, the enhancement of β-gal expression induced by AuNCs-Lf-PEG, AuNCs-Lf-PEI, AuNCs-Lf-PLL and AuNCs-DAB-Lf conjugates compared to unmodified AuNCs-Lf most likely resulted from the higher zeta potential of these DNA complexes due to the strong correlation between the cellular uptake and the positive charge density of the complexes (Futaki *et al.*, 2001). Moreover, the highest transfection efficacy of these gold conjugates could also result from the proton sponge effect of PEI, PLL and DAB, which highly facilitates endosomal escape (Creusat *et al.*, 2010; Kang *et al.*, 2011). Furthermore, the presence of gold nanocages in AuNCs-Lf-PEI, AuNCs-Lf-PLL and AuNCs-DAB-Lf could also play a role in improving their β-gal expression compared to PEI, PLL and DAB polyplex. This improvement in gene expression could be attributed to the presence of rigid gold nanoparticles in gene carriers that 1) preserved the 3D structures of the attached polymers, enabling the high condensation of DNA into small complexes, 2) promoted the mono-dispersity of these complexes, and 3) facilitated DNA internalisation into the cells, consequently resulting in enhanced gene transfection more than that obtained from polyplexes (Tencomnao *et al.*, 2011; Shan *et al.*, 2012). Also, this may be because the complexed DNA could be easily released from the gold conjugate after cell internalisation, whereas, for the polyplex, the DNA would be tightly condensed, thereby making the disassociation from the polyplex and release within the cells more difficult (Wong *et al.*, 2007). The shape of nanoparticles is another factor that may affect gene delivery efficacy and cell internalisation. Morgan *et al.* (2019) investigated the effect of the shape of three gold

nanoparticle formulations (nanocages, nanoshells and nanorods) that covalently attached to thiol-siRNA in HeLa cells under NIR laser irradiation. Both gold nanocages and nanoshells displayed high knockdown efficacy with high particle concentrations, demonstrating the efficient internalisation of gold nanocages and nanoshells into HeLa cells compared to that observed from gold nanorods. It was found that doubling the particle concentration of nanorods induced a 2-fold enhancement of GFP knockdown efficacy, demonstrating the need for a larger amount of nanorod particles to induce a similar GFP knockdown level to that observed for the nanocages and nanoshells. These findings highlighted the importance of cage shape when using gold nanoparticles as a gene delivery system by showing the strong impact of the gold nanoparticle shape on cellular internalisation and therefore on the efficacy of gene expression.

The cellular uptake of DNA complexed to AuNCs-Lf-PEI, AuNCs-Lf-PLL and AuNCs-DAB-Lf was significantly enhanced ($p < 0.05$) compared to that obtained with unmodified AuNCs-Lf due to the grafting of PEI, PLL and DAB that, as mentioned before, mediated the proton sponge effect, causing the endosomal escape of DNA. However, AuNCs-Lf-PEG showed a lower level of DNA uptake after 24 h incubation compared with AuNCs-Lf, leading to the hypothesis that DNA uptake following this treatment occurred at a later time owing to the PEG effect in reducing cellular uptake (Mishra *et al.*, 2004). Also, the cellular uptake level of the DNA complexed to AuNCs-Lf-PLL and AuNCs-DAB-Lf significantly exceeded that observed from the positive control DAB and PLL polyplexes (at a similar level when comparing AuNCs-Lf-PEI with PEI polyplex). The structure and unique morphology of gold nanocages could contribute to the enhancement of cellular uptake over other

types of nanoparticles. Robinson *et al.* (2015) found that gold nanocages were taken up by DU145 prostate cancer cells 28% more than gold nanorods. They were also taken up by HUVEC human umbilical vein endothelial cells 18% more than the nanorods. These findings indicate that the shape of gold nanocages plays a pivotal role in facilitating their cellular uptake in prostate cancer cells and in normal cells. In this study, the high cellular uptake of gold conjugates over the positive control polyplex could also be attributed to the rigid structure of gold nanoparticles, which has been reported to enhance cellular uptake compared to delivery systems bearing softer structures, such as liposomes and polymeric nanoparticles (Sun *et al.*, 2015). Liu *et al.* (2018) investigated the impact of nanoparticle rigidity on cellular uptake using G5 dendrimers as soft nanoparticles and dendrimers-coated gold nanoparticles as rigid nanoparticle models. They found that the cellular uptake of dendrimer-coated gold nanoparticles was 3.2-fold higher than that observed from dendrimers in both U87MG cancer cells and L929 normal cells. As the adsorption and cellular uptake of nanoparticles depend on their size, shape, charge and surface modification, the enhanced cellular uptake of the gold conjugates could also be due to the cationic polymer modification on the surface of gold nanocages and the positive surface charge of gold complexes. Cho *et al.* (2010) demonstrated that PAA-coated gold nanocages, which had a positive charge of +15.9 ± 2.7 mV, were taken by SK-BR-3 BC cells in larger amounts than negatively charged gold nanocages modified with anti-HER2 antibody (−2.7 ± 4.9 mV) and PEG-modified gold nanocages (−2.0 ± 5.4 mV).

Apoptosis (or controlled cell death) is a major technique utilised in gene therapy that involves facilitating cancer cells to express the cytokines necessary for this normal

physiological process. Cytokine expression occurs upon efficient delivery and transfection of plasmid DNA encoding these cytokines to the cells and nucleus, respectively. The TNFα cytokine was chosen for this study because of its well-known ability to induce apoptosis in different cancer cell lines (Aldawsari *et al.*, 2011a; Altwaijry *et al.*, 2018b).

The grafting of DAB and PLL to AuNCs-Lf significantly improved the *in vitro* therapeutic efficacy of the complexed DNA-encoding TNF in PC-3 prostate cancer cells, with lower IC_{50} values among AuNCs-Lf conjugates. The most efficacious treatment in this study was observed for AuNCs-DAB-Lf complexed with DNA encoding TNF, which enhanced the anti-proliferative activity by 9-fold compared to DAB dendriplex. The second-best treatment in this experiment was the AuNCs-Lf-PLL complex, which also induced an improvement of the anti-proliferative efficacy by 2.1-fold, compared to PLL polyplex. These findings could be attributed to improved gene expression efficacy and efficient cellular uptake followed by treatment with AuNCs-DAB-Lf and AuNCs-Lf-PLL complexes. Further, the MTT assay results of AuNCs-Lf complexes indicated that the therapeutic effect achieved could be attributed to the efficient delivery of the therapeutic gene, as AuNCs-Lf conjugates demonstrated a minimum anti-proliferative effect. In our previous study, Altwaijry *et al.* (2018b) found that Lf-bearing DAB (DAB-Lf) dendriplex-encoding TNF led to improved anti-proliferative activity by 1.9-fold in PC-3 cells compared with unmodified DAB dendriplex. Therefore, the higher anti-proliferative activity of AuNCs-DAB-Lf complex over DAB-Lf dendriplex compared with DAB dendriplex indicates the importance of AuNCs in improving gene therapeutic effect due to AuNCs' crucial role in enhancing transfection efficacy and cellular uptake.

Chapter 5: Conclusion and future works

5.1. Conclusion

This study revealed for the first time the effectiveness of using gold nanocages as targeted gene carriers for prostate cancer cells without external stimulation, resulting in a promising gene therapy platform to treat prostate cancer, even as a single therapy.

Using our modified protocol, gold nanocages with uniform shapes and controlled sizes were successfully prepared in large quantities. The large-scale production of the gold nanocages allowed us to conduct all experiments in this study using the same batch of gold nanocages. Further, the prepared gold nanocages had a particle size of less than 90 nm and exhibited UV-Vis spectra in the NIR region, which is ideal for gene delivery and photothermal therapy applications. This study revealed that lactoferrin-bearing gold nanocages alone or conjugated with cationic polymers were able to complex with plasmid DNA at conjugate:DNA weight ratios higher than 1:1, forming their smallest complex sizes with positive zeta potentials at the maximum tested weight ratio of 40:1. These results were translated *in vitro* into a higher DNA transfection level compared to the positive controls on PC-3 prostate cancer cells. Among the tested conjugates, AuNCs-DAB-Lf and AuNCs-Lf-PLL induced the highest transfection level on PC-3 cells compared to their positive controls, DAB dendriplex and PLL polyplex. This was probably due to the significant increase in cellular uptake of DNA in PC-3 cells following treatment with this complex compared with what was observed in cells treated with DAB dendriplex and PLL polyplex. This further resulted in a significant improvement in the anti-proliferative activity of therapeutic plasmid DNA-encoding TNFα by up to 9-fold and 2.1-fold when complexed with AuNCs-DAB-Lf and AuNCs-Lf-PLL, respectively, compared

to DAB dendriplex and PLL polyplex-encoding TNFα. To our knowledge, this is the first time that lactoferrin-bearing gold nanocage conjugates have been used to target prostate cancer cells, leading to enhanced DNA uptake, gene expression and anti-proliferative activity in PC-3 prostate cancer cells without involving external stimulation. Lactoferrin-bearing gold nanocage conjugates are therefore promising gene nanocarriers for prostate cancer cells and will be further investigated, alone or synergistically with other cancer therapies.

5.2. Future works

In this study, novel lactoferrin-bearing gold nanocage conjugates were developed, characterised and evaluated *in vitro* as potential targeted gene delivery systems for enhancing DNA uptake and gene expression in PC-3 prostate cancer cells while promoting the *in vitro* efficacy of therapeutic DNA without external stimulation. The results obtained from this study confirm the hypothesis that lactoferrin-bearing gold nanocage conjugates are highly promising gene carriers for single-approach cancer treatment and are encouraging for future development.

Based on the findings obtained, lactoferrin-bearing gold conjugates should be subjected to further *in vitro* evaluations of other prostate cancer cell lines, such as DU145 and LNCaP cells, as the lactoferrin receptors are also overexpressed on their surface membrane. Furthermore, the anti-proliferative efficacy of lactoferrin-bearing gold conjugates complexed with various therapeutic DNA, such as DNA-encoding tumour necrosis factor-related apoptosis-inducing ligand (TRAIL) or Interleukin (IL-12) could be examined. Moreover, to further confirm the hypothesis that using lactoferrin-bearing gold nanocages for targeted gene delivery would reduce secondary effects on healthy tissues, the cytotoxicity of lactoferrin-bearing gold conjugates should be evaluated in normal cell lines, such as WS1 skin fibroblast cells, MRC-5 lung fibroblast cells, HL-7702 hepatic cells and HK-2 renal epithelial cells. Before *in vivo* studies, it would be important to examine the interactions of AuNCs-Lf conjugates with the protein corona for potential *in vivo* applications. When exposed to biological fluids, nanoparticles tend to interact with biomolecules, thereby forming a complex layer of proteins called protein corona. The presence of this protein corona on the surface of nanoparticles has previously been shown to

impact the cellular internalisation of the delivery systems and the release of the entrapped drugs, modifying the biological response *in vivo* (Monopoli *et al.*, 2012; Van Hong Nguyen, 2017). It is hoped that the surface modification of AuNCs with Lf and cationic polymers will minimise protein adsorption and alter the corona composition, as previously reported. Further, Assali and colleagues demonstrated that functionalised gold nanoplatforms displayed fewer interactions with proteins and adsorbed less opsonin than their unmodified counterparts (Assali *et al.*, 2019). Therefore, future work should include measuring the size and zeta potential of the AuNCs-Lf complexes using a cell culture medium instead of glucose solution (5%). This would help investigate the impact of the protein corona on the physicochemical characteristics of the complex. Notably, all *in vitro* experiments (DNA cellular uptake, gene expression and MTT analysis) of the gold conjugates in this study were conducted in 10% serum supplemented medium. However, comparing these *in vitro* studies in serum-free medium and medium containing different serum concentrations would provide a better understanding of the cellular response to our gold formulations. Based on our positive *in vitro* results, an *in vivo* investigation, including the evaluation of the anti-cancer efficacy of the conjugates alone or complexed with various therapeutic DNA, would be promising to pursue.

REFERENCES

Aldawsari, H., Edrada-Ebel, R., Blatchford, D. R., Tate, R. J., Tetley, L. & Dufès, C. 2011a. Enhanced gene expression in tumors after intravenous administration of arginine-, lysine-and leucine-bearing polypropylenimine polyplex. *Biomaterials,* 32**,** 5889-5899.

Aldawsari, H., Raj, B. S., Edrada-Ebel, R., Blatchford, D. R., Tate, R. J., Tetley, L. & Dufès, C. 2011b. Enhanced gene expression in tumors after intravenous administration of arginine-, lysine-and leucine-bearing polyethylenimine polyplex. *Nanomedicine: Nanotechnology, Biology and Medicine,* 7**,** 615-623.

Altwaijry, N., Somani, S. & Dufès, C. 2018a. Targeted nonviral gene therapy in prostate cancer. *International Journal of Nanomedicine,* 13**,** 5753-5767.

Altwaijry, N., Somani, S., Parkinson, J. A., Tate, R. J., Keating, P., Warzecha, M., Mackenzie, G. R., Leung, H. Y. & Dufès, C. 2018b. Regression of prostate tumors after intravenous administration of lactoferrin-bearing polypropylenimine dendriplexes encoding TNF-α, TRAIL, and interleukin-12. *Drug Delivery,* 25**,** 679-689.

Assali, A., Razzazan, S., Akhavan, O., Mottaghitalab, F., Adeli, M. & Atyabi, F. 2019. The bio-interface between functionalized Au NR@ GO nanoplatforms with protein corona and their impact on delivery and release system. *Colloids and Surfaces B: Biointerfaces,* 173**,** 891-898.

Avvakumova, S., Pandolfi, L., Soprano, E., Moretto, L., Bellini, M., Galbiati, E., Rizzuto, M., Colombo, M., Allevi, R. & Corsi, F. 2019. Does conjugation strategy matter? Cetuximab-conjugated gold nanocages for targeting triple-negative breast cancer cells. *Nanoscale Advances,* 1**,** 3626-3638.

Baker, J. R. 2009. Dendrimer-based nanoparticles for cancer therapy. *ASH Education Program Book,* 2009**,** 708-719.

Bangham, A. 1993. Liposomes: the Babraham connection. *Chemistry and Physics of Lipids,* 64**,** 275-285.

Beik, J., Khateri, M., Khosravi, Z., Kamrava, S. K., Kooranifar, S., Ghaznavi, H. & Shakeri-Zadeh, A. 2019. Gold nanoparticles in combinatorial cancer therapy strategies. *Coordination Chemistry Reviews,* 387**,** 299-324.

Bertrand, N., Wu, J., Xu, X., Kamaly, N. & Farokhzad, O. C. 2014. Cancer nanotechnology: the impact of passive and active targeting in the era of modern cancer biology. *Advanced Drug Delivery Reviews,* 66**,** 2-25.

Bokkhim, H., Bansal, N., GrØndahl, L. & Bhandari, B. 2013. Physico-chemical properties of different forms of bovine lactoferrin. *Food Chemistry,* 141**,** 3007-3013.

Bonoiu, A. C., Mahajan, S. D., Ding, H., Roy, I., Yong, K.-T., Kumar, R., Hu, R., Bergey, E. J., Schwartz, S. A. & Prasad, P. N. 2009. Nanotechnology approach for drug addiction therapy: gene silencing using delivery of gold nanorod-siRNA nanoplex in dopaminergic neurons. *Proceedings of the National Academy of Sciences,* 106**,** 5546-5550.

Brown, S. D., Nativo, P., Smith, J.-A., Stirling, D., Edwards, P. R., Venugopal, B., Flint, D. J., Plumb, J. A., Graham, D. & Wheate, N. J. 2010. Gold nanoparticles for the improved anticancer drug delivery of the active component of oxaliplatin. *Journal of the American Chemical Society,* 132**,** 4678-4684.

Chen, J., Glaus, C., Laforest, R., Zhang, Q., Yang, M., Gidding, M., Welch, M. J. & Xia, Y. 2010a. Gold nanocages as photothermal transducers for cancer treatment. *Small,* 6**,** 811-817.

Chen, J., Wang, D., Xi, J., Au, L., Siekkinen, A., Warsen, A., Li, Z.-Y., Zhang, H., Xia, Y. & Li, X. 2007a. Immuno gold nanocages with tailored optical properties for targeted photothermal destruction of cancer cells. *Nano Letters,* 7**,** 1318-1322.

Chen, J., Yang, M., Zhang, Q., Cho, E. C., Cobley, C. M., Kim, C., Glaus, C., Wang, L. V., Welch, M. J. & Xia, Y. 2010b. Gold nanocages: a novel class of multifunctional nanomaterials for theranostic applications. *Advanced Functional Materials,* 20**,** 3684-3694.

Chen, Y.-H., Tsai, C.-Y., Huang, P.-Y., Chang, M.-Y., Cheng, P.-C., Chou, C.-H., Chen, D.-H., Wang, C.-R., Shiau, A.-L. & Wu, C.-L. 2007b. Methotrexate conjugated to gold nanoparticles inhibits tumor growth in a syngeneic lung tumor model. *Molecular Pharmaceutics,* 4**,** 713-722.

Cheng, Y., C. Samia, A., Meyers, J. D., Panagopoulos, I., Fei, B. & Burda, C. 2008. Highly efficient drug delivery with gold nanoparticle vectors for *in vivo* photodynamic therapy of cancer. *Journal of the American Chemical Society,* 130**,** 10643-10647.

Cheng, Y., Meyers, J. D., Broome, A.-M., Kenney, M. E., Basilion, J. P. & Burda, C. 2011. Deep penetration of a PDT drug into tumors by noncovalent drug-gold nanoparticle conjugates. *Journal of the American Chemical Society,* 133**,** 2583-2591.

Cheng, Y., Samia, A. C., Li, J., Kenney, M. E., Resnick, A. & Burda, C. 2009. Delivery and efficacy of a cancer drug as a function of the bond to the gold nanoparticle surface. *Langmuir,* 26**,** 2248-2255.

Cho, E. C., Au, L., Zhang, Q. & Xia, Y. 2010. The effects of size, shape, and surface functional group of gold nanostructures on their adsorption and internalization by cells. *Small,* 6**,** 517-522.

Cobley, C. M., Au, L., Chen, J. & Xia, Y. 2010. Targeting gold nanocages to cancer cells for photothermal destruction and drug delivery. *Expert Opinion on Drug Delivery,* 7**,** 577-587.

Cobley, C. M., Chen, J., Cho, E. C., Wang, L. V. & Xia, Y. 2011. Gold nanostructures: a class of multifunctional materials for biomedical applications. *Chemical Society Reviews,* 40**,** 44-56.

Creusat, G., Rinaldi, A.-S., Weiss, E., Elbaghdadi, R., Remy, J.-S., Mulherkar, R. & Zuber, G. 2010. Proton sponge trick for pH-sensitive disassembly of polyethylenimine-based siRNA delivery systems. *Bioconjugate Chemistry,* 21**,** 994-1002.

Desai, N., Trieu, V., Yao, Z., Louie, L., Ci, S., Yang, A., Tao, C., De, T., Beals, B. & Dykes, D. 2006. Increased antitumor activity, intratumor paclitaxel concentrations, and endothelial cell transport of cremophor-free, albumin-bound paclitaxel, ABI-007, compared with cremophor-based paclitaxel. *Clinical Cancer Research,* 12**,** 1317-1324.

Ding, Y., Jiang, Z., Saha, K., Kim, C. S., Kim, S. T., Landis, R. F. & Rotello, V. M. 2014. Gold nanoparticles for nucleic acid delivery. *Molecular Therapy,* 22**,** 1075-1083.

Dreaden, E. C., Alkilany, A. M., Huang, X., Murphy, C. J. & El-Sayed, M. A. 2012. The golden age: gold nanoparticles for biomedicine. *Chemical Society Reviews,* 41**,** 2740-2779.

Dreaden, E. C., Mackey, M. A., Huang, X., Kang, B. & El-Sayed, M. A. 2011. Beating cancer in multiple ways using nanogold. *Chemical Society Reviews,* 40**,** 3391-3404.

Dufès, C., Uchegbu, I. F. & Schätzlein, A. G. 2005. Dendrimers in gene delivery. *Advanced Drug Delivery Reviews,* 57**,** 2177-2202.

Duncan, R. & Izzo, L. 2005. Dendrimer biocompatibility and toxicity. *Advanced Drug Delivery Reviews,* 57**,** 2215-2237.

Ebara, M. & Uto, K. 2016. Gold nanomaterials for gene therapy *In:* nanoparticles, s. o. g. (ed.) *Polymers and Nanomaterials for Gene Therapy.* Woodhead Publishing.

Elbakry, A., Zaky, A., Liebl, R., Rachel, R., Goepferich, A. & Breunig, M. 2009. Layer-by-layer assembled gold nanoparticles for siRNA delivery. *Nano Letters,* 9**,** 2059-2064.

Faraday, M. 1857. The Bakerian Lecture: Experimental Relations of Gold (and Other Metals) to Light. *Philosophical Transactions of the Royal Society of London,* 147**,** 145-181.

Felgner, P. L., Gadek, T. R., Holm, M., Roman, R., Chan, H. W., Wenz, M., Northrop, J. P., Ringold, G. M. & Danielsen, M. 1987. Lipofection: a highly efficient, lipid-mediated DNA-transfection procedure. *Proceedings of the National Academy of Sciences,* 84**,** 7413-7417.

Fitzgerald, K. A., Rahme, K., Guo, J., Holmes, J. D. & O'Driscoll, C. M. 2016. Anisamide-targeted gold nanoparticles for siRNA delivery in prostate cancer–synthesis, physicochemical characterisation and *in vitro* evaluation. *Journal of Materials Chemistry B,* 4**,** 2242-2252.

Flynn, N. T., Tran, T. N. T., Cima, M. J. & Langer, R. 2003. Long-term stability of self-assembled monolayers in biological media. *Langmuir,* 19**,** 10909-10915.

Funkhouser, G. P., Arevalo, M. P., Glatzhofer, D. T. & O'Rear, E. A. 1995. Solubilization and adsolubilization of pyrrole by sodium dodecyl sulfate: polypyrrole formation on alumina surfaces. *Langmuir,* 11**,** 1443-1447.

Futaki, S., Ohashi, W., Suzuki, T., Niwa, M., Tanaka, S., Ueda, K., Harashima, H. & Sugiura, Y. 2001. Stearylated arginine-rich peptides: a new class of transfection systems. *Bioconjugate Chemistry,* 12**,** 1005-1011.

Ghosh, P., Han, G., De, M., Kim, C. K. & Rotello, V. M. 2008a. Gold nanoparticles in delivery applications. *Advanced Drug Delivery Reviews,* 60**,** 1307-1315.

Ghosh, P. S., Kim, C.-K., Han, G., Forbes, N. S. & Rotello, V. M. 2008b. Efficient gene delivery vectors by tuning the surface charge density of amino acid-functionalized gold nanoparticles. *ACS Nano,* 2**,** 2213-2218.

Giljohann, D. A., Seferos, D. S., Prigodich, A. E., Patel, P. C. & Mirkin, C. A. 2009. Gene regulation with polyvalent siRNA− nanoparticle conjugates. *Journal of the American Chemical Society,* 131**,** 2072-2073.

Godbey, W., Wu, K. K. & Mikos, A. G. 1999. Size matters: molecular weight affects the efficiency of poly (ethylenimine) as a gene delivery vehicle. *Journal of Biomedical Materials Research,* 45**,** 268-275.

Graff, J. N. & Chamberlain, E. D. 2015. Sipuleucel-T in the treatment of prostate cancer: an evidence-based review of its place in therapy. *Core Evidence,* 10**,** 1-10.

Han, L., Zhao, J., Zhang, X., Cao, W., Hu, X., Zou, G., Duan, X. & Liang, X.-J. 2012. Enhanced siRNA delivery and silencing gold–chitosan nanosystem with surface charge-reversal polymer assembly and good biocompatibility. *ACS Nano,* 6**,** 7340-7351.

Huang, S., Duan, S., Wang, J., Bao, S., Qiu, X., Li, C., Liu, Y., Yan, L., Zhang, Z. & Hu, Y. 2016. Folic-acid-mediated functionalized gold nanocages for targeted delivery of anti-miR-181b in combination of gene therapy and photothermal therapy against hepatocellular carcinoma. *Advanced Functional Materials,* 26**,** 2532-2544.

Hui, S. W., Langner, M., Zhao, Y.-L., Ross, P., Hurley, E. & Chan, K. 1996. The role of helper lipids in cationic liposome-mediated gene transfer. *Biophysical Journal,* 71**,** 590-599.

Jain, P. K., Qian, W. & El-Sayed, M. A. 2006. Ultrafast cooling of photoexcited electrons in gold nanoparticle−thiolated DNA conjugates involves the dissociation of the gold−thiol bond. *Journal of the American Chemical Society,* 128**,** 2426-2433.

Jain, R. K. & Stylianopoulos, T. 2010. Delivering nanomedicine to solid tumors. *Nature Reviews Clinical Oncology,* 7**,** 653-664.

Jaroch, K., Jaroch, A. & Bojko, B. 2018. Cell cultures in drug discovery and development: The need of reliable *in vitro-in vivo* extrapolation for pharmacodynamics and pharmacokinetics assessment. *Journal of Pharmaceutical and Biomedical Analysis,* 147**,** 297-312.

Johnsen, K. B., Bak, M., Kempen, P. J., Melander, F., Burkhart, A., Thomsen, M. S., Nielsen, M. S., Moos, T. & Andresen, T. L. 2018. Antibody affinity and valency impact brain uptake of transferrin receptor-targeted gold nanoparticles. *Theranostics,* 8**,** 3416-3436.

Kang, H. C., Kang, H.-J. & Bae, Y. H. 2011. A reducible polycationic gene vector derived from thiolated low molecular weight branched polyethyleneimine linked by 2-iminothiolane. *Biomaterials,* 32**,** 1193-1203.

Kelly, K. L., Coronado, E., Zhao, L. L. & Schatz, G. C. 2003. The optical properties of metal nanoparticles: The Influence of size, shape, and dielectric environment. *The Journal of Physical Chemistry B,* 107**,** 668-677.

Kim, S. T., Chompoosor, A., Yeh, Y.-C., Agasti, S. S., Solfiell, D. J. & Rotello, V. M. 2012. Dendronized gold nanoparticles for siRNA delivery. *Small,* 8**,** 3253-3256.

Kong, W.-H., Sung, D.-K., Shim, Y.-H., Bae, K. H., Dubois, P., Park, T. G., Kim, J.-H. & Seo, S.-W. 2009. Efficient intracellular siRNA delivery strategy through rapid and simple two steps mixing involving noncovalent post-PEGylation. *Journal of Controlled Release,* 138**,** 141-147.

Kura, A. U., Fakurazi, S., Hussein, M. Z. & Arulselvan, P. 2014. Nanotechnology in drug delivery: the need for more cell culture based studies in screening. *Chemistry Central Journal,* 8**,** 1-7.

Lammers, T., Kiessling, F., Hennink, W. E. & Storm, G. 2012. Drug targeting to tumors: principles, pitfalls and (pre-) clinical progress. *Journal of Controlled Release,* 161**,** 175-87.

Li, A., Qiu, J., Zhou, B., Xu, B., Xiong, Z., Hao, X., Shi, X. & Cao, X. 2020. The gene transfection and endocytic uptake pathways mediated by PEGylated PEI-entrapped gold nanoparticles. *Arabian Journal of Chemistry,* 13**,** 2558-2567.

Li, W., Cai, X., Kim, C., Sun, G., Zhang, Y., Deng, R., Yang, M., Chen, J., Achilefu, S. & Wang, L. V. 2011. Gold nanocages covered with thermally-responsive polymers for controlled release by high-intensity focused ultrasound. *Nanoscale,* 3**,** 1724-1730.

Li, Z., Liu, Y., Huang, X., Hu, C., Wang, H., Yuan, L., Brash, J. L. & Chen, H. 2019. One-step preparation of gold nanovectors using folate modified polyethylenimine and their use in target-specific gene transfection. *Colloids and Surfaces B: Biointerfaces,* 177**,** 306-312.

Lim, L. Y., Koh, P. Y., Somani, S., Al Robaian, M., Karim, R., Yean, Y. L., Mitchell, J., Tate, R. J., Edrada-Ebel, R. & Blatchford, D. R. 2015. Tumor regression following intravenous administration of lactoferrin-and lactoferricin-bearing dendriplexes. *Nanomedicine: Nanotechnology, Biology and Medicine,* 11**,** 1445-1454.

Liu, H., Wang, J., Li, W., Hu, J., Wang, M. & Kang, Y. 2018. Cellular uptake behaviors of rigidity-tunable dendrimers. *Pharmaceutics,* 10**,** 99-107.

Liu, Y. & Chiu, G. N. 2013. Dual-functionalized PAMAM dendrimers with improved P-glycoprotein inhibition and tight junction modulating effect. *Biomacromolecules,* 14**,** 4226-4235.

Luan, X., Rahme, K., Cong, Z., Wang, L., Zou, Y., He, Y., Yang, H., Holmes, J. D., O'Driscoll, C. M. & Guo, J. 2019. Anisamide-targeted PEGylated gold nanoparticles designed to target prostate cancer mediate: Enhanced systemic exposure of siRNA, tumour growth suppression and a synergistic therapeutic response in combination with paclitaxel in mice. *European Journal of Pharmaceutics and Biopharmaceutics,* 137**,** 56-67.

Maeda, H., Wu, J., Sawa, T., Matsumura, Y. & Hori, K. 2000. Tumor vascular permeability and the EPR effect in macromolecular therapeutics: a review. *Journal of Controlled Release,* 65**,** 271-284.

McCrudden, C. M. & McCarthy, H. O. 2013. Cancer gene therapy–key biological concepts in the design of multifunctional non-viral delivery systems, *InTech*.213-249

McIntosh, C. M., Esposito, E. A., Boal, A. K., Simard, J. M., Martin, C. T. & Rotello, V. M. 2001. Inhibition of DNA transcription using cationic mixed monolayer protected gold clusters. *Journal of the American Chemical Society,* 123**,** 7626-7629.

Minchinton, A. I. & Tannock, I. F. 2006. Drug penetration in solid tumours. *Nature Reviews Cancer,* 6**,** 583-592.

Mishra, S., Webster, P. & Davis, M. E. 2004. PEGylation significantly affects cellular uptake and intracellular trafficking of non-viral gene delivery particles. *European Journal of Cell Biology,* 83**,** 97-112.

Misra, R., Acharya, S. & Sahoo, S. K. 2010. Cancer nanotechnology: application of nanotechnology in cancer therapy. *Drug Discovery Today,* 15**,** 842-850.

Moghimi, S. M., Hunter, A. & Andresen, T. 2012. Factors controlling nanoparticle pharmacokinetics: an integrated analysis and perspective. *Annual Review of Pharmacology and Toxicology,* 52**,** 481-503.

Monnery, B. D., Wright, M., Cavill, R., Hoogenboom, R., Shaunak, S., Steinke, J. H. & Thanou, M. 2017. Cytotoxicity of polycations: Relationship of molecular weight and the hydrolytic theory of the mechanism of toxicity. *International Journal of Pharmaceutics,* 521**,** 249-258.

Monopoli, M. P., Åberg, C., Salvati, A. & Dawson, K. A. 2012. Biomolecular coronas provide the biological identity of nanosized materials. *Nature Nanotechnology,* 7**,** 779-786.

Moon, G. D., Choi, S.-W., Cai, X., Li, W., Cho, E. C., Jeong, U., Wang, L. V. & Xia, Y. 2011. A new theranostic system based on gold nanocages and phase-change materials with unique features for photoacoustic imaging and controlled release. *Journal of the American Chemical Society,* 133**,** 4762-4765.

Morgan, E., Wupperfeld, D., Morales, D. & Reich, N. 2019. Shape matters: Gold nanoparticle shape impacts the biological activity of siRNA delivery. *Bioconjugate Chemistry,* 30**,** 853-860.

Murphy, C. J., Thompson, L. B., Alkilany, A. M., Sisco, P. N., Boulos, S. P., Sivapalan, S. T., Yang, J. A., Chernak, D. J. & Huang, J. 2010. The many faces of gold nanorods. *The Journal of Physical Chemistry Letters,* 1**,** 2867-2875.

Nanjwade, B. K., Bechra, H. M., Derkar, G. K., Manvi, F. & Nanjwade, V. K. 2009. Dendrimers: emerging polymers for drug-delivery systems. *European Journal of Pharmaceutical Sciences,* 38**,** 185-196.

Oishi, M., Nakaogami, J., Ishii, T. & Nagasaki, Y. 2006. Smart PEGylated gold nanoparticles for the cytoplasmic delivery of siRNA to induce enhanced gene silencing. *Chemistry Letters,* 35**,** 1046-1047.

Pang, B., Yang, X. & Xia, Y. 2016. Putting gold nanocages to work for optical imaging, controlled release and cancer theranostics. *Nanomedicine: Nanotechnology, Biology, and Medicine,* 11**,** 1715-1728.

Park, T. G., Jeong, J. H. & Kim, S. W. 2006. Current status of polymeric gene delivery systems. *Advanced Drug Delivery Reviews,* 58**,** 467-486.

Patnaik, S. & Gupta, K. C. 2013. Novel polyethylenimine-derived nanoparticles for in vivo gene delivery. *Expert Opinion on Drug Delivery,* 10**,** 215-228.

Ping, Y., Liu, C., Zhang, Z., Liu, K. L., Chen, J. & Li, J. 2011. Chitosan-graft-(PEI-β-cyclodextrin) copolymers and their supramolecular PEGylation for DNA and siRNA delivery. *Biomaterials,* 32**,** 8328-8341.

Pouton, C. W., Lucas, P., Thomas, B. J., Uduehi, A. N., Milroy, D. A. & Moss, S. H. 1998. Polycation-DNA complexes for gene delivery: a comparison of the biopharmaceutical properties of cationic polypeptides and cationic lipids. *Journal of Controlled Release,* 53**,** 289-299.

Qiu, J., Xie, M., Wu, T., Qin, D. & Xia, Y. 2020. Gold nanocages for effective photothermal conversion and related applications. *Chemical Science,* 11**,** 12955-12973.

Ravi, M., Paramesh, V., Kaviya, S., Anuradha, E. & Solomon, F. P. 2015. 3D cell culture systems: advantages and applications. *Journal of Cellular Physiology,* 230**,** 16-26.

Robinson, R., Gerlach, W. & Ghandehari, H. 2015. Comparative effect of gold nanorods and nanocages for prostate tumor hyperthermia. *Journal of Controlled Release,* 220**,** 245-252.

Rosi, N. L., Giljohann, D. A., Thaxton, C. S., Lytton-Jean, A. K., Han, M. S. & Mirkin, C. A. 2006. Oligonucleotide-modified gold nanoparticles for intracellular gene regulation. *Science,* 312**,** 1027-1030.

Salameh, J. W., Zhou, L., Ward, S. M., Santa Chalarca, C. F., Emrick, T. & Figueiredo, M. L. 2020. Polymer-mediated gene therapy: Recent advances and merging of delivery techniques. *Wiley Interdisciplinary Reviews: Nanomedicine and Nanobiotechnology,* 12**,** e1598.

Seferos, D. S., Prigodich, A. E., Giljohann, D. A., Patel, P. C. & Mirkin, C. A. 2009. Polyvalent DNA nanoparticle conjugates stabilize nucleic acids. *Nano Letters,* 9**,** 308-311.

Shan, Y., Luo, T., Peng, C., Sheng, R., Cao, A., Cao, X., Shen, M., Guo, R., Tomás, H. & Shi, X. 2012. Gene delivery using dendrimer-entrapped gold nanoparticles as nonviral vectors. *Biomaterials,* 33**,** 3025-3035.

Shi, P., Ju, E., Ren, J. & Qu, X. 2014. Near-Infrared Light-Encoded Orthogonally Triggered and Logical Intracellular Release Using Gold Nanocage@ Smart Polymer Shell. *Advanced Functional Materials,* 24**,** 826-834.

Skrabalak, S. E., Au, L., Li, X. & Xia, Y. 2007. Facile synthesis of Ag nanocubes and Au nanocages. *Nature Protocols,* 2**,** 2182-2190.

Skrabalak, S. E., Chen, J., Sun, Y., Lu, X., Au, L., Cobley, C. M. & Xia, Y. 2008. Gold nanocages: synthesis, properties, and applications. *Accounts of Chemical Research,* 41**,** 1587-1595.

Somani, S., Laskar, P., Altwaijry, N., Kewcharoenvong, P., Irving, C., Robb, G., Pickard, B. S. & Dufès, C. 2018. PEGylation of polypropylenimine dendrimers: effects on cytotoxicity, DNA condensation, gene delivery and expression in cancer cells. *Scientific Reports,* 8**,** 1-13.

Sullivan, M. O., Green, J. & Przybycien, T. 2003. Development of a novel gene delivery scaffold utilizing colloidal gold–polyethylenimine conjugates for DNA condensation. *Gene Therapy,* 10**,** 1882-1890.

Sun, J., Zhang, L., Wang, J., Feng, Q., Liu, D., Yin, Q., Xu, D., Wei, Y., Ding, B. & Shi, X. 2015. Tunable rigidity of (polymeric core)–(lipid shell) nanoparticles for regulated cellular uptake. *Advanced Materials,* 27**,** 1402-1407.

Sun, T., Zhang, Y. S., Pang, B., Hyun, D. C., Yang, M. & Xia, Y. 2014. Engineered nanoparticles for drug delivery in cancer therapy. *Angewandte Chemie International Edition,* 53**,** 12320-12364.

Sun, Y., Mayers, B. T. & Xia, Y. 2002. Template-engaged replacement reaction: a one-step approach to the large-scale synthesis of metal nanostructures with hollow interiors. *Nano Letters,* 2**,** 481-485.

Sung, H., Ferlay, J., Siegel, R. L., Laversanne, M., Soerjomataram, I., Jemal, A. & Bray, F. 2021. Global cancer statistics 2020: GLOBOCAN estimates of incidence and mortality worldwide for 36 cancers in 185 countries. *CA: A Cancer Journal for Clinicians,* 71**,** 209-249.

Suresh, D., Zambre, A., Chanda, N., Hoffman, T. J., Smith, C. J., Robertson, J. D. & Kannan, R. 2014. Bombesin peptide conjugated gold nanocages internalize via clathrin mediated endocytosis. *Bioconjugate Chemistry,* 25**,** 1565-1579.

Tencomnao, T., Apijaraskul, A., Rakkhithawatthana, V., Chaleawlert-umpon, S., Pimpa, N., Sajomsang, W. & Saengkrit, N. 2011. Gold/cationic polymer nano-scaffolds mediated transfection for non-viral gene delivery system. *Carbohydrate Polymers,* 84**,** 216-222.

Thapa, B. & Narain, R. 2016. Mechanism, current challenges and new approaches for non viral gene delivery, *Woodhead Publishing.*

Thomas, M. & Klibanov, A. M. 2003. Conjugation to gold nanoparticles enhances polyethylenimine's transfer of plasmid DNA into mammalian cells. *Proceedings of the National Academy of Sciences,* 100**,** 9138-9143.

Tian, H., Guo, Z., Chen, J., Lin, L., Xia, J., Dong, X. & Chen, X. 2012. PEI conjugated gold nanoparticles: efficient gene carriers with visible fluorescence. *Advanced Healthcare Materials,* 1**,** 337-341.

Van Hong Nguyen, B.-J. L. 2017. Protein corona: a new approach for nanomedicine design. *International Journal of Nanomedicine,* 12**,** 3137-3151.

Waehler, R., Russell, S. J. & Curiel, D. T. 2007. Engineering targeted viral vectors for gene therapy. *Nature Reviews Genetics,* 8**,** 573-587.

Wagner, E. & Kloeckner, J. 2006. Gene delivery using polymer therapeutics. *Polymer Therapeutics***,** 135-173.

Wang, A. Z., Langer, R. & Farokhzad, O. C. 2012. Nanoparticle delivery of cancer drugs. *Annual Review of Medicine,* 63**,** 185-198.

Wang, W., Li, W., Ma, N. & Steinhoff, G. 2013a. Non-viral gene delivery methods. *Current Pharmaceutical Biotechnology,* 14**,** 46-60.

Wang, Y., Zheng, Y., Huang, C. Z. & Xia, Y. 2013b. Synthesis of Ag nanocubes 18–32 nm in edge length: the effects of polyol on reduction kinetics, size control, and reproducibility. *Journal of the American Chemical Society,* 135**,** 1941-1951.

Wicki, A., Witzigmann, D., Balasubramanian, V. & Huwyler, J. 2015. Nanomedicine in cancer therapy: challenges, opportunities, and clinical applications. *Journal of Controlled Release,* 200**,** 138-157.

Williams, H. D., Trevaskis, N. L., Charman, S. A., Shanker, R. M., Charman, W. N., Pouton, C. W. & Porter, C. J. 2013. Strategies to address low drug solubility in discovery and development. *Pharmacological Reviews,* 65**,** 315-499.

Wong, S. Y., Pelet, J. M. & Putnam, D. 2007. Polymer systems for gene delivery—past, present, and future. *Progress in Polymer Science,* 32**,** 799-837.

Xavier, P. L., Chaudhari, K., Verma, P. K., Pal, S. K. & Pradeep, T. 2010. Luminescent quantum clusters of gold in transferrin family protein, lactoferrin exhibiting FRET. *Nanoscale,* 2**,** 2769-2776.

Xia, X. & Xia, Y. 2014. Gold nanocages as multifunctional materials for nanomedicine. *Frontiers of Physics,* 9**,** 378-384.

Xia, X., Yang, M., Oetjen, L. K., Zhang, Y., Li, Q., Chen, J. & Xia, Y. 2011. An enzyme-sensitive probe for photoacoustic imaging and fluorescence detection of protease activity. *Nanoscale,* 3**,** 950-953.

Yang, X., Yang, M., Pang, B., Vara, M. & Xia, Y. 2015. Gold Nanomaterials at Work in Biomedicine. *Chemical Reviews,* 115**,** 10410-10488.

Yavuz, M. S., Cheng, Y., Chen, J., Cobley, C. M., Zhang, Q., Rycenga, M., Xie, J., Kim, C., Song, K. H. & Schwartz, A. G. 2009. Gold nanocages covered by smart polymers for controlled release with near-infrared light. *Nature Materials,* 8**,** 935-939.

Yuan, F., Dellian, M., Fukumura, D., Leunig, M., Berk, D. A., Torchilin, V. P. & Jain, R. K. 1995. Vascular permeability in a human tumor xenograft: molecular size dependence and cutoff size. *Cancer Research,* 55**,** 3752-3756.

Zamora-Justo, J. A., Abrica-González, P., Vázquez-Martínez, G. R., Muñoz-Diosdado, A., Balderas-López, J. A. & Ibáñez-Hernández, M. 2019. Polyethylene glycol-coated gold nanoparticles as DNA and atorvastatin delivery systems and cytotoxicity evaluation. *Journal of Nanomaterials,* 2019**,** 5982047-5982047.

Zhang, X. Q., Xu, X., Bertrand, N., Pridgen, E., Swami, A. & Farokhzad, O. C. 2012. Interactions of nanomaterials and biological systems: Implications to personalized nanomedicine. *Advanced Drug Delivery Reviews,* 64**,** 1363-1384.

Zhou, Z., Liu, X., Zhu, D., Wang, Y., Zhang, Z., Zhou, X., Qiu, N., Chen, X. & Shen, Y. 2017. Nonviral cancer gene therapy: Delivery cascade and vector nanoproperty integration. *Advanced Drug Delivery Reviews,* 115**,** 115-154.

Zinselmeyer, B. H., Mackay, S. P., Schatzlein, A. G. & Uchegbu, I. F. 2002. The lower-generation polypropylenimine dendrimers are effective gene-transfer agents. *Pharmaceutical Research,* 19**,** 960-967.

Appendix I: List of Publications

1. Almowalad, J., Somani, S., Laskar, P., Meewan, J., Tate, R., Mullin, M., and Dufès, C. 2021. Lactoferrin-bearing gold nanocages for gene delivery in prostate cancer cells *in vitro*. *International Journal of Nanomedicine*. 16, 4391-4407
2. Almowalad, J., Laskar, P., Somani, S., Meewan, J., Tate, R., Mullin, M., and Dufès, C. 2021. Dendrimer-conjugated, lactoferrin-bearing gold nanocages for gene delivery in prostate cancer cells *in vitro*. (Submitted for publication).

Appendix II: Conference Abstracts

1. Almowalad, J., Somani, S., Lasker, P., and Dufès, C. Development of novel gold nanocages as drug and gene delivery systems. The British Society for Nanomedicine Early Career Researcher's Meeting, Glasgow, UK (July 25-26, 2019), Poster presentation.

2. Almowalad, J., Somani, S., Lasker, P., and Dufès, C. Gold nanocages as drug and gene delivery systems. The International Conference On Nanomedicine And Nanobiotechnology (ICONAN), Munich, Germany, (October 16-18, 2019), Poster presentation.

Others

1. University of Strathclyde Postgraduate Travel Award for presenting a poster at the International Conference On Nanomedicine And Nanobiotechnology (ICONAN) (16-18th October 2019) in Munich, Germany.